รายงานวิจัยฉบับสมบูรณ์

โครงการ: Electroreduction of CO_2 to methane on Cu-based alloys: First-principle calculations

ปฏิกิริยาอิเลคโตรรีดักชั่นของคาร์บอนไดออกไซด์ไปเป็นมีเทนบนโลหะผสมทองแดง
โดยการคำนวณใช้ทฤษฎีเฟริส์พรินสิเพิ้ล

โดย ดร. ผุศนา หิรัญสิทธิ์

2 มิถุนายน 2558

สัญญาเลขที่ TRG5680015

รายงานวิจัยฉบับสมบูรณ์

โครงการ: Electroreduction of CO_2 to methane on Cu-based alloys: First-principle calculations
ปฏิกิริยาอิเลคโตรรีดักชั่นของคาร์บอนไดออกไซด์ไปเป็นมีเทนบนโลหะผสมทองแดง
โดยการคำนวณใช้ทฤษฎีเฟริส์พรินสิเพิ้ล

ผู้วิจัย ดร. ผุศนา หิรัญสิทธิ์ สังกัด ศูนย์นาโนเทคโนโลยีแห่งชาติ

สนับสนุนโดยสำนักงานกองทุนสนับสนุนการวิจัย และ ศูนย์นาโนเทคโนโลยีแห่งชาติ

Abstract

Project Code: TRG5680015

Project Title: Electroreduction of CO_2 to methane on Cu-based alloys: First-principle calculations

Investigator: Dr. Pussana Hirunsit National Nanotechnology Center, National Science and Technology Development Agency

E-mail Address: pussana@nanotec.or.th

Project Period: June 03, 2013 – June -02, 2015

A systematic investigation of CO_2 electroreduction to CH_4 and CH_3OH on copper-based alloys stepped surfaces, Cu, Cu_3Ag, Cu_3Au, Cu_3Ni, Cu_3Pd, Cu_3Pt, Cu_3Co, Cu_3Rh, and Cu_3Ir, was performed using density functional theory (DFT) calculations associated with the standard hydrogen electrode model. The calculation results were able to determine the correlations between CO adsorption energy and the other key $C_xH_yO_z$ intermediates adsorption energy, the overpotential, the limiting-potential elementary step, and selectivity to CH_4, CH_3OH, HCOOH, and H_2. The electrode efficiency decrease by OH* poisoning and the H_2 evolution is also investigated. The results demonstrate that the CO* protonation is the limiting-potential step on most surfaces, with the exception on Cu_3Au and Cu_3Co surfaces. In spite of the excessive strong CO* interaction on some surfaces, the overpotentials reduce when the degree of CO* adsorption energy and HCO*/COH* adsorption energy decoupling increases. The CO* adsorption energy is a good descriptor for linear scaling correlations with the other $C_xH_yO_z$ intermediates due to the similar charge transfer characteristics of the C-O bond in CO* and those intermediates. The formic acid production can be efficiently catalyzed on Cu_3Pt, Cu_3Ni, Cu_3Co, and Cu_3Rh surfaces. Methanol production is favorable on Cu_3Pd and Cu_3Pt surfaces, yet they show high overpotential (～0.7 V). The key of methanol selectivity is CH_2OH* intermediate formation favorability associated with the preference of CH_2OH* protonation at the C atom over the O atom. The calculations reveal that the electroreduction activity on Cu-based alloys catalysts do not show a volcano type relation as was previously found on pure metal catalysts

Keywords: CO_2 reduction, density functional theory, heterogeneous catalysis, and copper alloys

บทคัดย่อ

รหัสโครงการ: TRG5680015

ชื่อโครงการ: ปฏิกิริยาอิเลคโตรรีดักชั่นของคาร์บอนไดออกไซด์ไปเป็นมีเทนบนโลหะผสมทองแดงโดยการคำนวณใช้ทฤษฎีเฟิร์สพรินสิเพิ้ล

ชื่อนักวิจัย: ดร.ผุศนา หิรัญสิทธิ์ ศูนย์นาโนเทคโนโลยีแห่งชาติ สำนักงานพัฒนาวิทยาศาสตร์และเทคโนโลยีแห่งชาติ

E-mail Address: pussana@nanotec.or.th

ระยะเวลาโครงการ: 3 มิถุนายน พ.ศ.2556 - 2 มิถุนายน พ.ศ.2558

โครงการนี้ได้ทำการศึกษาการเกิดปฏิกิริยาอิเล็กโตรรีดักชั่นของคาร์บอนไดออกไซด์ไปเป็นมีเทนและเมทานอลบนพื้นผิวแบบขั้นของโลหะผสมทองแดง โดยใช้การคำนวณแบบ density functional theory ร่วมกับโมเดล standard hydrogen electrode โครงการนี้ทำการศึกษาอย่างเป็นระบบโดยผสมคอปเปอร์กับธาตุในหมู่ 9-11 ประกอบด้วย Cu, Cu_3Ag, Cu_3Au, Cu_3Ni, Cu_3Pd, Cu_3Pt, Cu_3Co, Cu_3Rh, และ Cu_3Ir ผลการคำนวณแสดงถึงความสัมพันธ์ระหว่างค่าพลังงานการดูดซับของ CO กับ ค่าพลังงานการดูดซับของสารตัวกลาง $C_xH_yO_z$, ขั้นตอนของปฏิกิริยาที่ถูกจำกัดทางศักย์ไฟฟ้า, และสมรรถนะการเลือกเกิดสารผลิตภัณฑ์ มีเทน, เมทานอล, กรดฟอร์มิก และ แก๊สไฮโดรเจน นอกจากนี้ยังรวมถึงการศึกษาถึงประสิทธิภาพของอิเล็กโทรดที่ลดลงเนื่องจากการเกิดสารตัวกลาง OH ปกคลุมพื้นผิว และเนื่องจากการเกิดแก๊สไฮโดรเจนซึ่งเป็นปฏิกิริยาข้างเคียง ผลการคำนวณแสดงให้เห็นว่า ขั้นตอนปฏิกิริยาการเติมโปรตอนให้ CO เป็นขั้นตอนที่ถูกจำกัดทางศักย์ไฟฟ้าบนพื้นผิวโลหะผสมทองแดงส่วนใหญ่ ยกเว้น บนพื้นผิวของ Cu_3Au และ Cu_3Co ถึงแม้ว่าการดูดซับ CO จะแข็งแรงมากบนบางพื้นผิวโลหะผสมทองแดง แต่การลดลงของ overpotential เกิดขึ้นได้เมื่อการควบคู่ระหว่างค่าพลังงานการดูดซับ CO กับ ค่าพลังงานการดูดซับ HCO/COH ลดลง ค่าพลังงานการดูดซับ CO เป็นตัวบอกที่ดีสำหรับการแสดงความสัมพันธ์แบบเส้นตรงกับ ค่าพลังงานการดูดซับสารตัวกลาง $C_xH_yO_z$ อื่นๆ เนื่องจากมีลักษณะการถ่ายเทอิเล็กตรอนที่คล้ายกันระหว่าง พันธะ C-O ใน CO และพันธะ C-O ในสารตัวกลาง $C_xH_yO_z$ อื่นๆ ปฏิกิริยาการเกิดกรดฟอร์มิกสามารถเกิดได้อย่างมีประสิทธิภาพที่ดีบนพื้นผิว Cu_3Pt, Cu_3Ni, Cu_3Co, และ Cu_3Rh ปฏิกิริยาการเกิดเมทานอลสามารถเอื้อให้เกิดขึ้นได้ดีกว่าปฏิกิริยาการเกิดมีเทนบนพื้นผิว Cu_3Pd และ Cu_3Pt แต่มี overpotential ที่สูงประมาณ 0.7 V ปัจจัยสำคัญต่อสมรรถนะการเลือกเกิดเมทานอลคือ การเอื้อให้เกิดสารตัวกลาง CH_2OH หรือไม่ ร่วมกับการเอื้อให้เกิดปฏิกิริยาเติมโปรตอนในขั้นต่อไปที่คาร์บอนอะตอม ไม่ใช่ที่ออกซิเจนอะตอมของสารตัวกลาง CH_2OH ผลการคำนวณยังแสดงให้เห็นถึงความแตกต่างของแนวโน้มความสามารถในการเกิดปฏิกิริยาอิเล็กโตรรีดักชั่นของคาร์บอนไดออกไซด์บนพื้นผิวแบบขั้นของโลหะผสมทองแดงซึ่งไม่แสดงความสัมพันธ์ในลักษณะของกราฟแบบภูเขาไฟซึ่งพบบนพื้นผิวแบบขั้นของธาตุบริสุทธิ์ในหมู่ 9-11

คำหลัก: ปฏิกิริยาอิเล็กโตรรีดักชั่นของคาร์บอนไดออกไซด์, density functional theory, การเร่งปฏิกิริยาแบบวิวิธพันธุ์ และ โลหะผสมทองแดง

1. Introduction

The electroreduction of CO_2 to valuable hydrocarbon products is a promising process that would create a significant impact to the global carbon balance by recycling waste CO_2 into usable hydrocarbons. The critical challenges for the CO_2 electroreduction process are that the reaction must be at a low overpotential as well as being selective. The overpotential is the difference between the applied potential and the equilibrium potential for the reaction. The faradic efficiency and selectivity of CO_2 electroreduction depends on a number of factors; the electrode materials, electrode surface structures, type of ionic species in electrolytes, local pH, and CO_2 concentration on the electrode.[1-9] The electrode material is crucial in that it plays essential roles in determining the overpotential, efficiency and selectivity. A variety of electrode materials have extensively been examined for CO_2 electroreduction, including ionic liquids[10], organometallic complexes[11-12], organic compounds[13-14], doped graphene[15], semiconductors[16], proteins[17] and enzymes (carbon monoxide dehydrogenase)[18-19]. Several excellent reviews provide important research advances regarding catalysis for CO_2 conversion and other important factors as well.[6, 9, 20-24]

A Copper electrode was found to perform the direct reduction of CO_2 to hydrocarbons (methane and ethylene) with a reasonable current density (5-10 $mA.cm^{-2}$) and current efficiency.[1, 24-26] A wider range of hydrocarbons such as ethanol and propanol can also be produced.[1, 27-30] The most common reactions and their equilibrium potentials vs RHE (reverse hydrogen electrode) are listed in reaction (1-6). Despite the unique hydrocarbons production from CO_2, copper inefficiently catalyzes CO_2 electroreduction to the point that the overpotential is quite high, approximately 1.0 V. Thermodynamically, the equilibrium potential of CO_2 reduction to CH_4 (reaction 5) is only +0.17 V_{RHE} at 18.5 °C. Nevertheless, it was experimentally shown that the potential of -0.8 V is required for the onset CH_4 production on a copper electrode and -1.0 V is required for a decent current (2 $mA.cm^{-2}$ to CH_4 production).[31] Hori et al. proposed that the reduction of COH* intermediate, which is formed upon CO* reduction, might be the rate determining step.[32] Several groups have also shown that the rate-limiting step occurs after the formation of CO*.[33-35] The density functional theory (DFT) calculations by Nørskov's group indicated that the limiting potential step of CO_2 reduction to CH_4 on Cu(211) surface is the protonation of adsorbed CO* to form adsorbed HCO* ($CO^* + H^+ + e^- \rightarrow HCO^*$).[36] The calculations suggested that when the adsorbed HCO* can be stabilized relative to adsorbed CO*, the overpotential can be significantly reduced leading to a more efficient process.

$CO_2 + 2(H^+ + e^-) \rightarrow HCOOH(aq)$ U = -0.20 V_{RHE} (1)

$CO_2 + 2(H^+ + e^-) \rightarrow CO + H_2O$ U = -0.12 V_{RHE} (2)

$CO_2 + 4(H^+ + e^-) \rightarrow CH_2O(aq) + H_2O$ U = -0.07 V_{RHE} (3)

$CO_2 + 6(H^+ + e^-) \rightarrow CH_3OH(aq) + H_2O$ U = +0.03 V_{RHE} (4)

$CO_2 + 8(H^+ + e^-) \rightarrow CH_4 + 2H_2O$ U = +0.17 V_{RHE} (5)

$2CO_2 + 12(H^+ + e^-) \rightarrow C_2H_4 + 4H_2O$ U = +0.08 V_{RHE} (6)

The CO_2 electroreduction on Cu catalyst yields the relatively high selectivity of methane and ethylene formation instead of methanol, while methanol is the majority product for the conventional CO_2 conversion. The selectivity still remains a crucial question.. Recently, the DFT calculation of the kinetic barrier of the CO_2 reduction paths by Nie et al[37-38] revealed that the selectivity step for methane versus methanol on Cu(111) occurs with hydrogenation of CO* to COH* (produce CH_4/C_2H_4) versus CHO* (produces CH_3OH).[37-38] The reduction of CO* to COH* is kinetically favored over CHO* when the potential-dependent barriers for hydrogenating the CO* are evaluated in the presence of a water molecule.[38] The polar O-H bond formation is stabilized through water-assisted proton shuttling coupled with electron transfer.[38] The less polar C-H bond requires direct surface interaction with both C and H at the transition state. Once COH* is produced, it is further reduced to C*, and then reduced to CH_4 and C_2H_4 products on Cu(111).[38] Thus, the proposed reaction path by Nie et al.[37] differs from the one proposed by Peterson et al.[36] for methane production which goes through CH_2O* and CH_3O* intermediates. Also, the DFT studies by Nie et al [37-38] indicate that surface CH_3O* will kinetically favor methanol production over methane due to higher barriers for methane formation. The methanol formation was also proposed to go through reduction of methanediol which is the hydrated form of formaldehyde.[39] The relative stabilities and rate of formation of CHO* versus COH* are dependent on various parameters, such as Cu surface structure, computational functional and approach of solvation inclusion. The intermediates adsorption is very sensitive to the electrode surface morphology resulting in the voltammetry feature changes and the change in voltage potential of the product formation.[40-41] Although copper is not an ideal catalyst, the understanding of this unique ability of a copper electrode is fruitful for better catalyst design.

In addition, several studies have investigated the pathway leading to C_2 species products and the step determining the favorability between C_1 and C_2 species.[38, 42-43] Nevertheless, the reduction reaction mechanism selectively leading to C_1 or C_2 species is still unclear. The previous experiment suggested that on a copper electrode the HCO* is the key intermediate towards the breaking of the C-O bond, leading to C_1 species (methane) production, while the key first step of the C_2 species products such as ethylene and ethanol was suggested to be the formation of CO dimer.[42, 44] The DFT calculations by Nie et al. also suggested that the effective barrier for ethylene formation occur at CH_2* reduction to CH_3* on Cu(111).[37] Though the rate constant favors ethylene selectivity at lower overpotentials on Cu(111), the relative coverage of CH_2* and H* will also affect the selectivity and might be expected to further promote methane formation at higher overpotentials.[37] Hansen et al. also predicted that the formation of both CH_4 and C_2H_4 are kinetically feasible from CH_2* on Cu(211) surface, with CH_4 being more kinetically favorable.[39] The presence of CH_2* allows for ethylene production from the same path as methane, which matches recent experimental studies[43] that indicate these two products share a common intermediate.

The electroreduction of CO_2 to hydrocarbons takes place on almost all metal electrodes, although the efficiencies and the selectivity are low.[22, 45-46] The CO_2 electroreduction using 0.1 M $KHCO_3$ electrolyte and a temperature of 18.5 ± 0.5 °C on various pure metal electrodes demonstrated that CO and formate are the main products on many metal electrodes.[22, 46] The CO formation occurred on Cu, Au, Ag, Zn, Pd, Ga, Ni and Pt and the formate formation took place on Pb, Hg, In, Sn, Cd and Tl.[22, 46] Also, the electrochemical reduction of CO_2 at a low-temperature of 0°C in 0.05 mol dm^{-3} $KHCO_3$ solution revealed a similar product selectivity group, that CO is mainly produced on Ti, Ni, Ag and Au electrodes and HCOOH is mainly yielded on Cd, In, Sn, Pb, Tl, and Hg electrodes.[45] Also, it was experimentally shown that Zn, Ag, Cu, Ni, and Pt are able to produce both methane and methanol and the selectivity may be determined by the C* and O* binding energy by modifying the surface to favor or disfavor C-O bond breakage.

Furthermore, the electrode potentials of CO_2 reduction on metals are well correlated with the potential of H_2 evolution which is a competitive side reaction and may obstruct the further reduction of hydrocarbon intermediate species.[22, 46] Many pure metal electrodes catalyze a major side reaction of H_2 evolution (HER); metals in group VA, VIA, Mn, Re, Fe, Ru, Co, Rh, and Ir.[45] Compared with all metals, Cu is the only metal that produces hydrocarbons (C_xH_y) efficiently. Based on DFT calculations by Nørskov's group, the analysis of CO_2 reduction to CH_4 on transition metals; Cu, Pt, Rh, Pd, Ni, Au and Ag revealed the "volcano" type of the activity diagram in which Cu is at the top among these metals.[47] The calculations clearly exhibit why Cu is the best-known metal electrocatalyst. Copper exhibits a better ability to perform CO* protonation than the other metals, but this is only associated with the poor activity of the hydrogen evolution reaction (HER), i.e., moderate negative potential for HER.[47] They suggested that the key to a substantially improved process efficiency is to find materials that have the binding energy of CO* and the binding energy of products upon CO* protonation (HCO* or COH*) decoupling, which leads to the reduction of the CO* and the protonation potential to be less negative.[47]

Alloying is an approach that may reduce the overpotential. It also leads to a major change in product distribution and faradic efficiency compared to those of the pure metals.[48] Many Cu alloys; Cu-Ni, Cu-Sn, Cu-Pb, Cu-Zn, Cu-Cd and Cu-Ag were experimentally studied for the CO_2 reduction in 0.05 M $KHCO_3$ aqueous solution.[48] These alloys were found to have selectivity toward CO and HCOOH products.[48] The alloy composition also highly influences the selectivity and product formation potential. Copper-gold alloy showed that the CO production increases markedly with the Au content, while the fraction of CH_4 decreases and the $Au_{50}Cu_{50}$ appears to be the composition giving the most efficient CO_2 conversion and yielding the highest faradic efficiency with CO as the major product.[49] The experimental onset potential of CO_2 electroreduction on the rich-Au nanoparticles (Au_2Cu) was positively shifted, indicating that copper-gold has the potential to lower the energy used for CO_2 conversion.[50] The alloying approach is anticipated to improve the HCO* intermediate stability on the surface leading to a significant reduction in the overpotential. In the previous theoretical work,[51] we found that the overpotential of CO_2 reduction to CH_4 on $Cu_3Au(211)$ is negatively shifted compared to the Cu(211) surface and the potential-limiting step is CO_2 protonation to form HOCO* while the overpotential on $Cu_3Ag(211)$ is similar to that on the Cu(211) surface with the same potential-limiting step of CO* protonation. However, the side reaction of H_2 evolution can pose a challenge on copper-gold and copper-silver alloys with Cu-rich composition.[51] CO is the major product on copper-gold and copper-silver alloys with higher Au and Ag content because it is challenged by the CO* desorption preference over further reduction of CO*.[51]

The exploration for electrocatalyst materials which can primarily meet the requirements of providing a more efficient process and being selective of CO_2 reduction is required for the process to advance. The development of more promising electrode materials requires a fundamental understanding of how electrode materials influence key reaction steps. The preferential adsorption of reactants, intermediates and products on electrode materials essentially contributes to the overpotential, catalytic activity and selectivity. This work aims to perform a systematic thermodynamic investigation of CO_2 electroreduction to CH_4 and CH_3OH on Cu-based alloys with Cu-rich composition of Cu_3X where X is Ag, Au, Co, Ni, Pd, Pt, Rh, and Ir using DFT calculations associated with the standard hydrogen electrode model[52]. The results of CO_2 conversion to CH_4 on Cu_3Au and Cu_3Ag and pure Cu surfaces were reported in the previous work[51] and are included here again to complete the systematic analysis. The goal of this work is to examine how copper alloying with transition metals modifies the CO_2 electroreduction activity and selectivity compared to that on pure Cu catalyst. The analysis provides useful theoretical insights for a better understanding of the chemical nature of the catalysts which could lead to improved catalyst development. We demonstrated how Cu-based alloys influence the electrocatalytic reactivity, the overpotential, the potential limiting step, the tendency of OH* surface poisoning, H_2 evolution and the selectivity to formic acid, methane and methanol products. The calculations suggest that alloying with some metals can reduce the overpotential of methane production and also affect the selectivity of methane, methanol and formic acid production.

2. Computational details

The structures of Cu_3X surfaces are modeled with $L1_2$ crystal lattice structures where X are metals in group 9-11 which are Ag, Au, Co, Ni, Pd, Pt, Rh, and Ir. The slab models of stepped (211) surface with a unit cell of 3×3 containing 6 layers of metal atoms and a vacuum region equivalent to more than 6 atomic layers (approximately 15 Å) were used for a search of the most stable binding sites. The bulk $L1_2$ crystal lattice structure of Cu_3X and the slab model of Cu_3X(211) are shown in Figure 1. The stepped surfaces (211) is chosen because it was generally found to be the most reactive for C-O bond breaking,[53] which is a crucial process here. The two atomic layers from the bottom of the slab were fixed, while the other layers were relaxed to their lowest energy configurations. The fixed layers were set to their bulk bond distances according to their optimized lattice constants that were determined from bulk calculations. The calculated lattice constants in Å are 3.63(Cu), 3.78(Cu_3Ag), 3.79 (Cu_3Au), 3.61(Cu_3Co), 3.70(Cu_3Ir), 3.60(Cu_3Ni), 3.72(Cu_3Pd), 3.73(Cu_3Pt), and 3.70(Cu_3Rh).

The impurity Au, Ag and Pd on the Cu host shows a moderate degree of segregation.[54] Also, the segregation may be induced by the strong affinity toward CO adsorption on those impurity metals. It should be noted that the segregation may induce the surface and near-surface composition change. The systematic investigation of Cu_3X in this work exhibits how the alloying effect produces a considerably different electrocatalytic activity trend from that found previously on pure metals and changes hydrocarbon products selectivity.

The fully periodic plane-wave DFT calculations as implemented in the Vienna *ab initio* Simulation Program (VASP)[55-56] were employed. Spin-polarized DFT calculations were performed with the exchange-correlation functional Perdew-Burke-Ernzerhof (PBE)[57-58] described within the generalized gradient approximation implemented with the projector augmented wavefunction (PAW)[59-60] method for representing the non-valence core electrons. The calculations employed 5×5×1 k-points Monkhorst-Pack mesh sampling in the surface Brillouin zone. The plane-wave cutoff energy was optimized at 400 eV. The results were checked for convergence with respect to the energy cutoff and number of k-points. The Methfessel-Paxton smearing of order 2 with a value of smearing parameter σ of 0.2 eV was applied. The convergence criteria for electronic self-consistent iteration were set to 1.5×10^{-7} eV and the ionic relaxation loop was limited for all forces smaller than 0.035 eV/Å for free atoms.

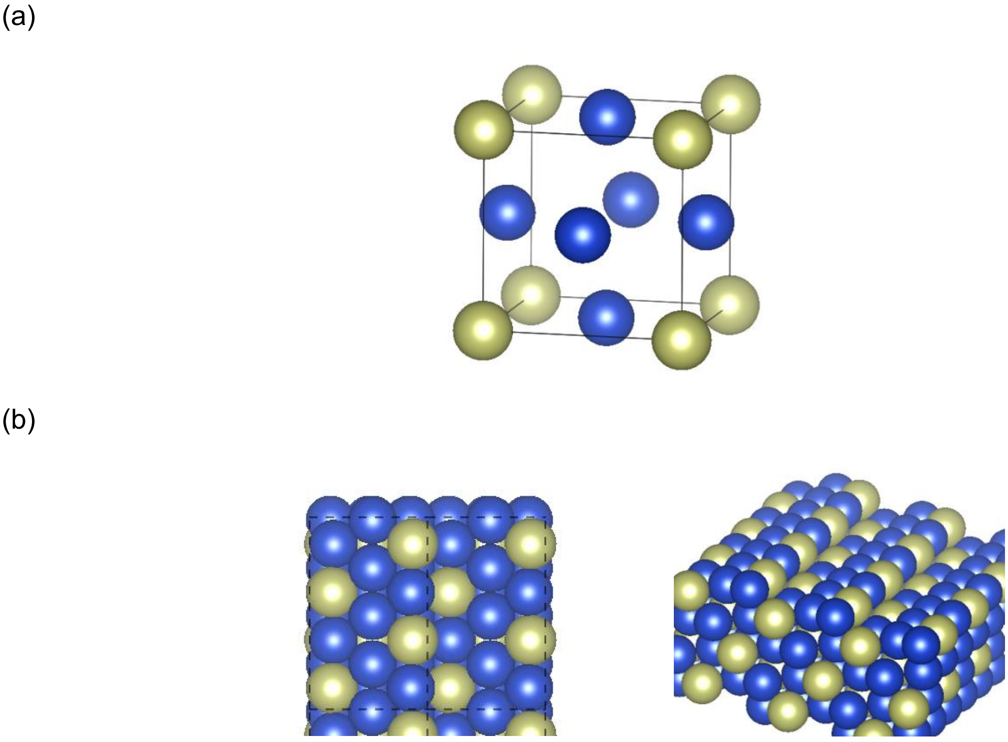

Top view side view

Figure 1. (a) The bulk $L1_2$ crystal lattice structure of Cu_3X , and (b) a unit cell of slab model of stepped (211) Cu_3X alloys surface. Cu atom-blue and X atom-green. The dashed line indicates a unit cell boundary.

The free energy diagrams of the electrochemical reactions for a given surface at 291.65 K were constructed according to the method proposed by Nørskov et al.[52] The method successfully described the overpotential of the oxygen reduction reaction on metal surfaces and CO_2 reduction to be methane on the Cu(211) surface.[36, 52] Details of calculations are described very well in Peterson *et al*.[36] Also, our previous work[51] includes the calculation details, the applied values of zero-point energy (*ZPE)*, $\int C_p dT$ and $T\Delta S$ correction terms of all adsorbed species and gas-phase species and the parameters taking into account the solvation effect on the adsorbate stabilization. The method[52] sets the reference potential to be the standard hydrogen electrode (SHE). This means, at $U \neq 0$, the free energy of the proton-electron pair can be treated by shifting the energy by -*e*U where U is the electrode potential relative to SHE. The reference electrode in this work is the theoretical reversible hydrogen electrode (RHE) which can relate to the standard hydrogen electrode (SHE) as $U_{RHE} = U_{SHE} - (kT \times pH \times ln10)$ where the pH value in this work is 6.8.

3. Results and discussion

Figure 2 shows the eight and six electrons and protons transferred pathways for CO_2 reduction to methane and methanol, which are investigated in this work. The pathways share the common first-three proton and electron transfer steps (seen in the top reaction scheme in Figure 2) of i) CO_2 protonation to be HOCO* ii) the protonation of HOCO* to be HCOOH or to form CO* + H_2O(aq) and iii) the protonation of CO* at C to form HCO* or at O to form COH. The second and third reaction scheme in Figure 2 shows the further proton and electron transfer steps when HCO* is favorable and when COH* is favorable, respectively. The protonation of HCO* (the second reaction scheme in Figure 2) at the C atom can form formaldehyde (OCH_2*) or at the O atom to form HCOH* leading to methane and methanol production. The protonation of COH* (the third reaction scheme in Figure 2) at the C atom can yield HCOH* or at the O atom can yield C*+H_2O leading to methane and methanol production as well. The theoretical work based on DFT calculations by Nørskov et al.[36, 41] suggested that the lowest free energy pathway from CO_2 to CH_4 on Cu(211) surface proceeds through the adsorbed formaldehyde intermediate and methane production is more energetically favorable than methanol production. However, this disagrees with the experimental results that formaldehyde reduction leads to methanol product rather than methane.[44] Recently, Nørskov et al. [39] has suggested that methanol is possibly formed by the reduction of methanediol rather than formaldehyde which could explain the contradiction. Their calculations showed that methandiol which is formed by hydration of formaldehyde is selectively reduced to methanol. Thus, methanol may be formed by reduction of methanediol rather than by reduction of adsorbed formaldehyde. This means the calculation results do not necessarily contradict the suggestion that CO/CO_2 reduction on Cu(211) surface goes through adsorbed formaldehyde intermediate to yield methane. In this work, we also include the investigation of methanediol reduction to methanol/methane and hydrogen evolution reaction (HER), which is a competitive side reaction.

The common first-three proton and electron transfer steps

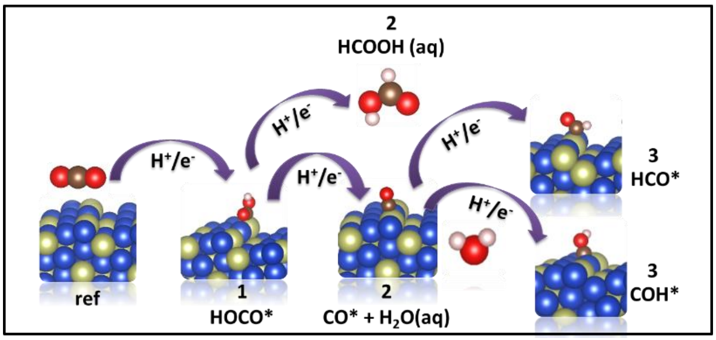

Pathways via HCO* intermediate

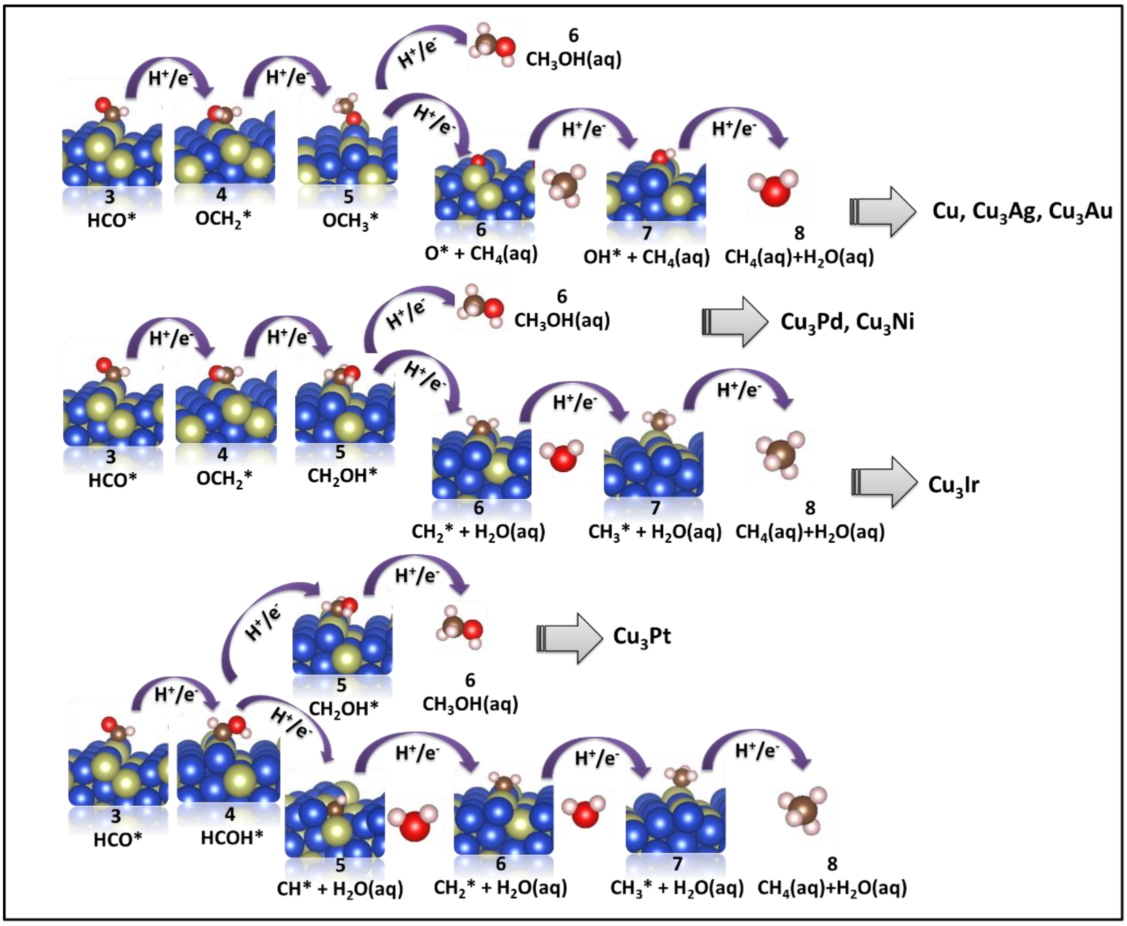

Pathways via COH* intermediate

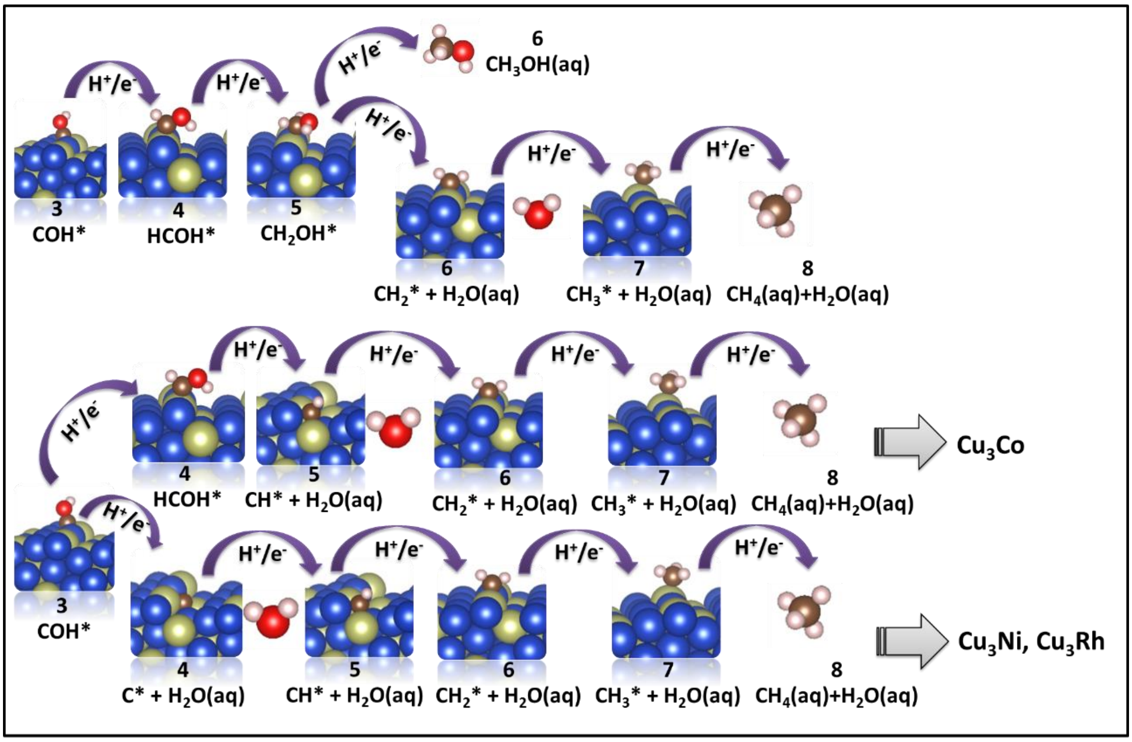

Methanediol Reduction Reaction

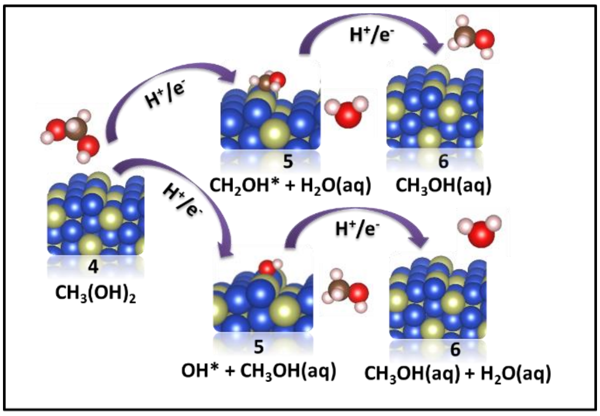

Hydrogen Evolution Reaction (HER)

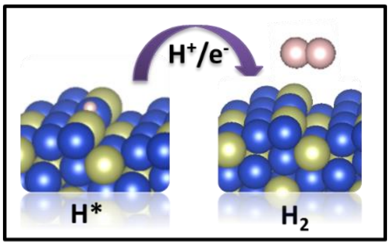

Figure 2. Six and eight protons/electrons transfer step pathways of CO_2 reduction to methanol and methane. The most thermodynamically favorable pathway on each surface is labeled on the right hand side. The top reaction scheme shows the common first-three electrons/protons transfer

step. The second and third reaction scheme shows the further protons and electrons transfer step when the favorable HCO* and COH* intermediate is formed, respectively. The steps for methanediol reduction to methanol/methane and hydrogen evolution reaction (HER) are shown in the last two reaction schemes. Cu atom-blue, X atom-green, C atom-brown, O atom-red, and H atom-white.

3.1 Surface Interaction with Intermediate Species

The affinity relation between intermediates and surfaces are of importance to the free energy change of the elementary steps. We begin with the analysis of the interaction between the key intermediates and the alloy surfaces (Figure 3). The most favorable adsorption configurations and adsorption energies of all intermediate species on Cu_3X surfaces are shown in Tables 1-3. It was previously reported that the pure Au and Ag surfaces show weaker CO* interaction compared to that on the pure Cu surface, but the other pure metal surfaces (i.e. Pd, Pt, Ni, Rh and Ir) show stronger CO* interaction.[47] Alloying the transition metals with copper reveals a similar general trend of CO* interaction with the pure metal surfaces. Figure 3a (top) shows that the CO* binding on Cu_3Ag and Cu_3Au surfaces are weaker than that on pure Cu surface and the CO* binding on the other alloy surfaces are stronger. The CO* intermediate binds strongest on Cu_3Ir and Cu_3Rh surfaces. The CO* adsorption energies on Cu_3Pt, Cu_3Ni and Cu_3Co are comparable. The O* binding energy trend on Cu_3X surfaces (Figure 3a) is similar to that of pure metals. Alloying Cu with metals which have weaker O* adsorption than Cu; namely Ag, Au, Pd and Pt, remain to have relatively weak O* adsorption and vice versa for the metals with strong O* adsorption; namely Ni, Co, Rh and Ir. In addition, we found that the high affinity of CO* with Cu, Pd, Co, and Rh may influence the segregation resulting in relatively high composition of those metals on the surface and near surface atomic layers. The calculations show that the binding energy can be affected by the composition change. The CO* binding energies on the segregated structures are weaker than those on the non-segregated structures by 0.02, 0.06 and 0.16 eV on Cu_3Pd, Cu_3Co and Cu_3Rh, respectively. Figure 4 shows CO* adsorption structures on Cu_3Pd, Cu_3Co and Cu_3Rh. The CO* binding energy on segregated Cu_3Ag structure is stronger than that on the non-segregated structure by 0.02 eV. The sensitivity of CO* binding energy to the change of surface composition due to segregation tends to increase on the surface with relatively strong CO* interaction.

Table 1. Adsorption energy of intermediate species, *B.E*[a], on Cu(211), $Cu_3Ag(211)$, and $Cu_3Au(211)$ in eV. Blue atom is Cu, gray atom is Ag, orange atom is Au, red atom is O, brown atom is C and white atom is H.

species	Cu(211)		$Cu_3Ag(211)$		$Cu_3Au(211)$	
	configuration	*B.E*[a]	configuration	*B.E*[a]	configuration	*B.E*[a]
O	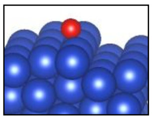	0.77	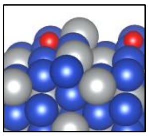	0.88	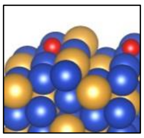	1.13
H	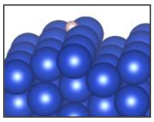	-0.28	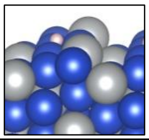	-0.19	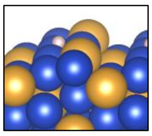	-0.17
C	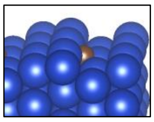	2.05	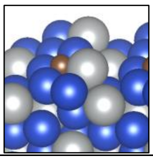	2.85	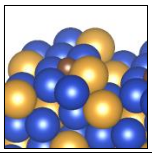	2.91
OH	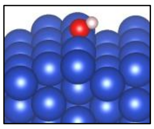	-0.28	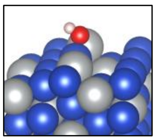	0.05	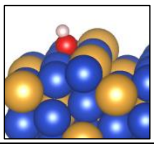	0.24
CO	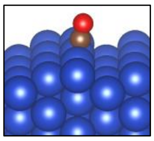	0.93	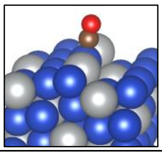	1.05	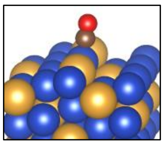	1.12
CH	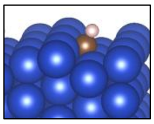	1.01	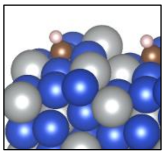	1.35	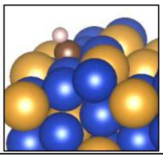	1.55
CH_2	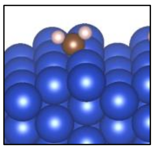	0.53	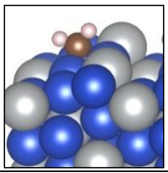	0.77	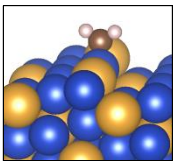	0.79
COH	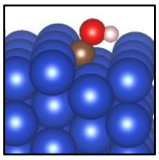	1.91	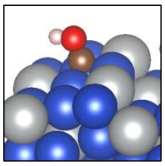	2.00	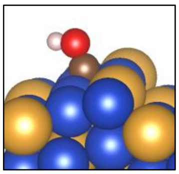	2.12

species	Cu(211)		Cu_3Ag(211)		Cu_3Au(211)	
	configuration	$B.E^a$	configuration	$B.E^a$	configuration	$B.E^a$
HCO	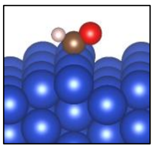	1.43	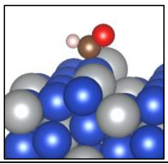	1.51	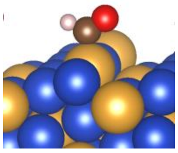	1.45
HCOH	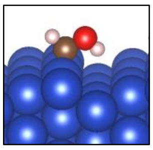	1.18	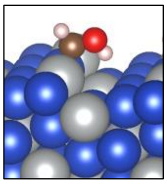	1.45	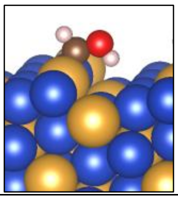	1.37
HOCO	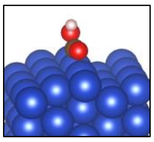	1.04	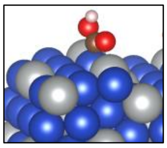	1.26	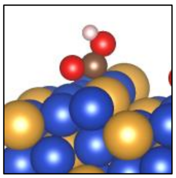	1.51
CH_3	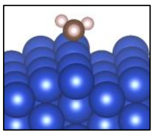	-0.61	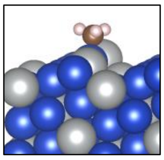	-0.39	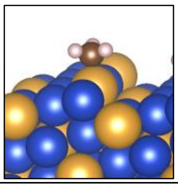	-0.40
OCH_2	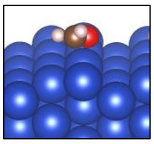	0.83	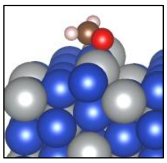	1.06	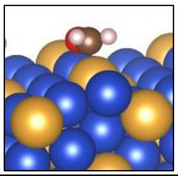	1.01
OCH_3	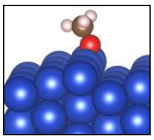	-0.27	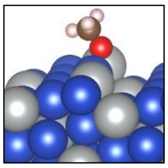	0.07	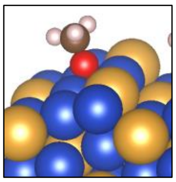	0.16
CH_2OH	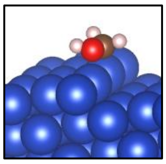	0.54	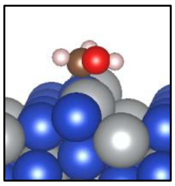	0.68	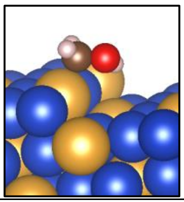	0.65

$^aB.E = E_{total(C_xH_yO_z)} - E_{slab} - xE(C) - yE(H) - zE(O)$

Where $E_{total(C_xH_yO_z)}$ is the total energy of the state, E_{slab} is the energy of the clean slab, $E(C)$is energy of C atom referenced to graphene, $E(H)$ is the energy of H atom referenced to 1/2H_2 and $E(O)$ is the energy of O atom referenced to (H_2O – H_2)

Table 2. Adsorption energy of intermediate species, $B.E^{a}$, on $Cu_3Pd(211)$, $Cu_3Pt(211)$, and $Cu_3Co(211)$ surfaces in eV. Blue atom is Cu, gray atom is Pd or Pt, dark blue atom is Co, red atom is O, brown atom is C and white atom is H.

species	$Cu_3Pd(211)$		$Cu_3Pt(211)$		$Cu_3Co(211)$	
	configuration	$B.E^{a}$	configuration	$B.E^{a}$	configuration	$B.E^{a}$
O	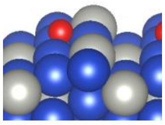	1.22	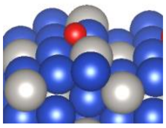	1.26	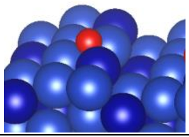	0.08
H	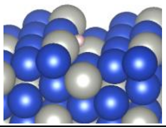	-0.31	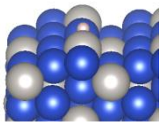	-0.40	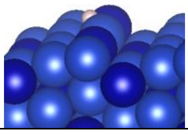	-0.46
C	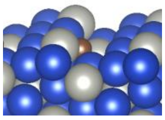	1.93	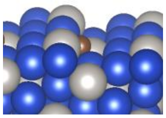	1.34	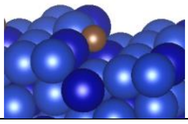	1.67
OH	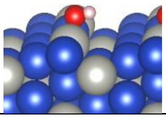	0.18	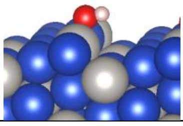	0.19	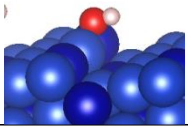	-0.63
CO	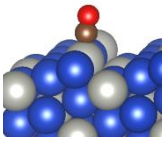	0.66	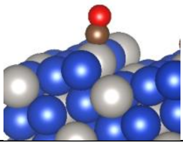	0.14	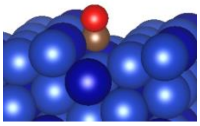	0.13
CH	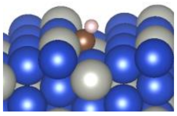	1.09	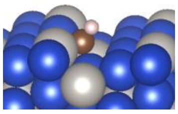	0.53	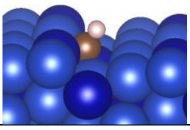	-0.15
CH_2	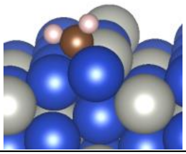	0.60	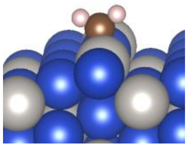	0.11	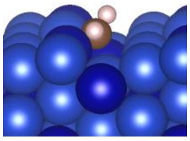	-0.18
COH	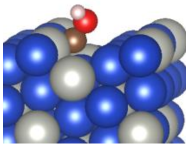	1.68	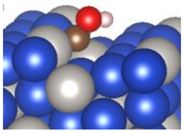	0.94	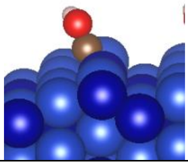	0.29
HCO	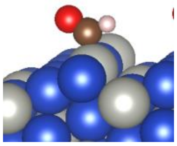	1.12	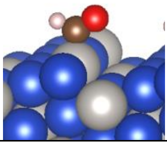	0.62	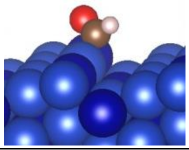	0.68

species	$Cu_3Pd(211)$		$Cu_3Pt(211)$		$Cu_3Co(211)$	
	configuration	*B.E*[a]	configuration	*B.E*[a]	configuration	*B.E*[a]
HCOH	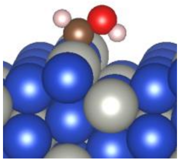	1.02	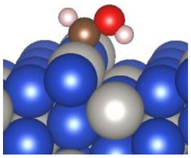	0.55	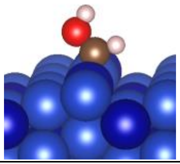	0.61
HOCO	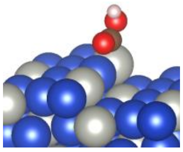	1.23	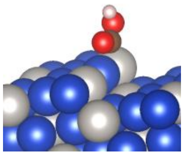	0.71	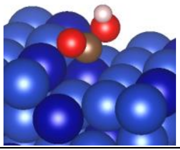	0.60
CH_3	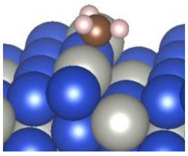	-0.51	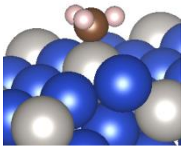	-0.84	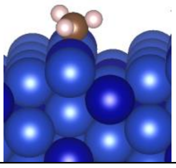	-0.83
OCH_2	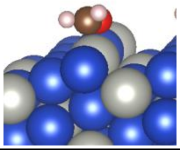	0.71	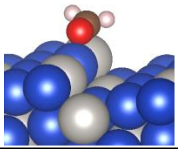	0.59	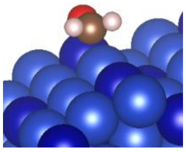	0.03
OCH_3	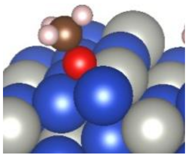	0.34	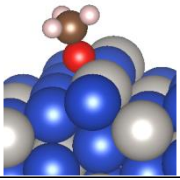	0.42	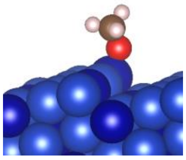	-0.42
CH_2OH	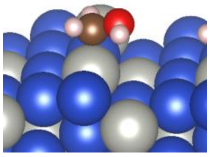	0.54	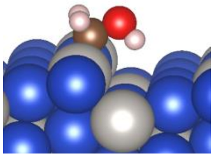	0.04	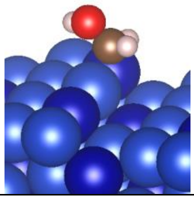	0.22

[a] $B.E = E_{total(C_xH_yO_z)} - E_{slab} - xE(C) - yE(H) - zE(O)$

Where $E_{total(C_xH_yO_z)}$ is the total energy of the state, E_{slab} is the energy of the clean slab, $E(C)$ is energy of C atom referenced to graphene, $E(H)$ is the energy of H atom referenced to $1/2H_2$ and $E(O)$ is the energy of O atom referenced to ($H_2O - H_2$)

Table 3. Adsorption energy of intermediate species, $B.E^a$, on $Cu_3Ni(211)$, $Cu_3Rh(211)$, and $Cu_3Ir(211)$ surfaces in eV. Blue atom is Cu, gray atom is Ni or Rh, green atom is Ir, red atom is O, brown atom is C and white atom is H.

species	$Cu_3Ni(211)$		$Cu_3Rh(211)$		$Cu_3Ir(211)$	
	configuration	$B.E^a$	configuration	$B.E^a$	configuration	$B.E^a$
O	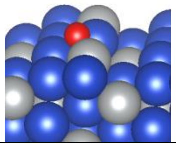	0.52	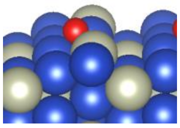	0.71	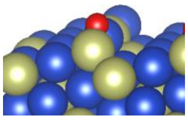	-0.16
H	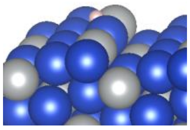	-0.47	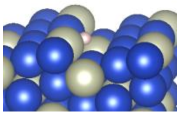	-0.61	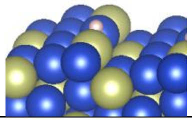	-0.66
C	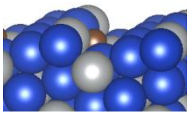	0.75	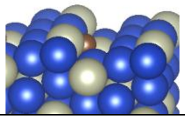	0.33	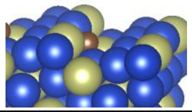	-0.12
OH	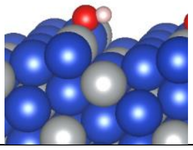	-0.41	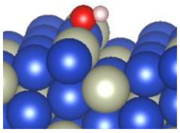	-0.12	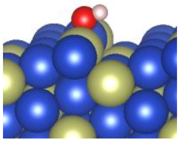	-0.29
CO	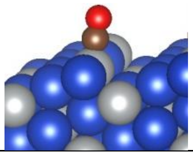	0.10	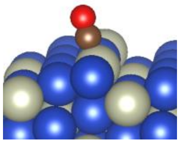	-0.13	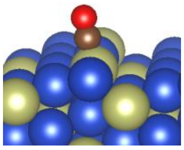	-0.62
CH	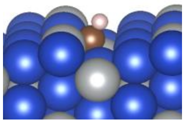	0.11	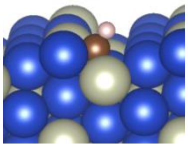	-0.10	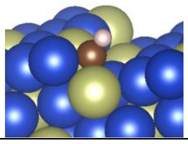	-0.60
CH_2	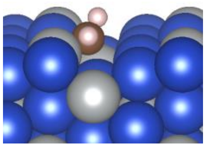	0.09	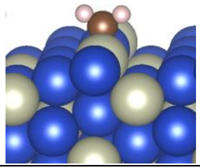	-0.13	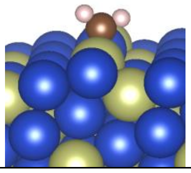	-1.59
COH	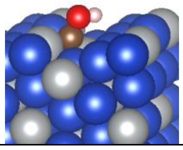	0.77	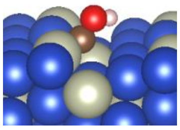	0.19	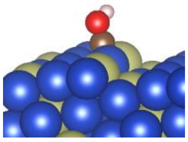	-0.39

species	$Cu_3Ni(211)$		$Cu_3Rh(211)$		$Cu_3Ir(211)$	
	configuration	*B.E*[a]	configuration	*B.E*[a]	configuration	*B.E*[a]
HCO	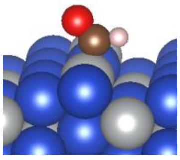	0.79	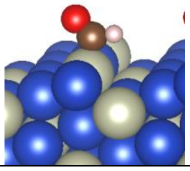	0.48	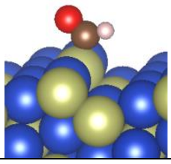	-0.57
HCOH	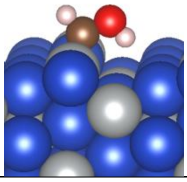	0.51	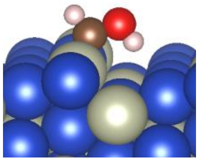	0.26	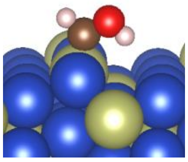	-0.36
HOCO	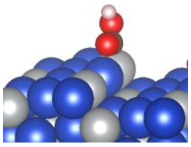	0.76	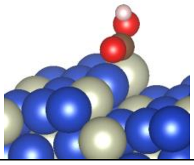	0.67	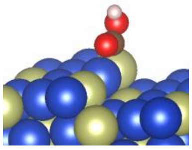	0.30
CH_3	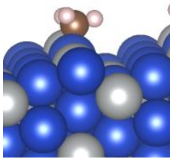	-0.90	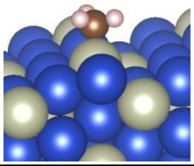	-0.86	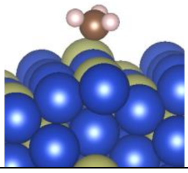	-2.11
OCH_2	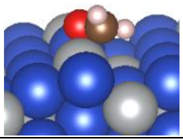	0.25	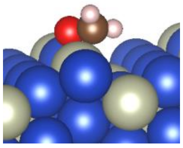	0.29	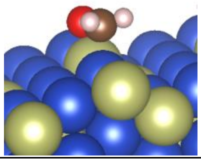	-0.64
OCH_3	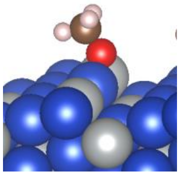	-0.37	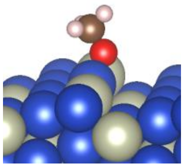	-0.06	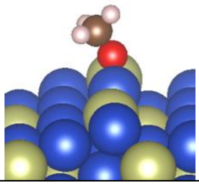	-0.70
CH_2OH	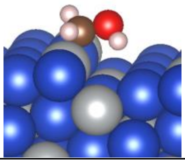	0.14	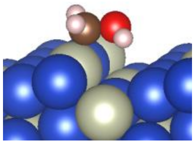	0.09	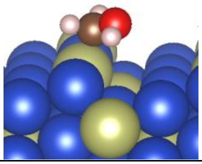	-0.50

$^{a}B.E = E_{total(C_xH_yO_z)} - E_{slab} - xE(C) - yE(H) - zE(O)$

Where $E_{total(C_xH_yO_z)}$is the total energy of the state, E_{slab} is the energy of the clean slab, $E(C)$is energy of C atom referenced to graphene, $E(H)$ is the energy of H atom referenced to $1/2H_2$ and $E(O)$is the energy of O atom referenced to (H_2O – H_2)

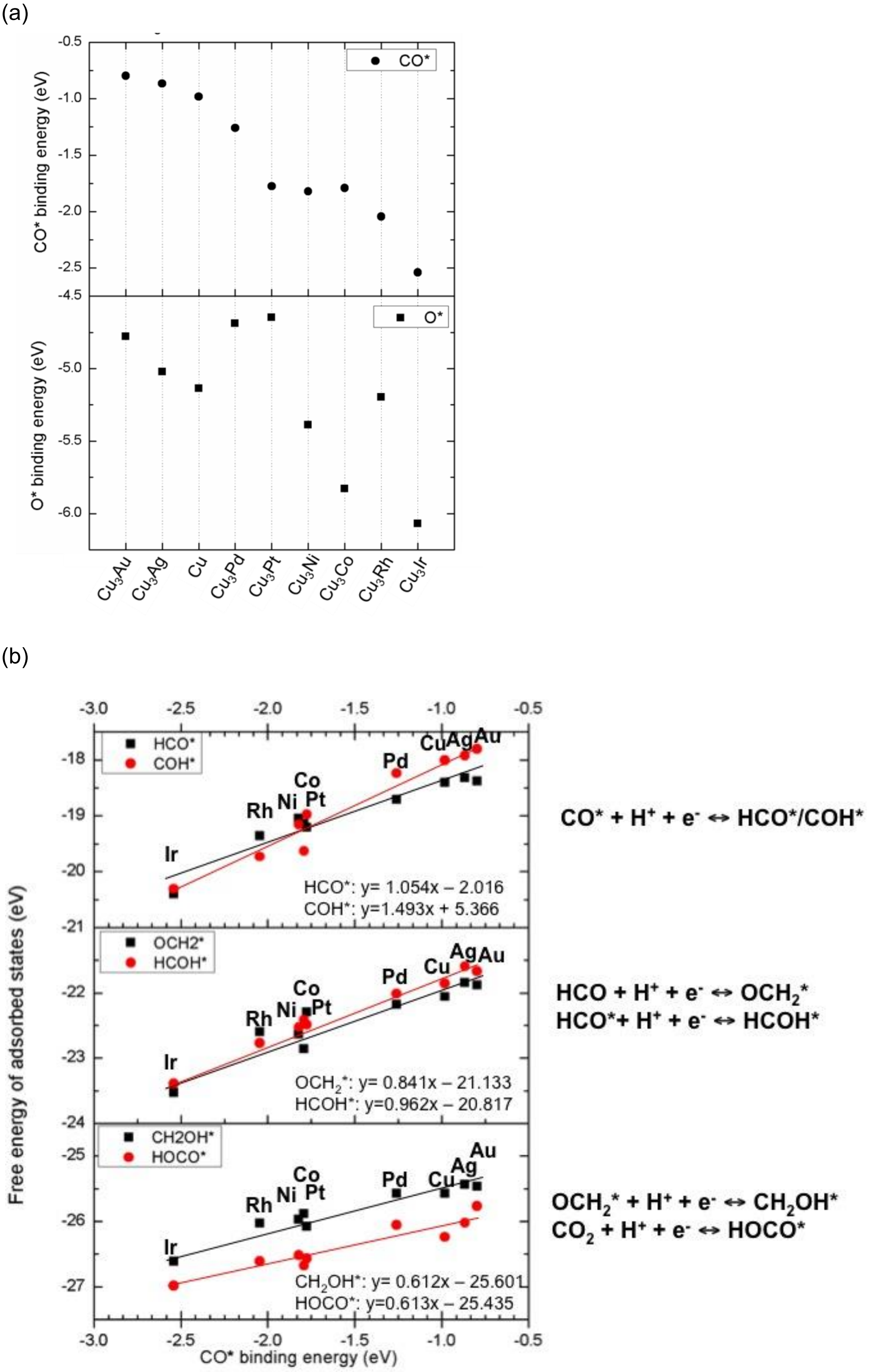

Figure 3. (a) CO* and O* binding energy (b) Linear scaling correlations of the free energy of the adsorbed HCO*, COH*, OCH_2*, HCOH*, CH_2OH* and HOCO* on Cu_3X surfaces as a function of

CO* binding energy. The X element is labeled at the data point. The binding energy is calculated by $E_{\text{total}} - E_{\text{clean slab}} - E_{\text{isolated adsorbate(gas)}}$. The free energy of the adsorbed states is calculated by $E_{\text{total}} - E_{\text{clean slab}}$ + (ZPE, entropy and enthalpy corrections). The binding is stronger with the more negative binding energy.

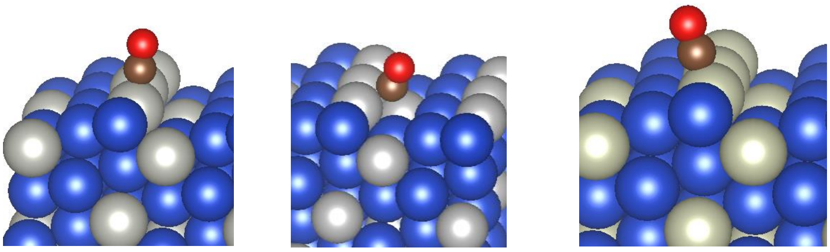
(a) (b) (c)

Figure 4. Structures of CO* adsorption on segregated structures of (a) $Cu_3Pd(211)$, (b) $Cu_3Co(211)$ and (c) $Cu_3Rh(211)$ surfaces.

The good linear scaling correlations between the CO* binding energy and the surface interaction with the other key intermediates i.e. HCO*, COH*, OCH_2*, HCOH*, CH_2OH and HOCO* on Cu_3X surfaces can be obtained as shown in Figure 3b. The coefficients determination (R^2) are in the range of 0.90-0.98 which represents a very strong relation between CO* binding energy and the surface interaction with those key intermediates. Similarly, the good correlation between adsorption energies of CO* and HCO* on pure transition metal (TM) surfaces was previously found as well.[47] Interestingly, the CO* interacts with the surfaces through the C atom, thus the CO* binding energies also show good linear scaling correlations with C* binding energies but very poor correlation with O* binding energies (Figure 5). Although, the intermediate HCO* and COH* binds to the alloy surfaces through the C atom, HCO*/COH* binding energies do not correlate with C* binding energies. Yet, they show very good correlation with CO* binding energies.

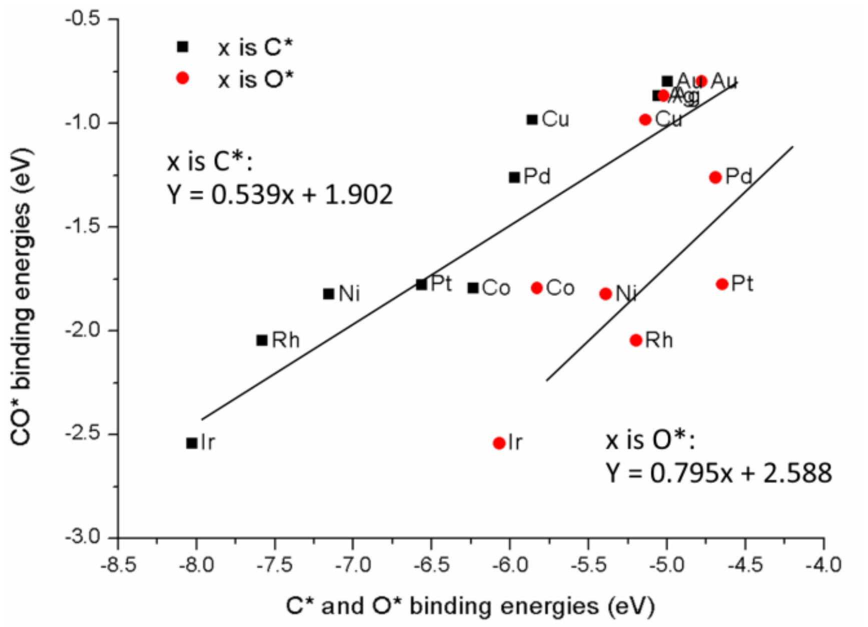

Figure 5. Linear scaling correlations between CO* binding energies and C* or O* binding energies on $Cu_3X(211)$ surfaces. The X element is labeled at the data point. The binding energies are calculated by $E_{total} - E_{clean\ slab} - E_{adsorbate\ (gas)}$.

The protonation of CO* forming HCO*/COH* is a crucial step. It was previously reported to be the limiting-potential step on pure Cu, Pd, Ni, Rh, Pt and Cu_3Ag surfaces.[36, 47, 51] The favorability of CO* protonation products between HCO* and COH* can be affected by alloying. Alloying Rh and Co with Cu results in COH* being more stable. The stability of HCO* and COH* is comparable on Cu_3Ni surface. It is interesting that the relatively higher stability of COH* than HCO* may occur on catalysts with relatively strong CO* interaction energy (Figure 3b). Also, it was previously reported that the HCO* or COH* favorability may be affected by the solvation effect through water-assisted proton shuttling coupled with electron transfer.[37] We also found that the favorability of HCO* or COH* formation carries on, being the same on the segregated and non-segregated structures. The sensitivity of HCO* binding energy due to segregation is low (<0.05 eV) on the surfaces with weak CO* interaction and it is large (>0.1 eV) on the surfaces with strong CO* interaction such as Cu_3Pd and Cu_3Co surfaces. The sensitivity of COH* binding energy due to segregation is larger so that the binding energy change ranges between 0.1-0.4 eV. Furthermore, the protonation of CO_2 to produce HOCO* was previously reported to be the limiting-potential step on pure Au, Ag and Cu_3Au surfaces.[47, 51] All the alloy surfaces show stronger HOCO* interaction than the Cu_3Au surface (Figure 3b). Thus, the significantly weak HOCO* interaction resulting in the CO_2 protonation to yield HOCO*, which proves to be the limiting-potential step, should not be problematic on the other alloy surfaces.

The electronic structures facilitate the understanding of the nature of CO bonding with the alloys surfaces. The charge density difference of CO* adsorption (Figure 6) on the Cu surface shows significant electron transfer from Cu surface atoms to C atom. However, on the Cu_3Co surface, electrons are mostly transferred from the Co surface atoms to the C atom rather than from the Cu surface atoms. The CO* adsorption trend on metal surfaces qualitatively agrees with the surface *d*-band center energy level trend (Table 4). The trends can be ascribed to the interaction between the metal *d* states and the CO $2\pi^*$ and 5σ states.[61] The *d*-band center energy levels of Cu_3Au and Cu_3Ag shift to lower energy than that of the Cu surface whereas the *d*-band center energy levels of the other alloy surfaces shift to higher energy compared to the Cu surface. This corresponds to the weaker chemisorption of CO* on Cu_3Ag and Cu_3Au surfaces than that on the Cu surface whereas CO* adsorption is relatively stronger on the other alloy surfaces. Also, the *d* states of Cu tends to interact with CO* rather than the *d* states of Au and Ag which manifests in the favorable CO* adsorption site to be on top of Cu on Cu_3Ag and Cu_3Au surfaces (see structures in Table 1). Similarly, the *d* states of the other X elements; namely Pd, Pt, Co, Ni, Rh and Ir tend to interact with CO* rather than the *d* states of Cu which results in the favorable CO* adsorption on a top site of those X atoms or the foot of the step site where CO* interacts with two X atoms (see structures in Tables 2-3).

Table 4. Surface *d*-band center energy level referenced on Fermi energy level.

Cu_3X(211)	*d*-band center energy level (eV)
Cu_3Ag	-2.68
Cu_3Au	-2.54
Cu	-2.16
Cu_3Pd	-1.83
Cu_3Pt	-1.85
Cu_3Ni	-1.49
Cu_3Co	-1.76
Cu_3Rh	-1.52
Cu_3Ir	-1.68

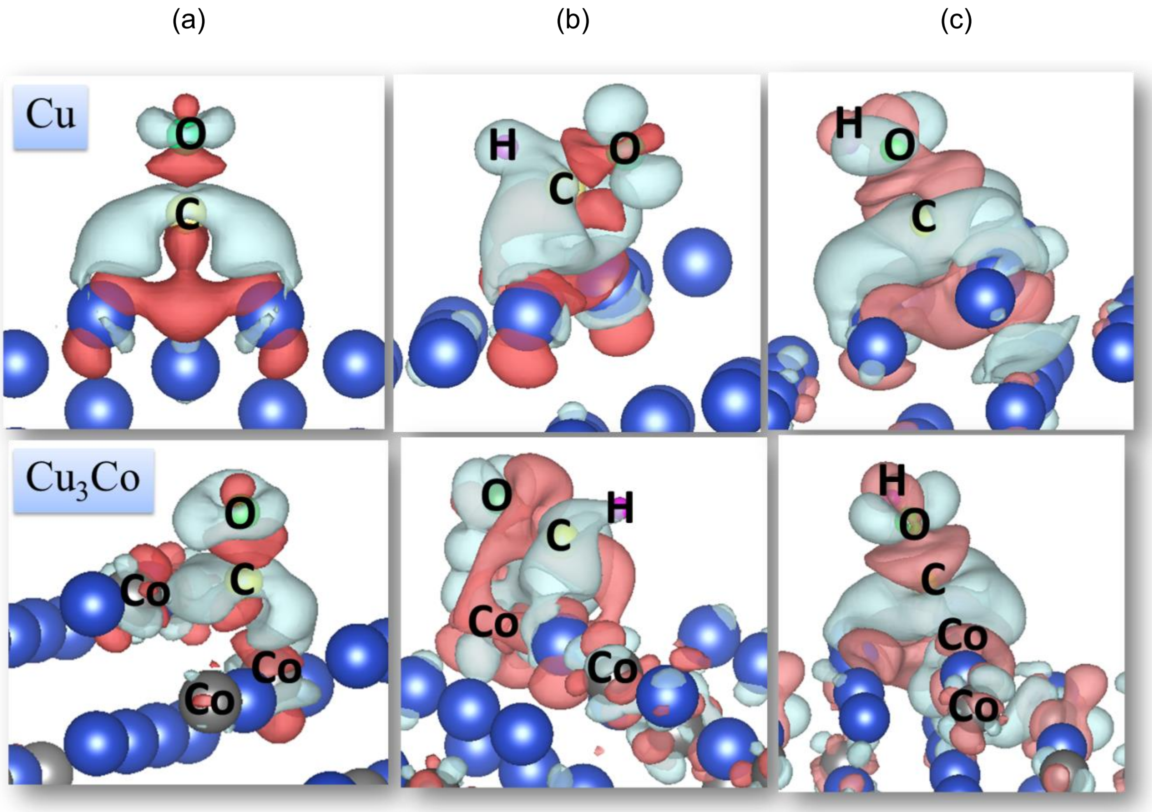

Figure 6 The isosurface of charge density differences of (a) CO* adsorption with the isosurface value of ±0.005 eV/Å^3 (b) HCO* adsorption with the isosurface value of ±0.002 eV/Å^3 and (c) COH* adsorption with the isosurface value of ±0.001 eV/Å^3. The top row is the adsorption on Cu(211) surface and the bottom row is the adsorption on Cu_3Co(211) surface. Red and blue colors represent charge depletion and accumulation, respectively. The blue atom is Cu and grey atom is Co.

The common features of charge density difference analysis seen in HCO* and COH* adsorption on both Cu and Cu_3Co surfaces (Figures 6b and 6c) are that electrons transfer from the Cu surface to the C atom. In Figure 6b, electron accumulation (blue) at the C-H bond and the electron depletion (red) at the C-O bond can be observed upon HCO* adsorption, whereas in Figure 6c, electron depletion (red) occurs at C-O and O-H bond upon COH* adsorption. Thus, electron depletion at both O-H and C-O bonds in COH* adsorption may induce the preference to COH* formation on a surface with a relatively high *d*-band center energy level and strong CO* adsorption; namely Cu_3Ni, Cu_3Co, Cu_3Rh and Cu_3Ir. Yet, electron accumulation at the C-H bond in HCO* adsorption may bring the favorability of HCO* formation on a surface with a relatively low *d*-band center energy level; namely Cu_3Au, Cu_3Ag, Cu, Cu_3Pd and Cu_3Pt. In addition, the poor correlation between HCO*/COH* adsorption energy with the C* adsorption energy may result from the difference of charge transfer characteristic at the C-H (HCO* adsorption) bond and at the O-H (COH* adsorption) bond. The charge transfer characteristic of the C-O bond in HCO* and CO* adsorption is similar, thus CO* adsorption energy is a good descriptor for correlations with HC* and COH* adsorption energy as well as with OCH_2*, HCOH*, CH_2OH and HOCO* adsorption energy.

3.2 Pathway Investigation

The investigated CO_2 reduction pathway to produce methane and methanol is shown in Figure 2. The pathways through COH* are considered on Cu_3Co, Cu_3Ni and Cu_3Rh surfaces because COH* formation is more favorable than HCO* formation on those surfaces. The pathways through HCO* are considered on Cu, Cu_3Ag, Cu_3Au, Cu_3Pd, and Cu_3Pt surfaces. The stability of adsorbed HCO* and COH* is comparable on Cu_3Ni and Cu_3Ir in which the free energies of HCO* and COH* states are very close with ~0.1 eV difference. Thus, the pathways through both HCO* and COH* intermediates are considered on Cu_3Ni and Cu_3Ir surfaces. From a thermodynamic point of view, the limiting-potential indicates the highest electrode potential at which the free energy of every elementary step is downhill and the reaction begins to have an evident rate. By constructing the free energy diagrams as a function of potential, the energetically favorable pathway and the limiting-potential step on surfaces can be indicated. The free energy diagrams at 0 V_{RHE} are shown in Figures 7-8. The most favorable pathway, the limiting-potential elementary step, the limiting-potential voltage, and the onset potential of HER and the H_2O formation step are summarized in Table 5.

The calculated free energy diagrams indicate that the Cu-based alloy catalysts mostly are more energetically favorable to yield methane than methanol product. Methanol production is found to be favorable on Cu_3Pd, and Cu_3Pt surfaces. On Cu_3Ni surface, the reduction to methanol shows a slightly higher limiting-potential of 0.1 V than the reduction to methane. The CO* protonation producing HCO* or COH* is the limiting-potential step on most surfaces with the exception of Cu_3Au, and Cu_3Co surfaces. The protonation of CO_2 yielding HOCO* is the limiting-potential step on Cu_3Au surface. The water formation step and the protonation of COH* to form HCOH* are the limiting-potential steps on Cu_3Co surface. Figure 9 displays the onset potentials of the CO_2 protonation, CO* protonation, and the formic acid formation step. It can be seen that the overpotentials on Cu_3Co, Cu_3Rh and Cu_3Ir surfaces are lower than that on pure Cu. The overpotentials on Cu_3Ag, Cu_3Pd and Cu_3Pt surfaces are similar to that on pure Cu and they show the same limiting-potential step.

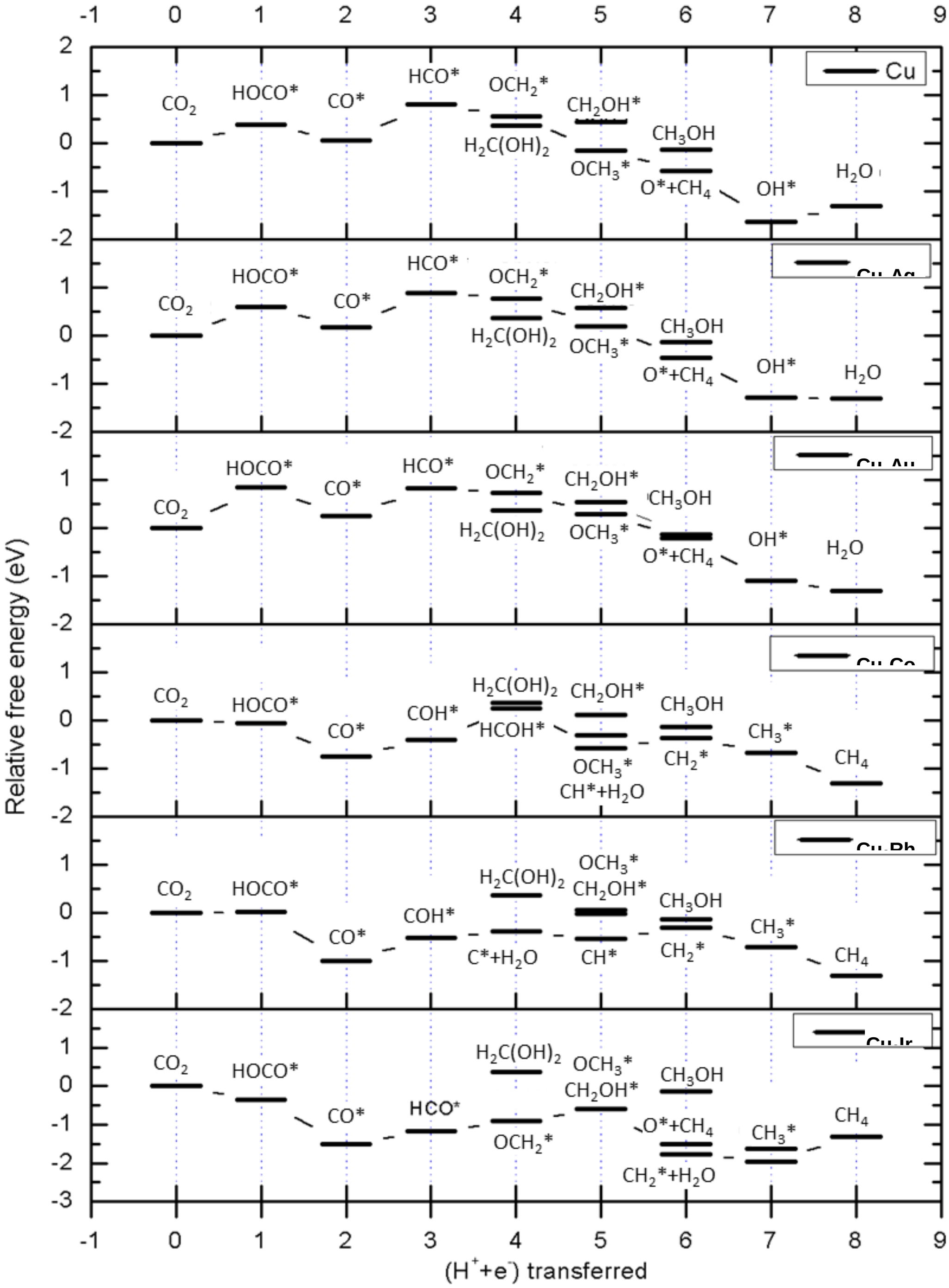

Figure 7. Free energy diagrams of the most favorable CH$_4$ pathway and the reduction of methanediol at 0 V$_{RHE}$ on Cu, Cu$_3$Ag, Cu$_3$Au, Cu$_3$Co, Cu$_3$Rh, and Cu$_3$Ir (211) surfaces.

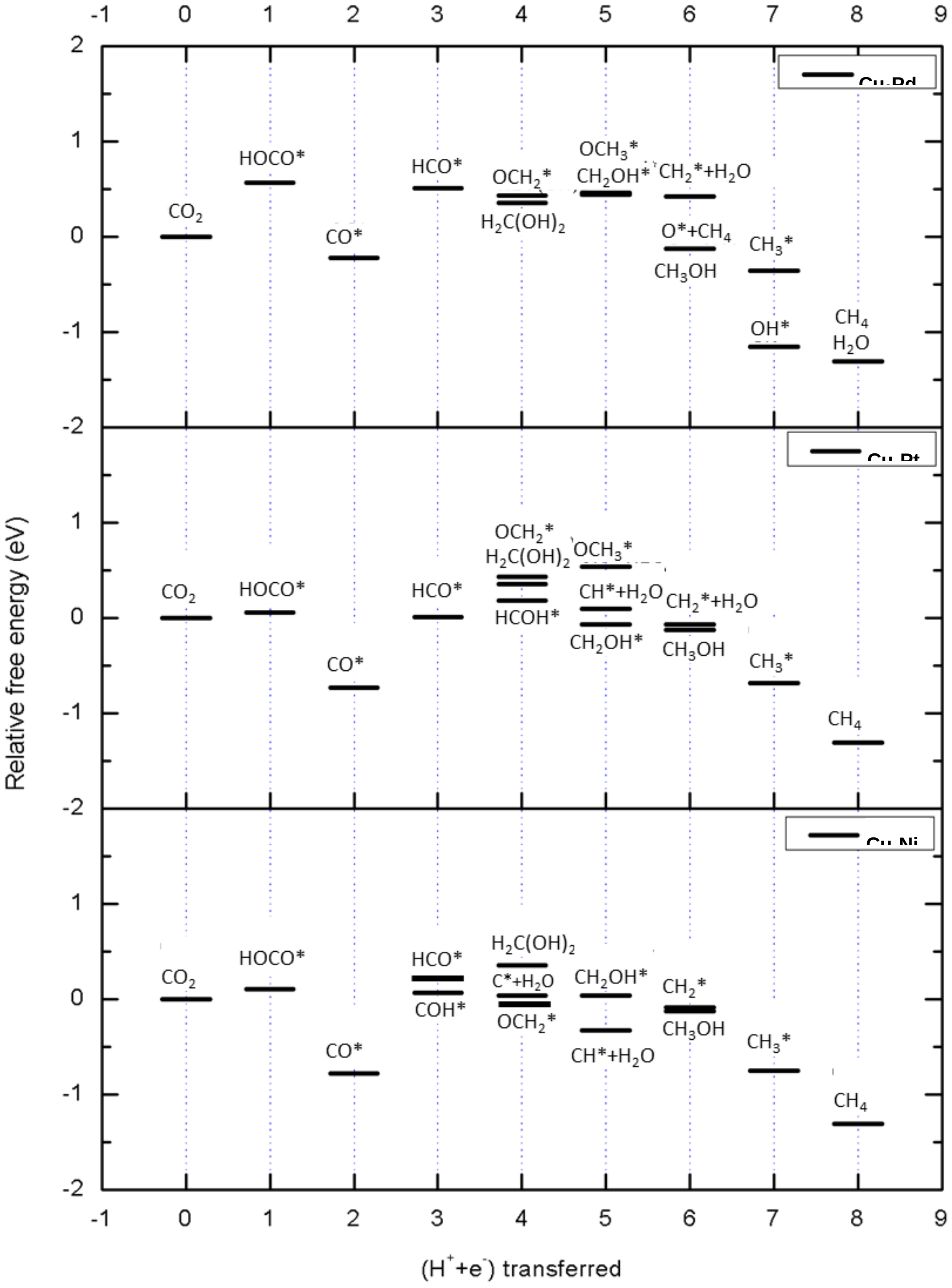

Figure 8. Free energy diagrams of the most favorable CH_3OH, CH_4 pathway and the reduction of methanediol at 0.0 V_{RHE} on Cu_3Pd, Cu_3Pt, and Cu_3Ni (211) surfaces.

Table 5. Summary of the most favorable pathway, the calculated limiting-potential voltage, the limiting-potential elementary step, and the calculated onset potential of H_2O formation and HER on $Cu_3X(211)$ surfaces.

	Most favorable pathway	The limiting-potential elementary step	Onset potential of the limiting-potential step (V_{RHE})	Onset potential of $OH^* + H^+ + e^- \rightarrow H_2O$ (V_{RHE})	Onset potential of HER (V_{RHE})
Cu	CH_4	$CO^* + H^+ + e^- \rightarrow HCO^*$	-0.75	-0.31	-0.10
Cu_3Au	CH_4	$CO_2 + H^+ + e^- \rightarrow HOCO^*$	-0.86	0.21	0.02
Cu_3Ag	CH_4	$CO^* + H^+ + e^- \rightarrow HCO^*$	-0.72	0.02	-0.01
Cu_3Pd	CH_3OH	$CO^* + H^+ + e^- \rightarrow HCO^*$	-0.72	0.16	-0.12
Cu_3Pt	CH_3OH	$CO^* + H^+ + e^- \rightarrow HCO^*$	-0.74	0.17	-0.21
Cu_3Ni	CH_4	$CO^* + H^+ + e^- \rightarrow COH^*$	-0.85	-0.44	-0.28
	CH_3OH	$CO^* + H^+ + e^- \rightarrow HCO^*$	-0.95		
Cu_3Co	CH_4	$COH^* + H^+ + e^- \rightarrow HCOH^*$	-0.67	-0.66	-0.27
		$OH^* + H^+ + e^- \rightarrow H_2O$	-0.66		
Cu_3Rh	CH_4	$CO^* + H^+ + e^- \rightarrow COH^*$	-0.49	-0.15	-0.42
Cu_3Ir	CH_4	$CO^* + H^+ + e^- \rightarrow HCO^*$	-0.32	-0.31	-0.47
		$OCH_2^* + H^+ + e^- \rightarrow OCH_3^*$	-0.33		

The Cu_3Au, and Cu_3Ni surfaces show the highest limiting-potential of -0.86 V_{RHE} (Table 5, Figure 9). The relatively very weak HOCO* adsorption on Cu_3Au (Figure 3b) contributes to the high limiting-potential of HOCO* formation. The HOCO* binding energies on the other surfaces are relatively stronger, thus the HOCO* formation is not a challenging step on the other surfaces. Furthermore, the two protons and electrons transfer steps of CO_2 reduction to formic acid take place at low potential close to the equilibrium potential of formic acid formation (-0.20 V_{RHE}, equation 1) on Cu_3Pt, Cu_3Ni, Cu_3Co, and Cu_3Rh surfaces (Figure 9). This suggests that these surfaces are thermodynamically favorable for HCOOH production. The experiments showed that the addition of 10% Ni into Cu shifts the onset potential of HCOOH production in a positive potential direction compared to Cu (~0.2 V).[48] The calculation results show the shift of HCOOH onset potential ~0.3 V on Cu_3Ni compared to Cu. Additionally, Cu-Ni experimentally showed the strong suppression of CO formation and is not a significant effect on faradaic efficiency or the overpotential for production.[48] This may result from the increase efficiency of HCOOH production, and consequently the suppression of CO formation.

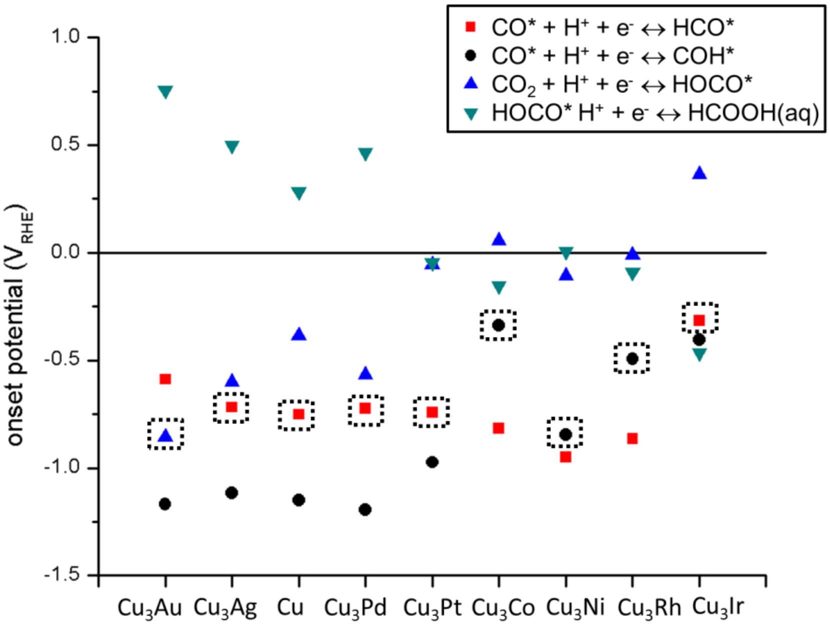

Figure 9. The onset potentials of the CO_2, $HOCO^*$, and CO^* protonation step. The dot squares indicate the calculated limiting-potential step on $Cu_3X(211)$ surfaces.

The very strong CO^* adsorption on Cu_3Ni induces the protonation of CO^* to be potentially limited at -0.85 V_{RHE} resulting in a relatively high overpotential for methane production. The Cu_3Co, Cu_3Rh and Cu_3Ir surfaces also show very strong CO^* and HCO^*/COH^* interaction (Figure 3b), however, the onset potentials of CO^* protonation step on these surfaces are less negative (-0.3 to -0.5 V_{RHE}) than that on Cu_3Ni surface. The strong adsorption of CO^* and HCO^*/COH^* is not essentially an indicator as to whether the onset potential of CO^* protonation is likely to be at high negative potential, yet the relative interaction between CO^* and HCO^* or COH^* on a surface is an important one. The difference in free energies of the adsorbed states of HCO^* or COH^* referenced on free energies of the adsorbed CO^* state on Cu_3Co, Cu_3Rh and Cu_3Ir are 2.9-3.1 eV whereas that on Cu_3Ni is 2.55 eV and they are ~2.7 eV on Cu_3Ag, Cu, Cu_3Pt and Cu_3Pd which show a similar onset potential of the CO^* protonation step. The larger of the free energy differences, the CO^* protonation step tends to take place at the less negative onset potential. The lowest calculated onset potential of CO^* protonation (-0.32 V_{RHE}) occur on Cu_3Ir surface in which the free energy difference is largest. The higher degree of CO^* and HCO^*/COH^* adsorption energy decoupling pronounces, the onset potential of CO^* protonation becomes less negative which increases the thermodynamic favorability of the CO^* protonation step. The theoretical overpotential on pure metal surfaces were shown to have a volcano-type relationship with copper situated near the top.[47] However, the volcano-type relationship is not seen on copper-based alloy surfaces.

3.3 Methanol Production

The investigated reaction pathways for methanol production as shown in Figure 2 may proceed through OCH_2^*, $HCOH^*$ intermediates and methanediol reduction. The equilibrium potential of $CO_2 + 6H^+ + 6e^- \rightarrow CH_3OH$ (aq) is 0.03 V_{RHE}. The free energy diagrams reveal that methanol production is more thermodynamically favorable than methane production on Cu_3Pd and Cu_3Pt surfaces, yet with high overpotential (~0.7 V) for methanol production. The favorable pathway on Cu_3Pd is through OCH_2^* intermediate and through $HCOH^*$ intermediate on Cu_3Pt. Then, the protonation of OCH_2^* and $HCOH^*$ yields a common intermediate of CH_2OH^*. This may suggest that the key of methanol selectivity is CH_2OH^* formation favorability associated with the preference of CH_2OH^* protonation at the C atom over the O atom. On Cu_3Ni surface, the most thermodynamically favorable production pathway for methane production proceeds through HCO^* and OCH_2^* and is only 0.1 V (Table 5) more energetically favorable than the methanol production pathway which goes through COH^* intermediate. This comes from the onset potential of HCO^* and COH^* formation is only 0.1 V difference on Cu_3Ni surface. The surface affinity with key species HCO^*/COH^* also plays a role on methanol and methane selectivity. In addition, the Cu-Ni alloy with 10% of Ni added was experimentally reported to have CH_3OH production in the potential region from -0.1 to -1.1 V_{RHE} with the maximum production at -0.5 V_{RHE} whereas it is absent on Cu and Ni catalysts.[48] The calculations in this work suggested that the onset potential of CH_3OH on Cu_3Ni is relatively high at -0.95 V_{RHE} and the OH^* removal step initially occurs at -0.44 V_{RHE} which may allow the high production at this potential.

The reduction of methanediol is also considered (Figure 2). Methanediol is formed via hydration of formaldehyde (OCH_2). At 0.0 V_{RHE}, the reduction of methanediol through CH_2OH^* intermediate (the first pathway) is energetically favorable on Cu_3Co, Cu_3Rh, Cu_3Pt, and Cu_3Ni surfaces. Yet, the formation of CH_2OH^* is the potential-limiting step on Cu, Cu_3Ag, Cu_3Au, Cu_3Pd surfaces with the limiting potential of -0.30, -0.21, -0.19 and -0.08 V_{RHE}, respectively. The protonation of CH_2OH^* to form CH_3OH is the potential-limiting step on Cu_3Ir surface with the limiting potential of -0.47 V_{RHE}. Additionally, an alternative pathway may occur with the protonation at carbon atoms of methanediol coupling with C-O breaking; $CH_2(OH)_2 + H^+ + e^- \rightarrow CH_3OH + OH^*$. The OH^* removal step is an important one for this pathway. This alternative pathway is the lowest free energy pathway to produce CH_3OH at 0.0 V_{RHE} on most surfaces except Cu_3Pt and Cu_3Ir surfaces.

However, the OH* removal step is a challenging step on Cu, Cu_3Ni, Cu_3Co, and Cu_3Rh surfaces where the onset OH* removal step takes place at negative potentials (Table 5).

3.4 H_2 Evolution and OH Removal

The OH* protonation to form water is a significant elementary step to inhibit the catalytic activity decrease via surface OH* poisoning. The OH* removal step to form H_2O is the potential-limiting step on Cu_3Co due to the excessively strong OH* binding energy (Figure 10). The OH* and H* binding energies are shown in Figure 10. Although the OH* removal step is not the potential-limiting step on the other surfaces with relatively high affinities for OH*(Figure 10); namely Cu, Cu_3Ni, Cu_3Rh and Cu_3Ir, the surfaces may be poisoned by OH* species due to the relatively high negative onset potential of the step (-0.2 to -0.7 V_{RHE}, Table 5). Thus, surface OH* poisoning may occur on the surface of Cu alloying with high OH affinity metals; namely Co, Ni, Rh and Ir. Likewise, alloying Cu with less affinity toward OH; namely Au, Ag, Pd and Pt metals improve the OH* removal step and prove to be more efficient than pure Cu.

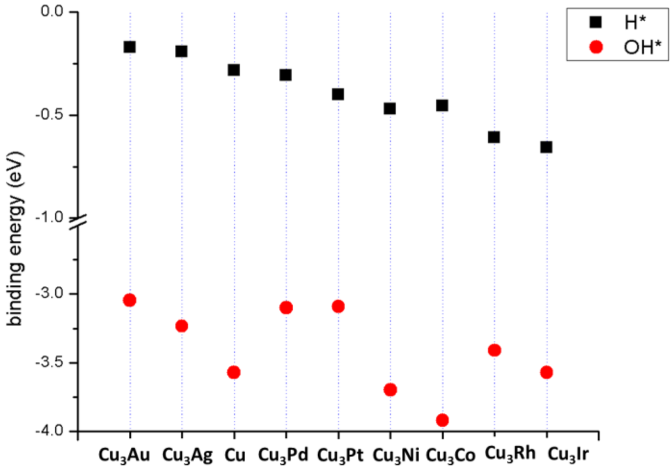

Figure 10. OH* and H* binding energies on $Cu_3X(211)$ surfaces. The binding energy is calculated by $E_{total} - E_{clean\ slab} - E_{isolated\ adsorbate(gas)}$.

Furthermore, the efficient CO_2 conversion catalyst would be expected to not overly catalyze HER and therefore dominate over CO_2 reduction, consequently the surface may mostly be covered by adsorbed H*. Also, the high activity of HER may lead to surface CO* poisoning which the adsorbed CO* is not further reduced. The pure Pd, and Pt surfaces were experimentally shown to mainly produce CO and HCOOH and prevent further CO_2 reduction with significant H_2 evolved as a side reaction.[46] The pure Co, Rh and Ir electrodes were experimentally shown to mainly produce H_2.[45] The HER on all alloy surfaces occurs at more negative potential than that on pure Cu with the exception on Cu_3Au and Cu_3Ag surfaces (Table 5). The approximately 0.0 V_{RHE} of

HER onset potential on Cu_3Ag and Cu_3Au surfaces possibly lead to much higher selectivity of H_2 on these surfaces.

The calculated HER on Cu surface is -0.1 V_{RHE} but almost entirely H_2 production on Cu is experimentally[31] observed at approximately -0.5 V_{RHE}. This may result from H*, O* and OH* binding to the same step sites and it would require the OH* removal step taking place in order to clear adsorbed OH* and enable H_2 evolution.[36] Similar to the Cu surface, the H_2 production on Cu_3Ni and Cu_3Co would occur at a more negative potential than the calculated HER onset potential shown in Table 5 and take place approximately at the onset potentials of their OH* removal step. Therefore, compared to the Cu surface, the HER would be suppressed due to high OH* coverage on the surfaces when alloying Cu with Ni, Co, and Ir. The H* binding energies shown in Figure 10 demonstrates that only H* on Cu_3Ag and Cu_3Au surfaces binds more weakly than on pure Cu surface. Thus, the Cu alloying results in the suppression of HER with the exception on Cu_3Ag and Cu_3Au surfaces.

4. Conclusions

This work systematically investigated thermodynamics of CO_2 electroreduction to methane and methanol on copper-based alloys (Cu_3X) where X are metals in group 9-11 using DFT calculations associated with the standard hydrogen electrode model. The affinity relation between intermediates and surfaces are crucial to the free energy change of the elementary steps, consequently, determining the overpotential, the potential-limiting step, and the selectivity. The key intermediates are CO*, HCO*, COH*, CH_2OH*, HOCO*, OH* and H,* and their interactions with the catalysts is required to be optimum in order to efficiently catalyze CO_2 conversion to methane and methanol, suppress H_2 production and avoid OH* surface poisoning.

The CO* protonation producing HCO* or COH* is the limiting-potential step on most surfaces with the exception on Cu_3Au, and Cu_3Co surfaces. In spite of the excessive strong CO* interaction which is even higher than that on pure Cu, the onset potentials of the CO* protonation step on Cu_3Co, Cu_3Rh and Cu_3Ir surfaces can be at less negative potential than that on pure Cu surface. The strong adsorption of CO* and HCO*/COH* is not necessarily an indicator as to whether the onset potential of CO* protonation is likely to be at high negative potential. Instead, the higher degree of CO* adsorption energy and HCO*/COH* adsorption energy decoupling produces, the onset potential of CO* protonation becomes less negative. This show that the CO* protonation step becomes more efficient. The selectivity between HCO* and COH* formation upon CO* protonation can be affected by alloying. The relatively higher stability of COH* than HCO* can be found on the surfaces with relatively strong CO* adsorption because they allow a relatively high degree of electron transfer to CO* corresponding to the electron deficiency at the O-H bond of COH*. The charge transfer characteristics of the C-O bond in HCO* and COH* adsorption is similar to that of CO*, therefore CO* adsorption energy is a good descriptor for linear scaling correlations with HCO* and COH* adsorption energies as well as with the other key intermediates of OCH_2*, HCOH*, CH_2OH*, and HOCO* binding energies. The selectivity of HCO* and COH* intermediates was not found to change due to the change of surface and near-surface compositions caused by segregation. Yet, the sensitivity of CO*, HCO* and COH* binding energies to the change of surface and near-surface compositions can be somewhat significant.

The Cu-based alloy catalysts mostly are more energetically favorable to yield methane than methanol product except on Cu_3Pd, and Cu_3Pt surfaces. The protonation of CO_2 yielding HOCO* is the limiting-potential step on Cu_3Au due to the significant weak HOCO* adsorption. The water formation step and the protonation of COH* to form HCOH* are the limiting-potential steps on Cu_3Co surface. The two proton and electron transfer steps of CO_2 reduction to yield formic acid takes place at low potential close to the equilibrium potential of formic acid formation on Cu_3Pt, Cu_3Ni, Cu_3Co, and Cu_3Rh surfaces. Thus, it suggests that these surfaces are thermodynamically favorable for formic acid production.

Methanol production is found to be more favorable than methane production on Cu_3Pd, and Cu_3Pt surfaces, yet they show high overpotential (~0.7 V). Both surfaces show that the key of methanol selectivity is CH_2OH* intermediate formation favorability associated with the preference of CH_2OH* protonation at the C atom over the O atom. The reduction of methanediol to methanol is energetically favorable at 0.0 V_{RHE} on most Cu-based alloy surfaces. However, the OH* removal step is a significant and challenging step in which its onset potential may take place at negative potentials resulting in OH* surface poisoning.

Alloying Cu with high OH affinity metals; namely Co, Ni, Ir, and Rh worsen surface OH* poisoning compared to pure Cu surface, yet it possibly suppresses the HER. Likewise, alloying Cu with less affinity toward OH; namely Au, Ag, Pd and Pt improve the OH* removal step to be more efficient than pure Cu, yet it may promote the HER. The HER on all alloy surfaces occurs at more negative potential than that on pure Cu with the exception on Cu_3Au and Cu_3Ag surfaces where HER is very efficient with the onset potentials at ~0.0 V_{RHE}.

References

1. Kuhl, K. P.; Cave, E. R.; Abram, D. N.; Jaramillo, T. F., New Insights into the Electrochemical Reduction of Carbon Dioxide on Metallic Copper Surfaces. *Energy Environ. Sci.* **2012,** *5*, 7050-7059.

2. Schouten, K. J. P.; Pérez Gallent, E.; Koper, M. T. M., Structure Sensitivity of the Electrochemical Reduction of Carbon Monoxide on Copper Single Crystals. *ACS Catal.* **2013,** *3*, 1292-1295.

3. Le, M.; Ren, M.; Zhang, Z.; Sprunger, P. T.; Kurtz, R. L.; Flake, J. C., Electrochemical Reduction of CO_2 to CH_3OH at Copper Oxide Surfaces. *J. Electrochem. Soc.* **2011,** *158*, E45-E49.

4. Varela, A. S.; Schlaup, C.; Jovanov, Z. P.; Malacrida, P.; Horch, S.; Stephens, I. E. L.; Chorkendorff, I., CO_2 Electroreduction on Well-Defined Bimetallic Surfaces: Cu Overlayers on Pt(111) and Pt(211). *J. Phys. Chem. C* **2013,** *117*, 20500-20508.

5. Nie, X.; Griffin, G. L.; Janik, M. J.; Asthagiri, A., Surface Phases of $Cu_2O(111)$ under CO_2 Electrochemical Reduction Conditions. *Catal. Commun.* **2014,** *52*, 88-91.

6. Gattrell, M.; Gupta, N.; Co, A., A Review of the Aqueous Electrochemical Reduction of CO_2 to Hydrocarbons at Copper. *J. Electroanal. Chem.* **2006,** *594*, 1-19.

7. Roy, S. C.; Varghese, O. K.; Paulose, M.; Grimes, C. A., Toward Solar Fuels: Photocatalytic Conversion of Carbon Dioxide to Hydrocarbons. *ACS Nano* **2010,** *4*, 1259-1278.

8. Schouten, K. J. P.; Pérez Gallent, E.; Koper, M. T. M., The Influence of pH on the Reduction of CO and to Hydrocarbons on Copper Electrodes. *J. Electroanal. Chem.* **2014,** *716*, 53-57.

9. Li, C. W.; Kanan, M. W., CO_2 Reduction at Low Overpotential on Cu Electrodes Resulting from the Reduction of Thick Cu_2O Films. *J. Am. Chem. Soc.* **2012,** *134*, 7231-7234.

10. Rosen, B. A.; Salehi-Khojin, A.; Thorson, M. R.; Zhu, W.; Whipple, D. T.; Kenis, P. J. A.; Masel, R. I., Ionic Liquid–Mediated Selective Conversion of CO_2 to CO at Low Overpotentials. *Science* **2011,** *334*, 643-644.

11. Hull, J. F.; Himeda, Y.; Wang, W.-H.; Hashiguchi, B.; Periana, R.; Szalda, D. J.; Muckerman, J. T.; Fujita, E., Reversible Hydrogen Storage Using CO_2 and a Proton-Switchable Iridium Catalyst in Aqueous Media under Mild Temperatures and Pressures. *Nat Chem* **2012,** *4*, 383-388.

12. Angamuthu, R.; Byers, P.; Lutz, M.; Spek, A. L.; Bouwman, E., Electrocatalytic CO_2 Conversion to Oxalate by a Copper Complex. *Science* **2010,** *327*, 313-315.

13. Barton Cole, E.; Lakkaraju, P. S.; Rampulla, D. M.; Morris, A. J.; Abelev, E.; Bocarsly, A. B., Using a One-Electron Shuttle for the Multielectron Reduction of CO_2 to Methanol: Kinetic, Mechanistic, and Structural Insights. *J. Am. Chem. Soc.* **2010,** *132*, 11539-11551.

14. Lim, C.-H.; Holder, A. M.; Hynes, J. T.; Musgrave, C. B., Reduction of CO_2 to Methanol Catalyzed by a Biomimetic Organo-Hydride Produced from Pyridine. *J. Am. Chem. Soc.* **2014,** *136*, 16081-16095.

15. Tripkovic, V.; Vanin, M.; Karamad, M.; Björketun, M. E.; Jacobsen, K. W.; Thygesen, K. S.; Rossmeisl, J., Electrochemical CO_2 and CO Reduction on Metal-Functionalized Porphyrin-Like Graphene. *J. Phys. Chem. C* **2013,** *117*, 9187-9195.

16. Dhakshinamoorthy, A.; Navalon, S.; Corma, A.; Garcia, H., Photocatalytic CO_2 Reduction by Tio2 and Related Titanium Containing Solids. *Energy Environ. Sci.* **2012,** *5*, 9217-9233.

17. Woolerton, T. W.; Sheard, S.; Reisner, E.; Pierce, E.; Ragsdale, S. W.; Armstrong, F. A., Efficient and Clean Photoreduction of CO_2 to CO by Enzyme-Modified Tio2 Nanoparticles Using Visible Light. *J. Am. Chem. Soc.* **2010,** *132*, 2132-2133.

18. Hansen, H. A.; Varley, J. B.; Peterson, A. A.; Nørskov, J. K., Understanding Trends in the Electrocatalytic Activity of Metals and Enzymes for CO_2 Reduction to CO. *J. Phys. Chem. Lett.* **2013,** *4*, 388-392.

19. Varley, J. B.; Hansen, H. A.; Ammitzbøll, N. L.; Grabow, L. C.; Peterson, A. A.; Rossmeisl, J.; Nørskov, J. K., Ni–Fe–S Cubanes in CO_2 Reduction Electrocatalysis: A Dft Study. *ACS Catal.* **2013,** *3*, 2640-2643.

20. Centi, G.; Quadrelli, E. A.; Perathoner, S., Catalysis for CO_2 Conversion: A Key Technology for Rapid Introduction of Renewable Energy in the Value Chain of Chemical Industries. *Energy Environ. Sci.* **2013,** *6*, 1711-1731.

21. Qiao, J.; Liu, Y.; Hong, F.; Zhang, J., A Review of Catalysts for the Electroreduction of Carbon Dioxide to Produce Low-Carbon Fuels. *Chem. Soc. Rev.* **2014,** *43*, 631-675.

22. Hori, Y., Electrochemical CO_2 Reduction on Metal Electrodes. In Modern Aspects of Electrochemistry, Vayenas, C. G.; White, R. E.; Gamboa-Aldeco, M. E., Eds. Springer New York: 2008; Vol. 42, pp 89-189.

23. Appel, A. M.; Bercaw, J. E.; Bocarsly, A. B.; Dobbek, H.; DuBois, D. L.; Dupuis, M.; Ferry, J. G.; Fujita, E.; Hille, R.; Kenis, P. J. A.; *et al.*, Frontiers, Opportunities, and Challenges in Biochemical and Chemical Catalysis of CO_2 Fixation. *Chem. Rev. (Washington, DC, U. S.)* **2013,** *113*, 6621-6658.

24. Kuhl, K. P.; Hatsukade, T.; Cave, E. R.; Abram, D. N.; Kibsgaard, J.; Jaramillo, T. F., Electrocatalytic Conversion of Carbon Dioxide to Methane and Methanol on Transition Metal Surfaces. *J. Am. Chem. Soc.* **2014,** *136*, 14107-14113.

25. Hori, Y.; Kikuchi, K.; Murata, A.; Suzuki, S., Production of Methane and Ethylene in Electrochemical Reduction of Carbon Dioxide at Copper Electrode in Aqueous Hydrogencarbonate Solution. *Chem. Lett.* **1986**, 897-898.

26. Hori, Y.; Kikuchi, K.; Suzuki, S., Production of CO and CH_4 in Electrochemical Reduction of CO_2 at Metal Electrodes in Aqueous Hydrogencarbonate Solution. *Chem. Lett.* **1985,** *14*, 1695-1698.

27. Hori, Y.; Murata, A.; Takahashi, R.; Suzuki, S., Enhanced Formation of Ethylene and Alcohols at Ambient Temperature and Pressure in Electrochemical Reduction of Carbon Dioxide at a Copper Electrode. *J. Chem. Soc., Chem. Commun.* **1988**, 17-19.

28. Noda, H.; Ikeda, S.; Oda, Y.; Ito, K., Potential Dependencies of the Products on Electrochemical Reduction of Carbon Dioxide at a Copper Electrode. *Chem. Lett.* **1989,** *18*, 289-292.

29. Shibata, H.; Moulijn, J.; Mul, G., Enabling Electrocatalytic Fischer–Tropsch Synthesis from Carbon Dioxide over Copper-Based Electrodes. *Catal. Lett.* **2008,** *123*, 186-192.

30. Centi, G.; Perathoner, S., Catalysis: Role and Challenges for a Sustainable Energy. *Top. Catal.* **2009,** *52*, 948-961.

31. Hori, Y.; Murata, A.; Takahashi, R., Formation of Hydrocarbons in the Electrochemical Reduction of Carbon Dioxide at a Copper Electrode in Aqueous Solution. *J. Chem. Soc., Faraday Trans. 1: Phys. Chem. Condens. Phases* **1989,** *85*, 2309-2326.

32. Hori, Y.; Takahashi, R.; Yoshinami, Y.; Murata, A., Electrochemical Reduction of CO at a Copper Electrode. *J. Phys. Chem. B* **1997,** *101*, 7075-7081.

33. DeWulf, D. W.; Jin, T.; Bard, A. J., Electrochemical and Surface Studies of Carbon Dioxide Reduction to Methane and Ethylene at Copper Electrodes in Aqueous Solutions. *J. Electrochem. Soc.* **1989,** *136*, 1686-1691.

34. Kim, J. J.; Summers, D. P.; Frese Jr, K. W., Reduction of CO_2 and CO to Methane on Cu Foil Electrodes. *J. Electroanal. Chem.* **1988,** *245*, 223-244.

35. Hori, Y.; Murata, A.; Takahashi, R.; Suzuki, S., Electroreduction of Carbon Monoxide to Methane and Ethylene at a Copper Electrode in Aqueous Solutions at Ambient Temperature and Pressure. *J. Am. Chem. Soc.* **1987,** *109*, 5022-5023.

36. Peterson, A. A.; Abild-Pedersen, F.; Studt, F.; Rossmeisl, J.; Norskov, J. K., How Copper Catalyzes the Electroreduction of Carbon Dioxide into Hydrocarbon Fuels. *Energy Environ. Sci.* **2010,** *3*, 1311-1315.

37. Nie, X.; Luo, W.; Janik, M. J.; Asthagiri, A., Reaction Mechanisms of CO_2 Electrochemical Reduction on Cu(111) Determined with Density Functional Theory. *J. Catal.* **2014,** *312*, 108-122.

38. Nie, X.; Esopi, M. R.; Janik, M. J.; Asthagiri, A., Selectivity of CO_2 Reduction on Copper Electrodes: The Role of the Kinetics of Elementary Steps. *Angew. Chem., Int. Ed.* **2013,** *52*, 2459-2462.

39. Hansen, H.; Montoya, J.; Zhang, Y.-J.; Shi, C.; Peterson, A.; Nørskov, J., Electroreduction of Methanediol on Copper. *Catal. Lett.* **2013,** *143*, 631-635.

40. Shaw, S. K.; Berna, A.; Feliu, J. M.; Nichols, R. J.; Jacob, T.; Schiffrin, D. J., Role of Axially Coordinated Surface Sites for Electrochemically Controlled Carbon Monoxide Adsorption on Single Crystal Copper Electrodes. *Phys. Chem. Chem. Phys.* **2011,** *13*, 5242-5251.

41. Durand, W. J.; Peterson, A. A.; Studt, F.; Abild-Pedersen, F.; Nørskov, J. K., Structure Effects on the Energetics of the Electrochemical Reduction of CO_2 by Copper Surfaces. *Surf. Sci.* **2011,** *605*, 1354-1359.

42. Calle-Vallejo, F.; Koper, M. T. M., Theoretical Considerations on the Electroreduction of CO to C2 Species on Cu(100) Electrodes. *Angew. Chem., Int. Ed.* **2013,** *52*, 7282-7285.

43. Schouten, K. J. P.; Qin, Z.; Gallent, E. P.; Koper, M. T. M., Two Pathways for the Formation of Ethylene in CO Reduction on Single-Crystal Copper Electrodes. *J. Am. Chem. Soc.* **2012,** *134*, 9864-9867.

44. Schouten, K. J. P.; Kwon, Y.; van der Ham, C. J. M.; Qin, Z.; Koper, M. T. M., A New Mechanism for the Selectivity to C1 and C2 Species in the Electrochemical Reduction of Carbon Dioxide on Copper Electrodes. *Chem. Sci.* **2011,** *2*, 1902-1909.

45. Azuma, M.; Hashimoto, K.; Hiramoto, M.; Watanabe, M.; Sakata, T., Electrochemical Reduction of Carbon Dioxide on Various Metal Electrodes in Low‐Temperature Aqueous $KHCO_3$ Media. *J. Electrochem. Soc.* **1990,** *137*, 1772-1778.

46. Hori, Y.; Wakebe, H.; Tsukamoto, T.; Koga, O., Electrocatalytic Process of CO Selectivity in Electrochemical Reduction of CO_2 at Metal Electrodes in Aqueous Media. *Electrochim. Acta* **1994,** *39*, 1833-1839.

47. Peterson, A. A.; Nørskov, J. K., Activity Descriptors for CO_2 Electroreduction to Methane on Transition-Metal Catalysts. *J. Phys. Chem. Lett.* **2012,** *3*, 251-258.

48. Watanabe, M.; Shibata, M.; Kato, A.; Azuma, M.; Sakata, T., Design of Alloy Electrocatalysts for CO_2 Reduction: Ⅲ . The Selective and Reversible Reduction of on Cu Alloy Electrodes. *J. Electrochem. Soc.* **1991,** *138*, 3382-3389.

49. Christophe, J.; Doneux, T.; Buess-Herman, C., Electroreduction of Carbon Dioxide on Copper-Based Electrodes: Activity of Copper Single Crystals and Copper–Gold Alloys. *Electrocatalysis* **2012,** *3*, 139-146.

50. Xu, Z.; Lai, E.; Shao-Horn, Y.; Hamad-Schifferli, K., Compositional Dependence of the Stability of Aucu Alloy Nanoparticles. *Chem. Commun. (Cambridge, U. K.)* **2012,** *48*, 5626-5628.

51. Hirunsit, P., Electroreduction of Carbon Dioxide to Methane on Copper, Copper–Silver, and Copper–Gold Catalysts: A Dft Study. *J. Phys. Chem. C* **2013,** *117*, 8262-8268.

52. Nørskov, J. K.; Rossmeisl, J.; Logadottir, A.; Lindqvist, L.; Kitchin, J. R.; Bligaard, T.; Jónsson, H., Origin of the Overpotential for Oxygen Reduction at a Fuel-Cell Cathode. *J. Phys. Chem. B* **2004,** *108*, 17886-17892.

53. Nørskov, J. K.; Bligaard, T.; Logadottir, A.; Bahn, S.; Hansen, L. B.; Bollinger, M.; Bengaard, H.; Hammer, B.; Sljivancanin, Z.; Mavrikakis, M.; Xu, Y.; Dahl, S.; Jacobsen, C. J. H., Universality in Heterogeneous Catalysis. *J. Catal.* **2002,** *209*, 275-278.

54. Ruban, A. V.; Skriver, H. L.; Nørskov, J. K., Surface Segregation Energies in Transition-Metal Alloys. *Phys. Rev. B* **1999,** *59*, 15990-16000.

55. Kresse, G.; Furthmüller, J., Efficient Iterative Schemes for Ab Initio Total-Energy Calculations Using a Plane-Wave Basis Set. *Phys. Rev. B* **1996,** *54*, 11169-11186.

56. Kresse, G.; Furthmüller, J., Efficiency of Ab-Initio Total Energy Calculations for Metals and Semiconductors Using a Plane-Wave Basis Set *Computational Materials Science* **1996,** *6*, 15-50.

57. Perdew, J. P.; Burke, K.; Ernzerhof, M., Generalized Gradient Approximation Made Simple. *Phys. Rev. Lett.* **1996,** *77*, 3865-3868.

58. Perdew, J. P.; Burke, K.; Ernzerhof, M., Generalized Gradient Approximation Made Simple [Phys. Rev. Lett. 77, 3865 (1996)]. *Phys. Rev. Lett.* **1997,** *78*, 1396-1396.

59. Blöchl, P. E., Projector Augmented-Wave Method. *Phys. Rev. B* **1994,** *50*, 17953.

60. Kresse, G.; Joubert, D., From Ultrasoft Pseudopotentials to the Projector Augmented-Wave Method. *Phys. Rev. B* **1999,** *59*, 1758-1775.

61. Hammer, B.; Morikawa, Y.; Nørskov, J. K., CO Chemisorption at Metal Surfaces and Overlayers. *Phys. Rev. Lett.* **1996,** *76*, 2141-2144.

Output จากโครงการวิจัยที่ได้รับทุนจาก สกว.

1. ผลงานตีพิมพ์ในวารสารวิชาการนานาชาติ

   P. Hirunsit*, W. Soodsawang, and J. Limtrakul, *CO_2 Electrochemical Reduction to Methane and Methanol on Copper-Based Alloys: Theoretical Insight.* J. Phys. Chem. C, 2015. 119: p. 8238-8249.

   P. Hirunsit*, *Electroreduction of carbon dioxide to methane on copper, copper-silver and copper-gold catalysts: A DFT study.* J. Phys. Chem. C, 2013. 117(16): p. 8262-8268.

2. การนำผลงานวิจัยไปใช้ประโยชน์
   - เชิงวิชาการ

     มีการนำเสนอผลงานในงานประชุมวิชาการนานาชาติในวงวิชาการและผู้สนใจด้านวิชาการทั้งในและต่างประเทศ ในหัวข้อ “Reactivity Trend of CO_2 Electroreduction on Copper Alloys from First Principles” ในงานการประชุม International Conference on Smart Materials and Surfaces, Bangkok, Thailand, Aug 26-28 2014

ภาคผนวก

THE JOURNAL OF
PHYSICAL CHEMISTRY C

Article

pubs.acs.org/JPCC

Electroreduction of Carbon Dioxide to Methane on Copper, Copper–Silver, and Copper–Gold Catalysts: A DFT Study

Pussana Hirunsit*

National Nanotechnology Center (NANOTEC), 111 Thailand Science Park, Phaholyothin Road, Klong 1, Klong Luang, Pathumthani 12120, Thailand

Ⓢ *Supporting Information*

ABSTRACT: The electrochemical reduction of CO_2 is a promising process capable of efficiently recycling CO_2 waste and converting it into hydrocarbon fuel. To date, copper is the best metal catalyst; however the overpotential to achieve this reaction on Cu is excessively high. It follows that the development of a catalyst to efficiently catalyze the conversion with a low overpotential at a reasonable current density is needed. Many aspects of the molecular details of the reaction are still unclear. In this work, DFT calculations are applied to investigate CO_2 electroreduction to CH_4 over Cu_3Ag and Cu_3Au stepped surfaces (211) compared to that over Cu(211). In the resulting analysis, the Cu_3Ag surface shows a slightly lower overpotential and suppresses OH poisoning compared to the Cu surface, yet the selectivity toward H_2 increases. The Cu_3Au is not a good candidate due to higher overpotential and a relatively weak CO adsorption resulting in CO desorption rather than further reduction. The CO desorption can also be problematic on Cu_3Ag as well. The thermodynamics and kinetics of the nonelectrochemical hydrogenations are also examined to explore alternative paths which might result in an absence of formaldehyde intermediate production during CO_2 reduction on Cu.

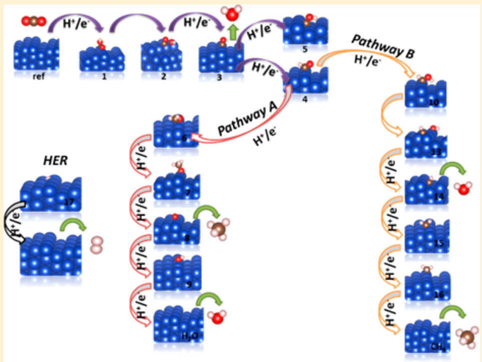

1. INTRODUCTION

The various environmental, economic, and societal impacts of Earth's climate change have been well documented. The observation that CO_2 plays a significant role is well-established: the higher the atmospheric CO_2 level, the better the atmosphere retains heat. Thus, CO_2 acts as a rule setter for climatic conditions and hence the need to creatively dispose of excess CO_2. A process capable of efficiently recycling CO_2 waste and converting it into hydrocarbon fuel would provide a renewable energy source that creates a more favorable carbon energy cycle. There are several approaches for CO_2 conversion to hydrocarbon. These include using biomass as well as thermochemical and electrochemical processes. The electrochemical process has an appealing advantage because it does not require high-temperature reactions and the production rate can be varied to follow the availability of electricity produced from clean resources such as solar cells. The types of CO_2 electroreduction products formed and faradic efficiency of the process depend on a number of factors, primarily the catalytic activity of the electrodes, type of ionic species in electrolytes, local pH, and CO_2 concentration on the electrode.[1,2] The electrode material plays a crucial role in determining the primary product and selectivity. The surface structure, surface crystallography, and its electronic configurations which influence the preferential adsorption of reactant, the intermediates, and the products are all important factors determining the catalytic activity of the electrode.[3−8] A key discovery was the direct reduction of CO_2 to hydrocarbons (methane and ethylene) on a copper electrode with reasonable current density (5−10 mA/cm^{-2}) and current efficiency by the group of Hori.[9,10] To date, the production of pure hydrocarbons has not yet been found. Interestingly, however, it was found that a wider range of hydrocarbons such as ethanol and propanol can also be produced.[11−14] It is an important challenge to discover promising electrode materials (electrocatalysts) which provide high efficiency and high hydrocarbon product selectivity. Thus, an understanding of the key reaction step and the structural and electronic effect of the electrodes on catalytic activity and selectivity is very crucial.

The satisfactory electrode for CO_2 reduction with high current efficiency should provide medium hydrogen overpotential, while catalyzing C−O bond breaking and strong CO adsorption and also allowing CO to be further reacted as well. Copper is a unique electrode which further reduces the CO intermediate to a more reduced species in significant amounts. The primary reactions occurring at a copper electrode during CO_2 reduction with the standard potentials calculated using formation energies are listed below.[1]

$$2H^+ + 2e^- \leftrightarrow H_2 \qquad U_0 = 0.0\ \text{V vs SHE (standard hydrogen electrode)} \tag{1}$$

Received: January 28, 2013
Revised: March 31, 2013
Published: April 2, 2013

dx.doi.org/10.1021/jp400937e | *J. Phys. Chem. C* 2013, 117, 8262−8268

$$2CO_2 + 12H^+ + 12e^- \leftrightarrow C_2H_4 + H_2O \quad U_0 = 0.079 \text{ V vs SHE} \tag{2}$$

$$CO_2 + 8H^+ + 8e^- \leftrightarrow CH_4 + 2H_2O \quad U_0 = 0.169 \text{ V vs SHE} \tag{3}$$

$$CO_2 + 2H^+ + 2e^- \leftrightarrow CO + H_2O \quad U_0 = -0.103 \text{ V vs SHE} \tag{4}$$

$$CO_2 + H^+ + 2e^- \leftrightarrow HCOO^- \quad U_0 = -0.225 \text{ V vs SHE} \tag{5}$$

Methane and ethylene should, in theory, thermodynamically occur at less cathodic potential; however, kinetically this does not occur. The factor of changing the dominant product from CO to CH_4 can be influenced by other factors such as electrode preparation and the amount of mass transport of CO.[1]

Several studies[15−18] clearly showed that during CO_2 reduction CO adsorption dominates on the electrode surface, suggesting that CO is a key intermediate. The high coverage of adsorbed CO found during CO_2 reduction also suggested that the reduction of adsorbed CO may be a key rate-determining step.[19,20] Furthermore, recent DFT calculations by Peterson et al.[21] have provided significant insights about how copper catalyzes CO_2 reduction to CH_4. The calculations suggested that the key step in the formation of CH_4 from CO_2 is the protonation of adsorbed CO* to form adsorbed HCO* ($CO^* + H^+ + e^- \rightarrow HCO^*$). If the adsorbed HCO* can be stabilized relative to adsorbed CO*, the overpotential can be significantly reduced, leading to a more efficient process. Therefore, the exploration of potential electrocatalyst materials which can primarily meet the requirements of providing a more efficient process of CO_2 reduction should be expanded.

The nature of the metal electrodes has a great influence on the product distribution from CO_2 reduction as it affects whether the reactants, intermediates, and products are adsorbed or not and also the strength of the adsorption. The analysis based on DFT calculations of the key adsorbates which are intermediates in the proposed mechanism of CO_2 reduction to CH_4 by Peterson et al.[21] on transition metals, Cu, Pt, Rh, Pd, Ni, Au, and Ag, has presented an activity diagram of the "volcano" type in which Cu is at the top among these metals, reflecting why Cu is the best-known metal electrocatalyst.[22] Copper exhibits a better ability to perform CO* protonation than the other metals, but this is only associated with the poor activity of the hydrogen evolution reaction (HER), i.e., moderate negative potential for HER. Peterson et al.[22] suggested that effective catalysts must catalyze the protonation of adsorbed CO* effectively and simultaneously show poor activity for the competitive HER.

This work aims to perform an analysis of Cu_3Ag and Cu_3Au as electrocatalysts for CO_2 reduction to yield methane using DFT calculations in conjunction with the standard hydrogen electrode model.[23] The goal is to examine the potential of these catalysts for CO_2 electroreduction to methane and to provide the insights as to how these Cu alloyed electrodes modify CO_2 reduction activity compared to pure Cu electrodes. Ultimately, the analysis will provide useful guidance for catalyst search and design, which will lead to further improvements in CO_2 electroreduction catalytic efficiency. Also, we perform thermodynamics and kinetics investigations on the alternative nonelectrochemical reactions in an attempt to understand the absence of formaldehyde intermediate suggested experimentally for CO_2 reduction to methane on Cu since a formaldehyde intermediate is theoretically favorable during the reduction.

2. COMPUTATIONAL DETAILS

The fully periodic plane-wave DFT calculations as implemented in the Vienna ab initio Simulation Program (VASP)[24,25] were employed. The slab models of a stepped (211) surface with a unit cell of 3 × 3 (shown in Figure 1) containing six layers of metal atoms and a vacuum region of more than six layers (approximately 15 Å) were used for a search of the most stable binding sites. The calculations were carried out on stepped surfaces (211) because it was generally found to be the most reactive for C−O bond breaking[26] which is a crucial process here. The structures of Cu_3X surfaces are modeled with $L1_2$ crystal lattice structures, where X is Ag and Au. It should be noted that Au and Ag have a moderate degree of segregation on the Cu host.[27] However, the favor of CO adsorption on Cu could reduce the tendency of Ag and Au segregation.

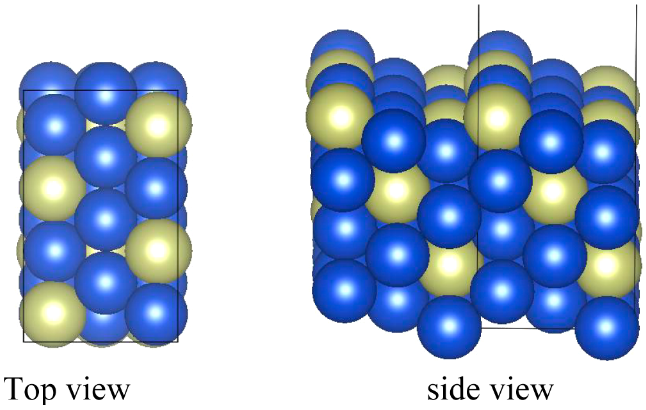

Figure 1. Unit cell of a slab model of a stepped (211) Cu_3X alloy surface. Cu atom, blue; and X atom, green. The solid line indicates a unit cell boundary.

The two atomic layers from the bottom of the slab were fixed, while the other layers were relaxed to their lowest energy configurations. The fixed layers were set to their bulk bond distances according to their optimized lattice constants that were determined from bulk calculations. The calculated lattice constants are 3.63 Å for Cu, 3.78 Å for Cu_3Ag, and 3.79 Å for Cu_3Au bulk compositions. Spin-polarized DFT calculations were performed with the exchange-correlation functional Perdew−Burke−Ernzerhof (PBE)[28,29] described within the generalized gradient approximation implemented with the Projector Augmented Wave function (PAW)[30,31] method for representing the nonvalence core electrons. The calculations employed 5 × 5 × 1 k-point Monkhorst−Pack mesh sampling in the surface Brillouin zone. The plane-wave cutoff energy was optimized at 400 eV. The results were checked for convergence with respect to energy cutoff and number of k-points. The Methfessel−Paxton smearing of order 2 with a value of smearing parameter σ of 0.2 eV was applied. The convergence criteria for electronic self-consistent iteration were set to 1.5×10^{-7} eV, and the ionic relaxation loop was limited for all forces smaller than 0.035 eV/Å for free atoms.

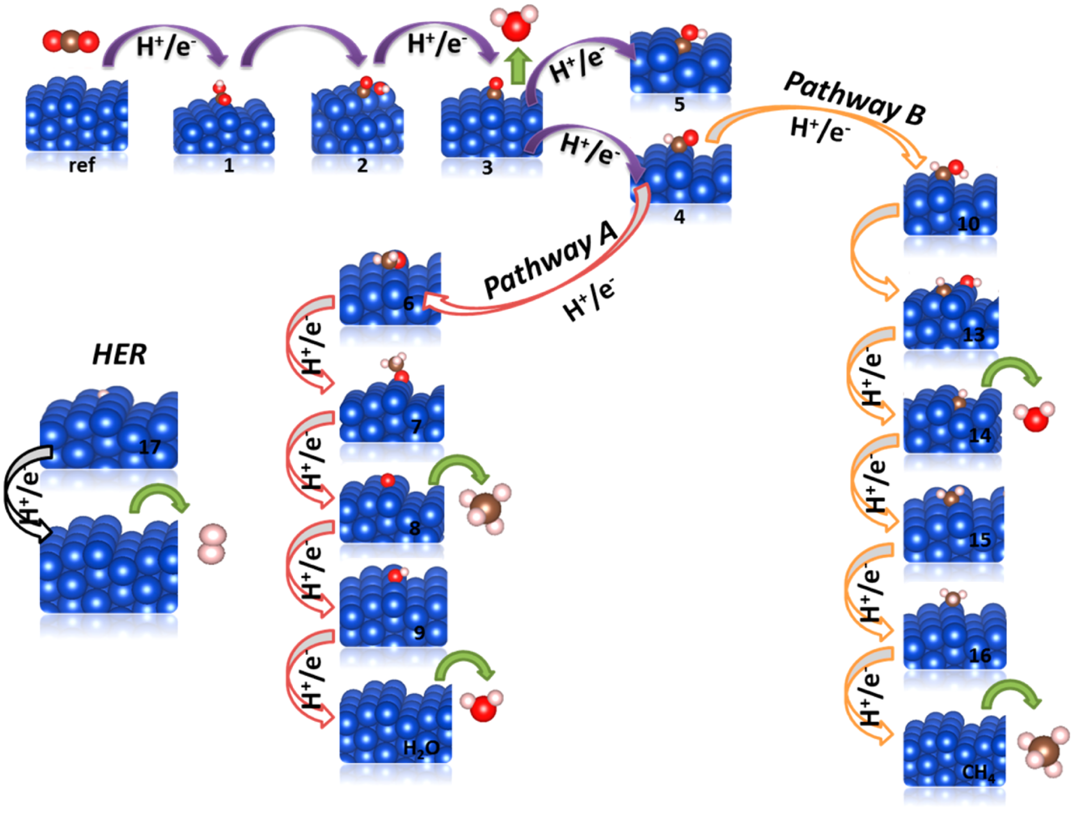

Figure 2. Studied CO_2 reduction pathways; hydrogen evolution reaction (HER), pathway A and pathway B. In pathway A, the protonation of HCO* forms formaldehyde (state 6), while it forms HCOH* (state 10) in pathway B. State 11(not shown here) in which HCO* dissociates to be CH* + O* is less stable (~ 0.4 eV) than state 10 (HCOH*). The intermediate configurations and adsorption energies are reported in the Supporting Information.

To construct the free energy diagrams, the free energy of the electrochemical reactions for a given surface at 291.65 K was calculated according to the method proposed by Nørskov et al.[23] Details of calculations are described very well in ref 21. The model is based on the thermochemistry of the reaction with an assumption of very small barriers due to proton and electron transfer to metal surfaces and includes the effect of solvation, electrode potential, zero-point energy (ZPE), heat capacity ($\int C_p dT$), and entropy ($T\Delta S$) corrections. The values of ZPE, $\int C_p dT$, and $T\Delta S$ correction terms of all adsorbed species and gas-phase species are shown in the Supporting Information. Those of adsorbed species were calculated by performing normal-mode vibrational analysis treating all $3N$ degrees of freedom of the adsorbate as vibrational and assuming the vibrations of metal surfaces due to the presence of adsorbate are minimal; all vibrations were treated in the harmonic oscillator approximation. The solvation effect on adsorbate stabilization was estimated according to those shown in ref 21; OH* and R−OH* adsorbates (OH does not directly bond to surfaces) are stabilized by approximately 0.5 and 0.25 eV, respectively. CO*, HCO*, and COH* adsorbates are stabilized by approximately 0.1 eV.

The method sets the reference potential to be the standard hydrogen electrode (SHE). This means that at pH = 0 in the electrolyte and 1 bar of H_2 in the gas phase at 298 K the reaction free energy of $1/2H_2(g) \leftrightarrow H^+(aq) + e^-$ is zero at zero electrode potential ($U = 0$). Therefore, at the standard conditions, the free energy of the reaction $HA^* \leftrightarrow A + H^+ + e^-$ can be calculated as the free energy of $^*AH \leftrightarrow A + 0.5H_{2(g)}$. At $U \neq 0$, the free energy of the proton−electron pair can be treated by shifting the energy by $-eU$ where U is the electrode potential relative to SHE. The reference electrode in this work is the theoretical reversible hydrogen electrode (RHE) which can relate to the standard hydrogen electrode (SHE) by subtracting $kT \times \text{pH} \times \ln 10$ where the pH value in this work is 6.8.

The nonelectrochemical barrier energies are calculated by using the nudged elastic band (NEB)[32]and dimer[33]methods to locate transition state structures. All transition states are verified by the number of imaginary frequencies = 1.

3. RESULTS AND DISCUSSION

The CO_2 electroreduction pathways included in this study are illustrated in Figure 2. Pathway A and pathway B have common intermediates up to state 5. Both pathways involve eight proton−electron pairs transferred. The difference between two pathways begins at the protonation of HCO*(state 4). State 5(COH*) is not likely to form as state 4 is more thermodynamically stable (>0.5 eV) on all studied surfaces. The pathway A is similar to the proposed mechanism by Nørskov et al. on Cu.[21] They have studied a number of possible pathways in the electroreduction of CO_2 on a Cu(211) surface and found pathway A has the lowest free energy. However, the reduction of formaldehyde on copper experimentally led to both methanol and methane products, while methanol is not produced during the reduction of CO_2 on copper. Thus, it was suggested that formaldehyde may not be an intermediate of CO_2 reduction on copper.[34] Thus, the pathway B in which the formaldehyde intermediate does not present is also included in this work. Although HCOH* (state 10) in pathway B is less thermodynamically stable than formaldehyde (state 6) in pathway A, pathway B may be of importance for the impact on the kinetics which will also be investigated in this work. The CO_2 reduction to CH_4 is thermodynamically possible at +0.17 V_{RHE} which is very close to the equilibrium of HER which occurs at 0.00 V_{RHE}. CO_2 reduction to CH_4 is in competition with HER at all negative potentials. Therefore, the hydrogen evolution reaction (HER) is also included in the calculations.

From a thermodynamic point of view, the limiting potential indicates the electrode potential at which the reaction begins to have an evident rate. It is the highest potential at which the free energy of the entire elementary step is downhill. Figure 3 shows the limiting potential of the common steps of pathways A and B. On Cu(211) and $Cu_3Ag(211)$ surfaces, U34 (protonation of CO*) is at the highest potential in which the elementary steps up to state 4 are free energy downhill, whereas it is Urefl (protonation of CO_2) on the $Cu_3Au(211)$ surface. The Urefl is theoretically found to be the limiting-potential step on pure Ag(211) and Au(211).[22]

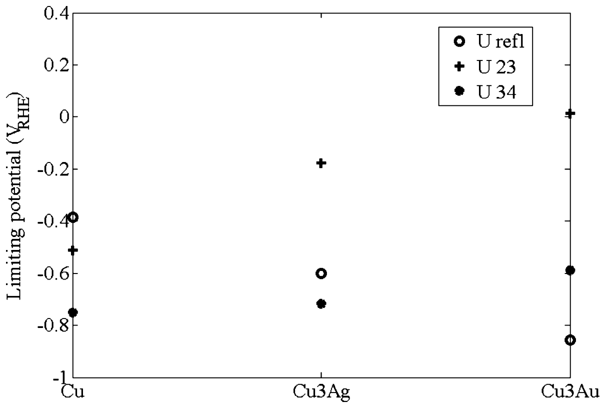

Figure 3. Limiting potential (V_{RHE}) of common elementary steps of pathways A and B. The legends indicate, for example, that U23 means the limiting potential of the elementary step of state 2 to state 3. The adsorbate corresponding to each state refers to Figure 2.

The limiting potentials of the steps after HCO* formation in pathways A and B are shown in Figures 4 and 5. Considering Figures 3 and 4 (pathway A), the most limiting potential step of pathway A is U34 (CO* protonation) on Cu and Cu_3Ag surfaces at −0.75 and −0.72 V_{RHE}, respectively, while it is Urefl (CO_2 protonation) on the Cu_3Au surface at −0.86 V_{RHE}. The second most limiting step in pathway A on Cu is the OH removal steps (U23 and U9−H_2O), while it is CO_2 protonation (Urefl) on Cu_3Ag and CO* protonation (U34) on Cu_3Au. The prediction of the most limiting potential step of Cu_3Ag and Cu_3Au closely follows the volcano plot by Peterson and Nørskov.[22] The CO adsorption energies of Cu_3Au and Cu_3Ag lie between those of Cu and Au with the values closer to Cu than Au. The most limiting step of Cu_3Ag is on the CO* → CHO* line in the volcano plot at slightly less negative potential than Cu, and the most limiting step of Cu_3Au falls on the CO_2 → COOH* line after the top of the volcano plot (the intersection between CO_2 → COOH* and CO* → CHO* lines) which predicts the most limiting step of Cu_3Au to be CO_2 → COOH* at more negative potential than Cu. The OH* removal steps (OH* + H^+ + e^- → H_2O) are likely to reduce Cu catalyst effectiveness, but it can be significantly improved by alloying with Au and Ag. This results in a less negative limiting potential of U23 and U9−H_2O. The limiting potentials of HER (U17−H_2) on Cu, Cu_3Ag, and Cu_3Au are −0.10, −0.01, and 0.02 V_{RHE}, respectively. The medium overpotential of HER on Cu suppresses HER activity,[21] while the reduction in overpotential of HER on Cu_3Ag and Cu_3Au may promote the HER, leading to the higher selectivity of H_2 compared to that on Cu. It should be noted that very small calculated overpotentials for HER on Cu_3Au and Cu_3Ag suggest that these catalysts would be remarkable HER catalysts.

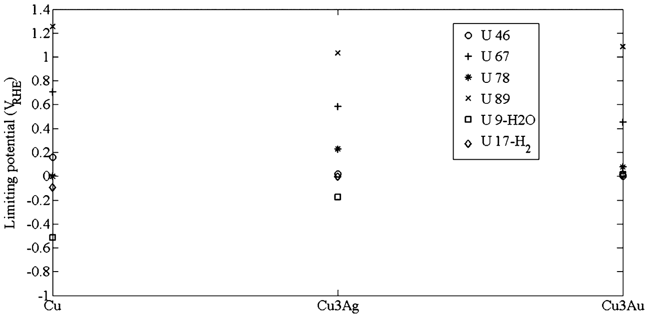

Figure 4. Limiting potential (V_{RHE}) of the elementary steps after state 4 in pathway A and the limiting potential of HER (U17−H_2).

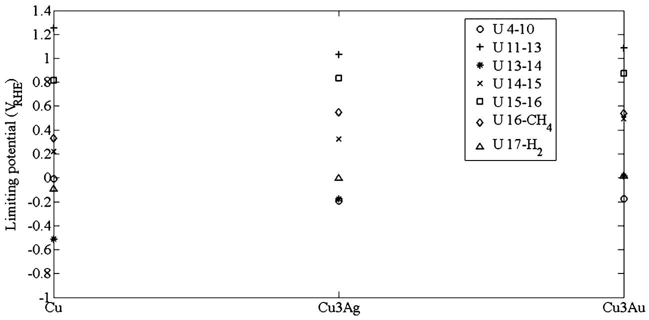

Figure 5. Limiting potential (V_{RHE}) of the elementary steps after state 4 in pathway B and the limiting potential of HER (U17−H_2).

Alloying Cu with Ag does not change the limiting-potential step and results in slightly smaller overpotential compared to pure Cu. Although Ag assists to promote the OH* removal step, it causes the CO_2 protonation step (Urefl) to be more difficult. The theoretical overpotential becomes less favorable when alloying Cu with Au, and the limiting-potential step changes. Alloying Cu with Au and Ag does not have a significant effect on HCO* adsorption where the HCO* adsorption energies on $Cu_3Ag(211)$ and $Cu_3Au(211)$ are different from that on Cu(211) by less than 0.1 eV. Comparing the adsorption of all intermediates, the HCO* adsorption is found to be the least sensitive to the alloying effect with Au and Ag. However, Au and Ag significantly affect HOCO* (state 1) adsorption energies (0.2−0.5 eV difference) due to the bonding through both C and O atoms. The CO_2 reductions which were carried out on copper−gold electrodes by Christophe et al.[35] showed that the CO production increases markedly with the Au content, while the fraction of CH_4 diminishes. This relates to the strong sensitivity between the higher Au content and the reduction in CO* adsorption energy and the smaller CO* desorption barrier energy. This induces CO* to desorb rather than to be further reduced. CO* adsorption energy on Cu_3Au is weaker than Cu by 0.19 eV. Cu_3Ag may also present the same challenge of CO* desorption because CO* adsorbs on Cu_3Ag more strongly than on Cu_3Au only by 0.07 eV. In addition, it was found that Au-rich alloy of Au_2Cu has relatively lower CO_2 reduction onset potentials than Au and Cu.[36] This indicates the strong effect of alloy composition which can lower energy used for CO_2 reduction.

The difference between pathway A and pathway B begins after state 4 where the protonation of HCO* produces HCOH* in pathway B instead of OCH_2*. The OCH_2* adsorption is approximately 0.4 eV more stable than HCOH* adsorption. Considering Figures 3 and 5 (pathway B), the potential limiting step of pathway B remains the same as the limiting step with pathway A on all surfaces. The most limiting of the later steps is still the OH* removal step (U13−14) for the high oxygen affinity surface like Cu. The limiting potential of the protonation of HCO* to become HCOH*(U4−10) on Cu_3Ag and Cu_3Au surfaces is comparable with that of the OH* removal step (U13−14). The calculated free energy diagrams of both pathways at the limiting potential of Cu and Cu_3Ag are shown in Figures 6 and 7, and for Cu_3Au it is shown in the Supporting Information.

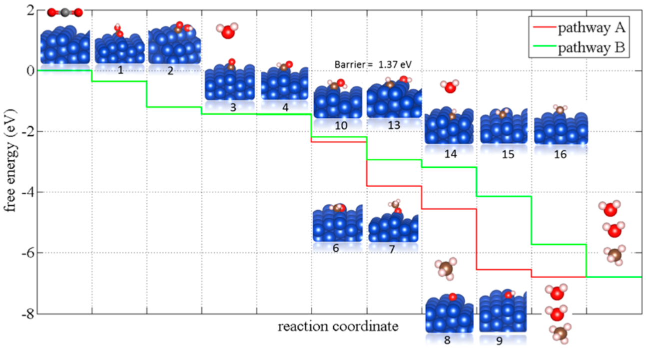

Figure 6. Cu(211) free energy diagram following reaction steps in pathway A and pathway B at limiting potential $U = -0.75$ V_{RHE}.

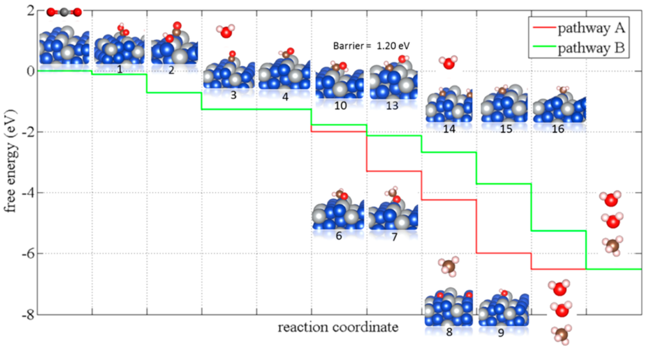

Figure 7. Cu_3Ag(211) free energy diagram following reaction steps in pathway A and pathway B at limiting potential $U = -0.72$ V_{RHE}.

Adsorbed CO*, HCO*, HOCO*, and OH* are the key intermediates that require an optimum binding energy among them to achieve an effective catalyst; nevertheless, their natures are not quite related. Alloying Cu with Au or Ag does not induce significant change on CO* and HCO* adsorption energies compared to Cu (<0.2 eV), while the adsorption energies of HOCO* and OH* show a significant change (0.2−0.5 eV). The insensitivity with the surface affinity toward O or C of CO* and HCO* adsorption energy, while HOCO* and OH* are strongly related to surface affinity toward O, creates a great challenge for a search of effective catalysts.

The reaction free energies and barrier energies of the nonelectrochemical reactions involving adsorbed H* are also investigated as shown in Table1. The corresponding transition state configurations are shown in the Supporting Information. The CO* protonation is favorable up to the potential −0.75 and −0.72 V_{RHE} on Cu and Cu_3Ag, respectively, while the nonelectrochemical CO* hydrogenation by adsorbed H* to form HCO* is not energetically favorable on all surfaces. Furthermore, the barrier energies of H* + CO* → HCO* are relatively high. Therefore, it is more likely that the HCO* formation takes the route of CO* electro-reduction rather than the nonelectrochemical hydrogenation of CO*, and it is also supported by the good agreement between the theoretical limiting potential (−0.75 V) and the experimental onset potential of CH_4 formation on Cu catalyst (−0.8 V).[19]

The OCH_2* adsorption is approximately 0.4 eV (electronic energy) more stable than HCOH* adsorption, thus the pathway A is more thermodynamically favorable than pathway B. OCH_2* adsorption is more stable on the surface than HCOH* because OCH_2* bonds through both oxygen and carbon atoms while HCOH* bonds through the carbon atom only. However, the experimental result by Schouten et al.[34] suggested that formaldehyde may not be an intermediate of CO_2 reduction on Cu. Table 1 shows that the formation of HCOH* and OCH_2* via hydrogenation of adsorbed H* is energetically favorable on all surfaces except for the formation of HCOH* on Cu_3Ag. The barriers of HCOH* formation are comparable to those of OCH_2* formation except on Cu_3Ag in which HCOH* formation has much higher barriers than OCH_2* formation. Thus, the formation of both HCOH* and OCH_2* via hydrogenation of HCO* can be facilitated on Cu and Cu_3Au surfaces. However, on Cu_3Ag, the formation of OCH_2* is more likely than the formation of HCOH*. The dissociation of OCH_2* back to HCO* is difficult due to energetically unfavorable and relatively high energy barriers. Thus, once OCH_2* is formed it is more likely to be further protonated to be OCH_3* (step 67). The thermodynamic and kinetics point of view indicates that the nonelectrochemical formation of both HCOH* and OCH_2* is feasible on Cu. Considering the results from both electro and nonelectrochemical reactions, the absence of a formaldehyde intermediate on Cu catalyst suggested by Schouten et al.[34] is, however, still unclear. Nevertheless, the coverage of HCO* may play a role in the favorability of species formed by HCO* hydrogenation. We found that the presence of HCO* adsorbed on the adjacent site influences the adsorption energy of OCH_2* to be more stable than HCOH* by 0.27 eV, while it is by 0.4 eV without the coadsorption of HCO*.

In addition, the first C−O bond breaking in both pathways id found in step 1 → 2, and the second C−O bond breaking step in pathway A occurs at step 7 → 8. In pathway B, it occurs at step 10 → 13. Step 10 → 13 is not an electrochemical reaction in nature, thus the free energy change will be expected to be roughly constant and does not depend on applied potentials. In pathway B, once HCOH* formed, it is energetically favorable for C−O bond breaking to result in CH* and OH* (state 13) except on the Cu_3Au surface. Nevertheless, the CH_4 formation via pathway B may be kinetically limited at the C−O bond breaking step (10 → 13) as the barrier energies are approximately 1.2−1.4 eV.

Table 1. Nonelectrochemical Reaction Free Energies (ΔG), Reaction Energy (ΔE, Only Electronic Energy), and Barrier Energies (E_a, Only Electronic Energy) of Elementary Steps Involving HCO*, OCH_2*, and HCOH* Intermediates (in eV)[a]

	Cu(211)			Cu_3Ag (211)			Cu_3Au (211)		
elementary step	E_a	ΔE	ΔG	E_a	ΔE	ΔG	E_a	ΔE	ΔG
H* + CO* → HCO*	+0.96	+0.75	+0.82	+0.58	+0.53	+0.60	+0.98	+0.46	+0.54
HCO* + H* → OCH_2*	+0.66	−0.32	−0.07	+0.37	−0.39	−0.13	+0.66	−0.52	−0.27
OCH_2* → HCO* + H*	+0.98	+0.32	+0.07	+0.76	+0.39	+0.13	+1.18	+0.52	+0.27
HCO* + H* → HCOH*	+0.60	−0.10	−0.03	+0.74	+0.01	+0.07	+0.72	−0.07	0.00
HCOH* → HCO* + H*	+0.70	+0.10	+0.03	+0.74	−0.01	−0.07	+0.79	+0.07	0.00
HCOH* → CH* + OH*	+1.37	−0.05	−0.36	+1.20	+0.10	−0.21	+1.64	+0.48	+0.18

[a] ΔG includes ZPE, enthalpic, entropy, and solvation effect corrections, but E_a and ΔE do not.

4. CONCLUSIONS

This work investigated the pathways for CO_2 electroreduction to CH_4 on Cu(211), Cu_3Ag(211), and Cu_3Au(211) using DFT calculations associated with the standard hydrogen electrode model . The limiting potential step is the protonation of HCO* on Cu and Cu_3Ag surfaces which is limited at −0.75 and −0.72 V_{RHE}, respectively. The limiting potential step is CO_2 protonation on the Cu_3Au surface at −0.86 $V_{RHE.}$ The higher overpotential makes Cu_3Au less efficient than Cu and Cu_3Ag. Cu_3Ag can be slightly more efficient than Cu considering lower overpotential. OH poisoning can be suppressed on Cu_3Ag and Cu_3Au compared to Cu. However, the efficiency of Cu_3Ag and Cu_3Au can be reduced due to the higher selectivity toward H_2. The CO* desorption preference over further reduction of CO* with the higher Au content is also a challenge. This also can be expected on Cu_3Ag in which the CO* adsorption is relatively weak as it also is on Cu_3Au. The adsorbed CO*, HCO*, HOCO*, and OH* species are the key intermediates that require an optimum binding energy among them to achieve an effective catalyst; nevertheless, their natures are not quite related. The HCO* and CO* adsorptions are insensitive with the surface affinity toward O or C, while HOCO* and OH* are strongly related to surface affinity toward O, creating a great challenge in the search for effective catalysts.

The alternative pathway which goes through HCOH* instead of the formaldehyde intermediate and the hydrogenation via nonelectrochemical reaction were also investigated to seek an understanding of the possible pathway that may not involve a formaldehyde intermediate. The protonation of HCO* is more favorable to form a formaldehyde intermediate than a HCOH* intermediate. The thermodynamic and kinetics points of view indicate that both HCOH* and formaldehyde intermediates are favorable via the nonelectrochemical hydrogenation of HCO* with comparable barrier energies. Nonetheless, the absence of a formaldehyde intermediate on the Cu catalyst during CO_2 reduction suggested experimentally is still unclear. However, we suggest that the coverage of HCO* plays an important role in influencing the species formed by HCO* hydrogenation, and the high coverage of HCO* possibly affects the adsorption energies of HCOH* to be comparable with that of OCH_2*

■ ASSOCIATED CONTENT

Ⓢ Supporting Information

Tables S1−S4 and Figure S1. This material is available free of charge via the Internet at http://pubs.acs.org.

■ AUTHOR INFORMATION

Notes

The authors declare no competing financial interest.

■ ACKNOWLEDGMENTS

The author acknowledged the financial support from the National Nanotechnology Center (NANOTEC) and Thailand Research Funding (TRF) and the computing resource from National e-Science Infrastructure Consortium.

■ REFERENCES

(1) Gattrell, M.; Gupta, N.; Co, A. *J. Electroanal. Chem.* **2006**, *594* (1), 1−19.
(2) Roy, S. C.; Varghese, O. K.; Paulose, M.; Grimes, C. A. *ACS Nano* **2010**, *4* (3), 1259−1278.
(3) Durand, W. J.; Peterson, A. A.; Studt, F.; Abild-Pedersen, F.; Nørskov, J. K. *Surf. Sci.* **2011**, *605* (15−16), 1354−1359.
(4) Tang, W.; Peterson, A. A.; Varela, A. S.; Jovanov, Z. P.; Bech, L.; Durand, W. J.; Dahl, S.; Norskov, J. K.; Chorkendorff, I. *Phys. Chem. Chem. Phys.* **2012**, *14* (1), 76−81.
(5) Shaw, S. K.; Berna, A.; Feliu, J. M.; Nichols, R. J.; Jacob, T.; Schiffrin, D. J. *Phys. Chem. Chem. Phys.* **2011**, *13* (12), 5242−5251.
(6) Takahashi, I.; Koga, O.; Hoshi, N.; Hori, Y. *J. Electroanal. Chem.* **2002**, *533* (1−2), 135−143.
(7) Hori, Y.; Takahashi, I.; Koga, O.; Hoshi, N. *J. Mol. Catal. A: Chem.* **2003**, *199* (1−2), 39−47.
(8) Hori, Y. Electrochemical CO_2 Reduction on Metal Electrodes. In *Modern Aspects of Electrochemistry*; Vayenas, C. G., White, R. E., Gamboa-Aldeco, M. E., Eds.; Springer: New York, 2008; Vol. *42*, pp 89−189.
(9) Hori, Y.; Kikuchi, K.; Murata, A.; Suzuki, S. *Chem. Lett.* **1986**, 897−898.
(10) Hori, Y.; Kikuchi, K.; Suzuki, S. *Chem. Lett.* **1985**, *14* (11), 1695−1698.
(11) Hori, Y.; Murata, A.; Takahashi, R.; Suzuki, S. *J. Chem. Soc., Chem.\ Commun.* **1988**, *1*, 17−19.
(12) Noda, H.; Ikeda, S.; Oda, Y.; Ito, K. *Chem. Lett.* **1989**, *18* (2), 289−292.
(13) Shibata, H.; Moulijn, J.; Mul, G. *Catal. Lett.* **2008**, *123* (3), 186−192.
(14) Centi, G.; Perathoner, S. *Top. Catal.* **2009**, *52* (8), 948−961.
(15) Smith, B. D.; Irish, D. E.; Kedzierzawski, P.; Augustynski, J. *J. Electrochem. Soc.* **1997**, *144* (12), 4288−4296.
(16) McQuillan, A. J.; Hendra, P. J.; Fleischmann, M. *J. Electroanal. Chem.* **1975**, *65* (2), 933−944.
(17) Ichinohe, Y.; Wadayama, T.; Hatta, A. *J. Raman Spectrosc.* **1995**, *26* (5), 335−340.
(18) Phillips, J. M.; Leibsle, F. M.; Holder, A. J.; Keith, T. *Surf. Sci.* **2003**, *545* (1−2), 1−7.
(19) Hori, Y.; Murata, A.; Takahashi, R. *J. Chem. Soc., Faraday Trans. 1: Phys. Chem. Condens. Phases* **1989**, *85* (8), 2309−2326.
(20) Kim, J. J.; Summers, D. P.; Frese, K. W., Jr. *J. Electroanal. Chem.* **1988**, *245* (1−2), 223−244.

(21) Peterson, A. A.; Abild-Pedersen, F.; Studt, F.; Rossmeisl, J.; Norskov, J. K. *Energy Environ. Sci.* **2010**, *3* (9), 1311−1315.

(22) Peterson, A. A.; Nørskov, J. K. *J. Phys. Chem. Lett.* **2012**, *3* (2), 251−258.

(23) Nørskov, J. K.; Rossmeisl, J.; Logadottir, A.; Lindqvist, L.; Kitchin, J. R.; Bligaard, T.; Jónsson, H. *J. Phys. Chem. B* **2004**, *108* (46), 17886−17892.

(24) Kresse, G.; Furthmüller, J. *Phys. Rev. B* **1996**, *54* (16), 11169−11186.

(25) Kresse, G.; Furthmüller, J. *Comput. Mater. Sci.* **1996**, *6* (1), 15−50.

(26) Nørskov, J. K.; Bligaard, T.; Logadottir, A.; Bahn, S.; Hansen, L. B.; Bollinger, M.; Bengaard, H.; Hammer, B.; Sljivancanin, Z.; Mavrikakis, M.; Xu, Y.; Dahl, S.; Jacobsen, C. J. H. *J. Catal.* **2002**, *209* (2), 275−278.

(27) Ruban, A. V.; Skriver, H. L.; Nørskov, J. K. *Phys. Rev. B* **1999**, *59* (24), 15990−16000.

(28) Perdew, J. P.; Burke, K.; Ernzerhof, M. *Phys. Rev. Lett.* **1996**, *77* (18), 3865−3868.

(29) Perdew, J. P.; Burke, K.; Ernzerhof, M. *Phys. Rev. Lett.* **1997**, *78* (7), 1396−1396.

(30) Blöchl, P. E. *Phys. Rev. B* **1994**, *50* (24), 17953.

(31) Kresse, G.; Joubert, D. *Phys. Rev. B* **1999**, *59* (3), 1758.

(32) Henkelman, G.; Jonsson, H. *J. Chem. Phys.* **2000**, *113* (22), 9978−9985.

(33) Henkelman, G.; Jonsson, H. *J. Chem. Phys.* **1999**, *111* (15), 7010−7022.

(34) Schouten, K. J. P.; Kwon, Y.; van der Ham, C. J. M.; Qin, Z.; Koper, M. T. M. *Chem. Sci.* **2011**, *2* (10), 1902−1909.

(35) Christophe, J.; Doneux, T.; Buess-Herman, C. *Electrocatalysis* **2012**, *3* (2), 139−146.

(36) Xu, Z.; Lai, E.; Shao-Horn, Y.; Hamad-Schifferli, K. *Chem. Commun.* **2012**, *48* (45), 5626−5628.

Supplementary Information for "Electroreduction of carbon dioxide to methane on copper, copper-silver and copper-gold catalysts: A DFT study"

Pussana Hirunsit

National Nanotechnology Center (NANOTEC), 111 Thailand Science Park, Phaholyothin Road,
Klong 1, Klong Luang, Pathumthani 12120, Thailand

Table S1. Adsorption energy of intermediate species, *B.E*, on Cu(211), $Cu_3Ag(211)$, and $Cu_3Au(211)$ in eV.

	Cu(211)		$Cu_3Ag(211)$		$Cu_3Au(211)$	
species	configuration	*B.E*	configuration	*B.E*	configuration	*B.E*
O	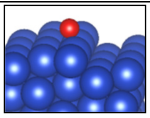	0.77	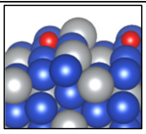	0.88	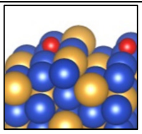	1.13
H	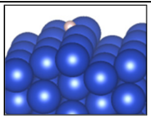	-0.28	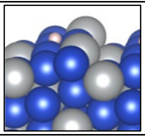	-0.19	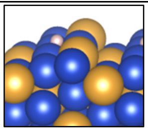	-0.17
C	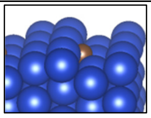	2.05	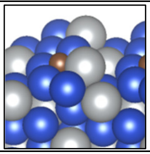	2.85	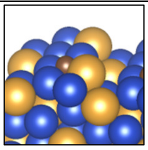	2.91
OH	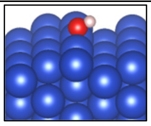	-0.28	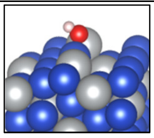	0.05	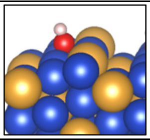	0.24
CO	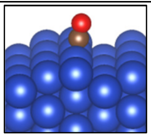	0.93	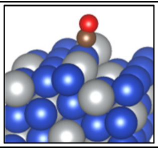	1.05	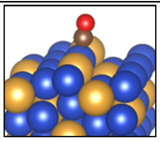	1.12
CH	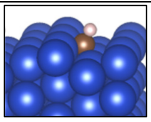	1.01	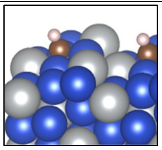	1.35	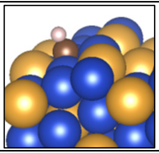	1.55
CH_2	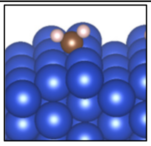	0.53	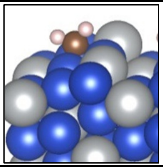	0.77	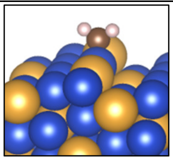	0.79
COH	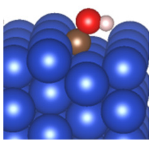	1.91	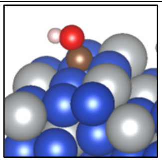	2.00	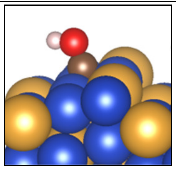	2.12

	$Cu(211)$		$Cu_3Ag(211)$		$Cu_3Au(211)$	
species	configuration	*B.E*	configuration	*B.E*	configuration	*B.E*
HCO	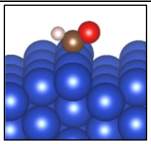	1.43	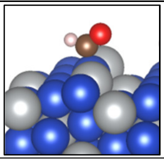	1.51	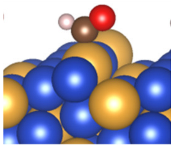	1.45
HCOH	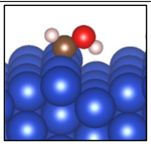	1.18	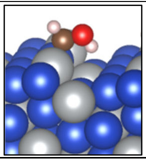	1.45	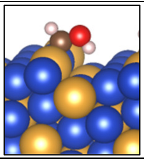	1.37
HOCO	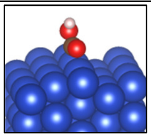	1.04	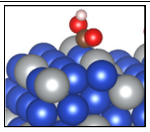	1.26	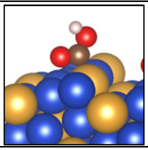	1.51
CH_3	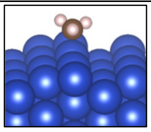	-0.61	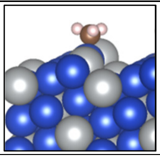	-0.39	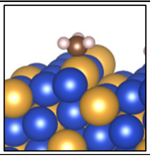	-0.40
OCH_2	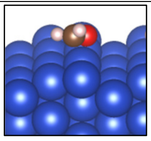	0.83	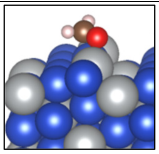	1.06	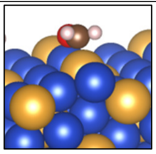	1.01
OCH_3	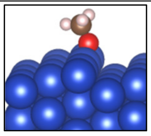	-0.27	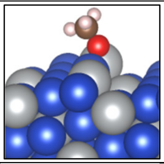	0.07	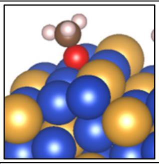	0.16
[a] CO* + H*	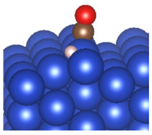	0.68	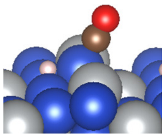	0.86	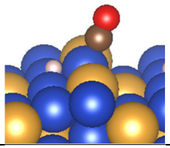	0.99
[a] HCO* + H*	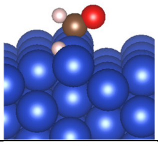	1.15	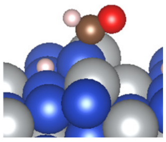	1.44	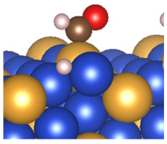	1.33
[a] CH* + OH*	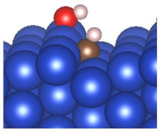	0.94	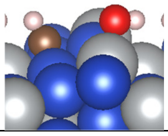	1.54	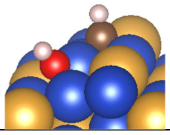	1.85

$$B.E = E_{total(C_xH_yO_z)} - E_{slab} - xE(C) - yE(H) - zE(O)$$

Where $E_{total(C_xH_yO_z)}$ is the total energy of the state, E_{slab} is the energy of the clean slab, $E(C)$is energy of C atom referenced to graphene, $E(H)$ is the energy of H atom referenced to $1/2H_2$ and $E(O)$ is the energy of O atom referenced to $(H_2O - H_2)$

[a] The adsorption energies corresponds to the co-adsorption of the two adsorbates.

Table S2. Calculated zero-point energy correction, enthalpic temperature and entropic corrections for adsorbed species.

adsorbed species	ZPE (eV)	$\int C_p dT$ (eV)	$-TS$ (eV)	ZPE + $\int C_p dT - TS$ (eV)
H*	0.160	0.005	-0.007	0.158
O*	0.072	0.025	-0.038	0.059
C*	0.097	0.017	-0.025	0.089
OH*	0.364	0.046	-0.079	0.331
CO*	0.192	0.076	-0.153	0.115
HCO*	0.444	0.086	-0.184	0.346
COH*	0.451	0.068	-0.110	0.409
HOCO*	0.624	0.096	-0.178	0.542
HCOH*	0.765	0.068	-0.109	0.724
OCH_2*	0.758	0.091	-0.190	0.659
OCH_3*	1.108	0.093	-0.179	1.022
CH*	0.348	0.028	-0.039	0.337
CH_2*	0.589	0.049	-0.075	0.563
CH_3*	0.900	0.060	-0.096	0.864

Table S3. Calculated zero-point energy correction, enthalpic temperature and entropic corrections for gas-phase species taken from ref [1].

adsorbed species	ZPE (eV)	$\int C_p dT$ (eV)	$-TS$ (eV)	ZPE + $\int C_p dT - TS$ (eV)
H_2	0.27	0.09	-0.42	-0.06
CO_2	0.31	0.10	-0.65	-0.24
H_2O	0.58	0.10	-0.65	0.03
CH_4	1.20	0.10	-0.06	1.24

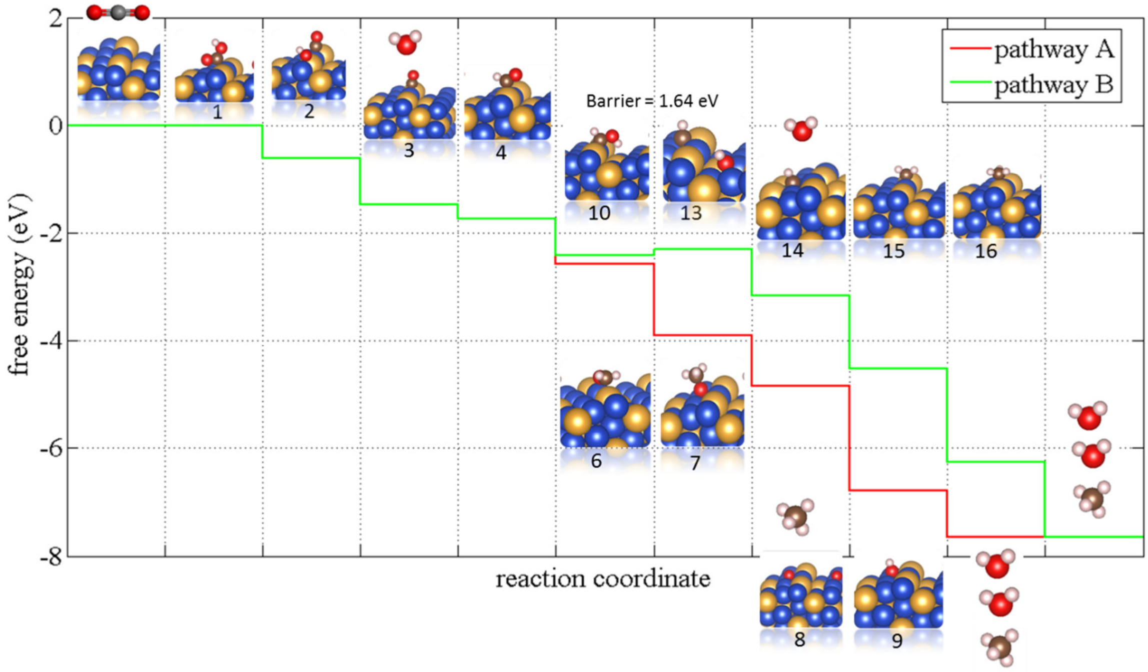

Figure S1. $Cu_3Au(211)$ free energy diagram following reaction steps in pathway A and pathway B at limiting potential U = -0.86 V_{RHE}.

Table S4. Transition state structures corresponding to the calculated barrier energies shown in Table 1.

Elementary step	Cu(211)		Cu$_3$Ag (211)		Cu$_3$Au (211)	
	Ea		Ea		Ea	
H* + CO* → HCO*	+0.96	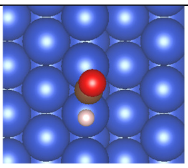	+0.48	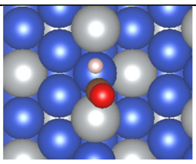	+0.98	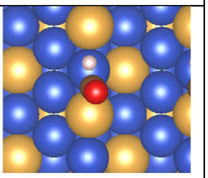
HCO* + H* → OCH$_2$*	+0.66	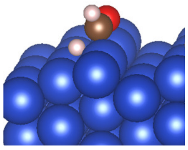	+0.37	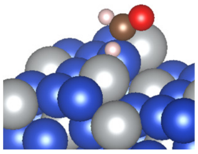	+0.66	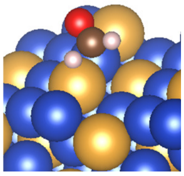
HCO* + H* → HCOH*	+0.60	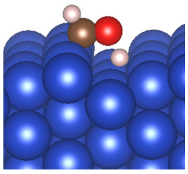	+0.74	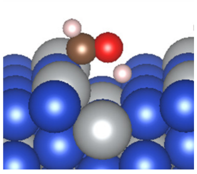	+0.72	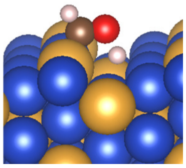
HCOH* → CH* + OH*	+1.37	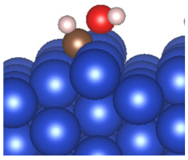	+1.20	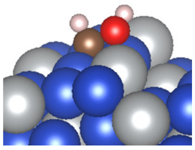	+1.64	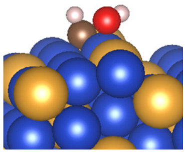

Reference

1. Peterson, A.A., et al., *How copper catalyzes the electroreduction of carbon dioxide into hydrocarbon fuels.* Energy & Environmental Science, 2010. **3**(9): p. 1311-1315.

THE JOURNAL OF PHYSICAL CHEMISTRY C

Article

pubs.acs.org/JPCC

CO_2 Electrochemical Reduction to Methane and Methanol on Copper-Based Alloys: Theoretical Insight

Pussana Hirunsit,*,[†] Wiwaporn Soodsawang,[†] and Jumras Limtrakul[‡,§,⊥]

[†] National Nanotechnology Center (NANOTEC), National Science and Technology Development Agency (NSTDA), 111 Thailand Science Park, Thanon Phahonyothin, Tambon Khlong Nueng, Amphoe Khlong Luang, Pathum Thani, Thailand

[‡] Department of Chemistry and NANOTEC Center for Nanoscale Materials Design for Green Nanotechnology, Faculty of Science, Kasetsart University, Bangkok 10900, Thailand

[§] PTT Group Frontier Research Center, PTT Public Company Limited, 555 Vibhavadi Rangsit Road, Chatuchak, Bangkok 10900, Thailand

[⊥] Department of Materials Science and Engineering, Vidyasirimedhi Institute of Science and Technology, Rayong 21210, Thailand

S Supporting Information

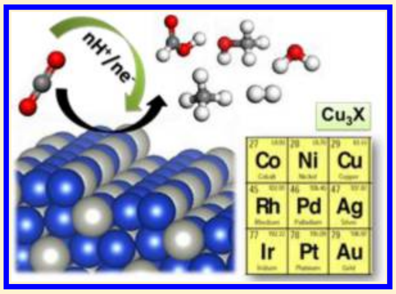

ABSTRACT: We performed a systematic investigation of CO_2 electroreduction to CH_4 and CH_3OH on copper-based alloys stepped surfaces using density functional theory calculations associated with the standard hydrogen electrode model. We determined the correlations between CO adsorption energy and the other key $C_xH_yO_z$ intermediates adsorption energy, the overpotential, the limiting-potential elementary step, and selectivity to CH_4, CH_3OH, HCOOH, and H_2. The electrode efficiency decrease by OH* poisoning and the H_2 evolution is also investigated. The results demonstrate that the CO* protonation is the limiting-potential step on most surfaces, with the exception on Cu_3Au and Cu_3Co surfaces. In spite of the excessive strong CO* interaction on some surfaces, the overpotentials reduce when the degree of CO* adsorption energy and HCO*/COH* adsorption energy decoupling increases. The CO* adsorption energy is a good descriptor for linear scaling correlations with the other $C_xH_yO_z$ intermediates due to the similar charge transfer characteristics of the C−O bond in CO* and those intermediates. The formic acid production can be efficiently catalyzed on Cu_3Pt, Cu_3Ni, Cu_3Co, and Cu_3Rh surfaces. Methanol production is favorable on Cu_3Pd and Cu_3Pt surfaces, yet they show high overpotential (~0.7 V). The key of methanol selectivity is CH_2OH* intermediate formation favorability associated with the preference of CH_2OH* protonation at the C atom over the O atom. The calculations reveal that the electroreduction activity on Cu-based alloys catalysts do not show a volcano-type relation as was previously found on pure metal catalysts.

1. INTRODUCTION

The electroreduction of CO_2 to valuable hydrocarbon products is a promising process that would create a significant impact to the global carbon balance by recycling waste CO_2 into usable hydrocarbons. The critical challenges for the CO_2 electroreduction process are that the reaction must be at a low overpotential as well as being selective. The overpotential is the difference between the applied potential and the equilibrium potential for the reaction. The faradic efficiency and selectivity of CO_2 electroreduction depends on a number of factors; the electrode materials, electrode surface structures, type of ionic species in electrolytes, local pH, and CO_2 concentration on the electrode.[1−9] The electrode material is crucial in that it plays essential roles in determining the overpotential, efficiency, and selectivity. A variety of electrode materials have extensively been examined for CO_2 electroreduction, including ionic liquids,[10] organometallic complexes,[11,12] organic compounds,[13,14] doped graphene,[15] semiconductors,[16] proteins,[17] and enzymes (carbon monoxide dehydrogenase).[18,19] Several excellent reviews provide important research advances regarding catalysis for CO_2 conversion and other important factors as well.[6,9,20−24]

A copper electrode was found to perform the direct reduction of CO_2 to hydrocarbons (methane and ethylene) with a reasonable current density (5−10 mA·cm^{-2}) and current efficiency.[1,24−26] A wider range of hydrocarbons such as ethanol and propanol can also be produced.[1,27−30] The most common reactions and their equilibrium potentials versus RHE (reverse hydrogen electrode) are listed in reactions 1−6. Despite the unique hydrocarbons production from CO_2, copper inefficiently catalyzes CO_2 electroreduction to the point that the overpotential is quite high, approximately 1.0 V. Thermodynamically, the equilibrium potential of CO_2 reduction to CH_4 (reaction 5) is only +0.17 V_{RHE} at 18.5 °C. Nevertheless, it was experimentally shown that the potential of −0.8 V is required for the onset CH_4 production on a copper electrode and −1.0 V is required for a decent current (2 mA·cm^{-2} to CH_4

Received: February 16, 2015
Revised: March 20, 2015
Published: April 7, 2015

DOI: 10.1021/acs.jpcc.5b01574
J. Phys. Chem. C 2015, 119, 8238−8249

production).[31] Hori et al. proposed that the reduction of COH* intermediate, which is formed upon CO* reduction, might be the rate-determining step.[32] Several groups have also shown that the rate-limiting step occurs after the formation of CO*.[33−35] The density functional theory (DFT) calculations by Nørskov's group indicated that the limiting potential step of CO_2 reduction to CH_4 on Cu(211) surface is the protonation of adsorbed CO* to form adsorbed HCO* ($CO^* + H^+ + e^- \rightarrow HCO^*$).[36] The calculations suggested that when the adsorbed HCO* can be stabilized relative to adsorbed CO*, the overpotential can be significantly reduced leading to a more efficient process.

$$CO_2 + 2(H^+ + e^-) \rightarrow HCOOH(aq) \quad U = -0.20\ V_{RHE} \tag{1}$$

$$CO_2 + 2(H^+ + e^-) \rightarrow CO + H_2O \quad U = -0.12\ V_{RHE} \tag{2}$$

$$CO_2 + 4(H^+ + e^-) \rightarrow CH_2O(aq) + H_2O \quad U = -0.07\ V_{RHE} \tag{3}$$

$$CO_2 + 6(H^+ + e^-) \rightarrow CH_3OH(aq) + H_2O \quad U = +0.03\ V_{RHE} \tag{4}$$

$$CO_2 + 8(H^+ + e^-) \rightarrow CH_4 + 2H_2O \quad U = +0.17\ V_{RHE} \tag{5}$$

$$2CO_2 + 12(H^+ + e^-) \rightarrow C_2H_4 + 4H_2O \quad U = +0.08\ V_{RHE} \tag{6}$$

The CO_2 electroreduction on Cu catalyst yields the relatively high selectivity of methane and ethylene formation instead of methanol, while methanol is the majority product for the conventional CO_2 conversion. The selectivity still remains a crucial question. Recently, the DFT calculation of the kinetic barrier of the CO_2 reduction paths by Nie et al.[37,38] revealed that the selectivity step for methane versus methanol on Cu(111) occurs with hydrogenation of CO* to COH* (produce CH_4/C_2H_4) versus CHO* (produces CH_3OH).[37,38] The reduction of CO* to COH* is kinetically favored over CHO* when the potential-dependent barriers for hydrogenating the CO* are evaluated in the presence of a water molecule.[38] The polar O−H bond formation is stabilized through water-assisted proton shuttling coupled with electron transfer.[38] The less polar C−H bond requires direct surface interaction with both C and H at the transition state. Once COH* is produced, it is further reduced to C*, and then reduced to CH_4 and C_2H_4 products on Cu(111).[38] Thus, the proposed reaction path by Nie et al.[37] differs from the one proposed by Peterson et al.[36] for methane production which goes through CH_2O^* and CH_3O^* intermediates. Also, the DFT studies by Nie et al.[37,38] indicate that surface CH_3O^* will kinetically favor methanol production over methane due to higher barriers for methane formation. The methanol formation was also proposed to go through reduction of methanediol which is the hydrated form of formaldehyde.[39] The relative stabilities and rate of formation of CHO* versus COH* are dependent on various parameters, such as Cu surface structure, computational functional and approach of solvation inclusion. The intermediates adsorption is very sensitive to the electrode surface morphology resulting in the voltammetry feature changes and the change in voltage potential of the product formation.[40,41] Although copper is not an ideal catalyst, the understanding of this unique ability of a copper electrode is fruitful for better catalyst design.

In addition, several studies have investigated the pathway leading to C_2 species products and the step determining the favorability between C_1 and C_2 species.[38,42,43] Nevertheless, the reduction reaction mechanism selectively leading to C_1 or C_2 species is still unclear. The previous experiment suggested that on a copper electrode the HCO* is the key intermediate toward the breaking of the C−O bond, leading to C_1 species (methane) production, while the key first step of the C_2 species products such as ethylene and ethanol was suggested to be the formation of CO dimer.[42,44] The DFT calculations by Nie et al. also suggested that the effective barrier for ethylene formation occur at CH_2^* reduction to CH_3^* on Cu(111).[37] Though the rate constant favors ethylene selectivity at lower overpotentials on Cu(111), the relative coverage of CH_2^* and H* will also affect the selectivity and might be expected to further promote methane formation at higher overpotentials.[37] Hansen et al. also predicted that the formation of both CH_4 and C_2H_4 are kinetically feasible from CH_2^* on Cu(211) surface, with CH_4 being more kinetically favorable.[39] The presence of CH_2^* allows for ethylene production from the same path as methane, which matches recent experimental studies[43] that indicate these two products share a common intermediate.

The electroreduction of CO_2 to hydrocarbons takes place on almost all metal electrodes, although the efficiencies and the selectivity are low.[22,45,46] The CO_2 electroreduction using 0.1 M $KHCO_3$ electrolyte and a temperature of 18.5 ± 0.5 °C on various pure metal electrodes demonstrated that CO and formate are the main products on many metal electrodes.[22,46] The CO formation occurred on Cu, Au, Ag, Zn, Pd, Ga, Ni, and Pt and the formate formation took place on Pb, Hg, In, Sn, Cd, and Tl.[22,46] Also, the electrochemical reduction of CO_2 at a low-temperature of 0 °C in 0.05 mol dm^{-3} $KHCO_3$ solution revealed a similar product selectivity group, that CO is mainly produced on Ti, Ni, Ag and Au electrodes and HCOOH is mainly yielded on Cd, In, Sn, Pb, Tl, and Hg electrodes.[45] Also, it was experimentally shown that Zn, Ag, Cu, Ni, and Pt are able to produce both methane and methanol and the selectivity may be determined by the C* and O* binding energy by modifying the surface to favor or disfavor C−O bond breakage.

Furthermore, the electrode potentials of CO_2 reduction on metals are well correlated with the potential of H_2 evolution which is a competitive side reaction and may obstruct the further reduction of hydrocarbon intermediate species.[22,46] Many pure metal electrodes catalyze a major side reaction of H_2 evolution (HER); metals in group VA, VIA, Mn, Re, Fe, Ru, Co, Rh, and Ir.[45] Compared with all metals, Cu is the only metal that produces hydrocarbons (C_xH_y) efficiently. Based on DFT calculations by Nørskov's group, the analysis of CO_2 reduction to CH_4 on transition metals; Cu, Pt, Rh, Pd, Ni, Au, and Ag revealed the "volcano" type of the activity diagram in which Cu is at the top among these metals.[47] The calculations clearly exhibit why Cu is the best-known metal electrocatalyst. Copper exhibits a better ability to perform CO* protonation than the other metals, but this is only associated with the poor activity of the hydrogen evolution reaction (HER), that is, moderate negative potential for HER.[47] They suggested that the key to a substantially improved process efficiency is to find materials that have the binding energy of CO* and the binding energy of products upon CO* protonation (HCO* or COH*) decoupling, which leads to the reduction of the CO* and the protonation potential to be less negative.[47]

Alloying is an approach that may reduce the overpotential. It also leads to a major change in product distribution and faradic efficiency compared to those of the pure metals.[48] Many Cu alloys, Cu−Ni, Cu−Sn, Cu−Pb, Cu−Zn, Cu−Cd, and Cu−Ag, were experimentally studied for the CO_2 reduction in 0.05 M $KHCO_3$ aqueous solution.[48] These alloys were found to have

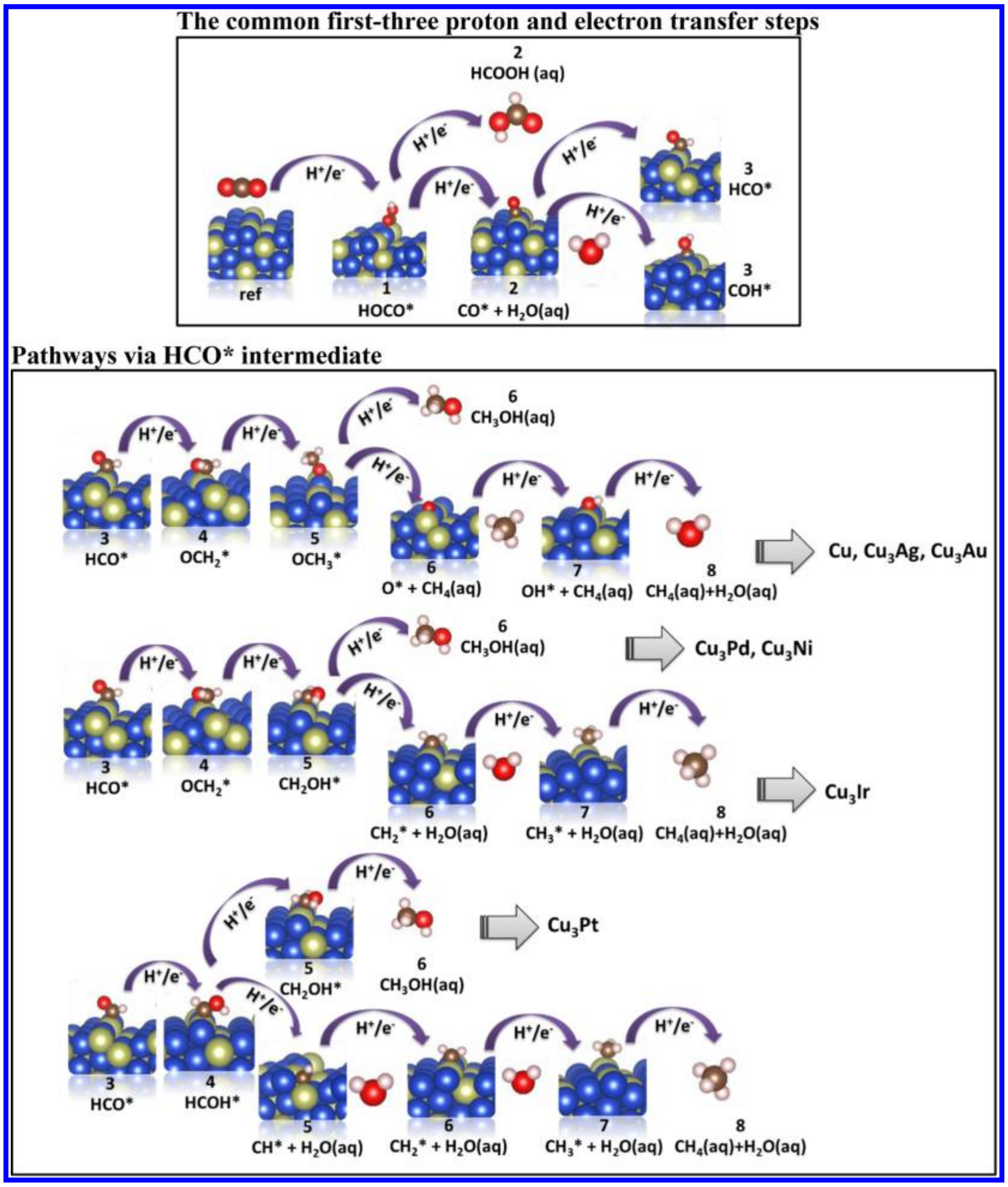

Figure 1. continued

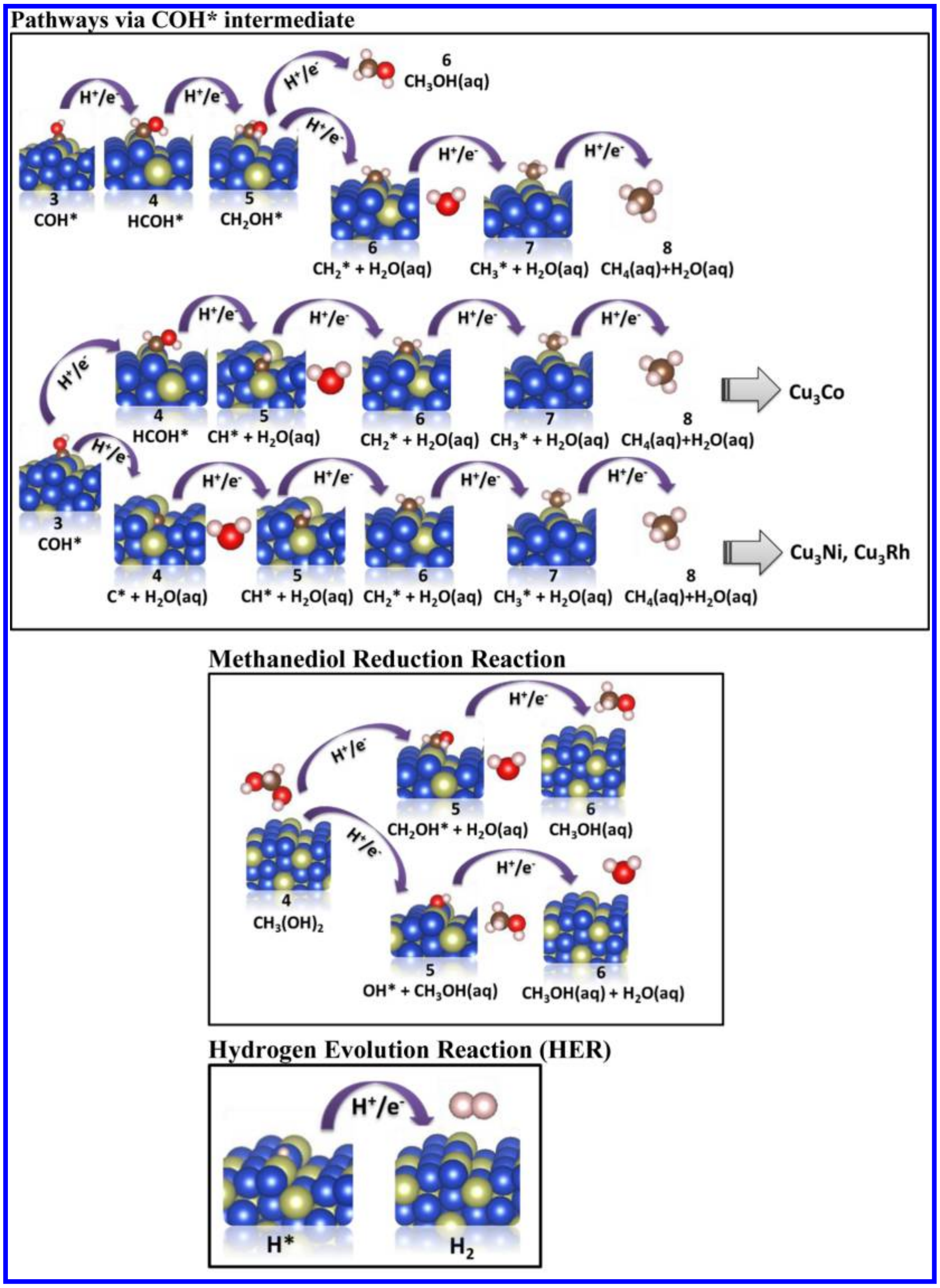

Figure 1. Six and eight protons/electrons transfer step pathways of CO_2 reduction to methanol and methane. The most thermodynamically favorable pathway on each surface is labeled on the right-hand side. The top reaction scheme shows the common first-three electrons/protons transfer step. The second and third reaction scheme shows the further protons and electrons transfer step when the favorable HCO* and COH* intermediate is formed, respectively. The steps for methanediol reduction to methanol/methane and hydrogen evolution reaction (HER) are shown in the last two reaction schemes. Cu atom, blue; X atom, green; C atom, brown; O atom, red; and H atom, white.

selectivity toward CO and HCOOH products.[48] The alloy composition also highly influences the selectivity and product formation potential. Copper−gold alloy showed that the CO production increases markedly with the Au content, while the fraction of CH_4 decreases and the $Au_{50}Cu_{50}$ appears to be the composition giving the most efficient CO_2 conversion and yielding the highest faradic efficiency with CO as the major product.[49] The experimental onset potential of CO_2 electroreduction on the rich-Au nanoparticles (Au_2Cu) was positively shifted, indicating that copper−gold has the potential to lower the energy used for CO_2 conversion.[50] The alloying approach is anticipated to improve the HCO* intermediate stability on the surface leading to a significant reduction in the overpotential. In the previous theoretical work,[51] we found that the overpotential of CO_2 reduction to CH_4 on $Cu_3Au(211)$ is negatively shifted compared to the Cu(211) surface and the potential-limiting step is CO_2 protonation to form HOCO* while the overpotential on $Cu_3Ag(211)$ is similar to that on the Cu(211) surface with the same potential-limiting step of CO* protonation. However, the side reaction of H_2 evolution can pose a challenge on copper−gold and copper−silver alloys with Cu-rich composition.[51] CO is the major product on copper−gold and copper−silver alloys with higher Au and Ag content because it is challenged by the CO* desorption preference over further reduction of CO*.[51]

The exploration for electrocatalyst materials which can primarily meet the requirements of providing a more efficient process and being selective of CO_2 reduction is required for the process to advance. The development of more promising electrode materials requires a fundamental understanding of how electrode materials influence key reaction steps. The preferential adsorption of reactants, intermediates and products on electrode materials essentially contributes to the overpotential, catalytic activity and selectivity. This work aims to perform a systematic thermodynamic investigation of CO_2 electroreduction to CH_4 and CH_3OH on Cu-based alloys with Cu-rich composition of Cu_3X, where X is Ag, Au, Co, Ni, Pd, Pt, Rh, and Ir using DFT calculations associated with the standard hydrogen electrode model.[52] The results of CO_2 conversion to CH_4 on Cu_3Au and Cu_3Ag and pure Cu surfaces were reported in the previous work[51] and are included here again to complete the systematic analysis. The goal of this work is to examine how copper alloying with transition metals modifies the CO_2 electroreduction activity and selectivity compared to that on pure Cu catalyst. The analysis provides useful theoretical insights for a better understanding of the chemical nature of the catalysts which could lead to improved catalyst development. We demonstrated how Cu-based alloys influence the electrocatalytic reactivity, the overpotential, the potential limiting step, the tendency of OH* surface poisoning, H_2 evolution, and the selectivity to formic acid, methane, and methanol products. The calculations suggest that alloying with some metals can reduce the overpotential of methane production and also affect the selectivity of methane, methanol, and formic acid production.

2. COMPUTATIONAL DETAILS

The structures of Cu_3X surfaces are modeled with $L1_2$ crystal lattice structures, where X are metals in groups 9−11, which are Ag, Au, Co, Ni, Pd, Pt, Rh, and Ir. The slab models of stepped (211) surface with a unit cell of 3 × 3 containing six layers of metal atoms and a vacuum region equivalent to more than six atomic layers (approximately 15 Å) were used for a search of the most stable binding sites. The bulk $L1_2$ crystal lattice structure of Cu_3X and the slab model of $Cu_3X(211)$ are shown in Figure S1. The stepped surfaces (211) is chosen because it was generally found to be the most reactive for C−O bond breaking,[53] which is a crucial process here. The two atomic layers from the bottom of the slab were fixed, while the other layers were relaxed to their lowest energy configurations. The fixed layers were set to their bulk bond distances according to their optimized lattice constants that were determined from bulk calculations. The calculated lattice constants in Å are 3.63 (Cu), 3.78 (Cu_3Ag), 3.79 (Cu_3Au), 3.61 (Cu_3Co), 3.70 (Cu_3Ir), 3.60 (Cu_3Ni), 3.72 (Cu_3Pd), 3.73 (Cu_3Pt), and 3.70 (Cu_3Rh).

The impurity Au, Ag, and Pd on the Cu host shows a moderate degree of segregation.[54] Also, the segregation may be induced by the strong affinity toward CO adsorption on those impurity metals. It should be noted that the segregation may induce the surface and near-surface composition change. The systematic investigation of Cu_3X in this work exhibits how the alloying effect produces a considerably different electrocatalytic activity trend from that found previously on pure metals and changes hydrocarbon products selectivity.

The fully periodic plane-wave DFT calculations as implemented in the Vienna Ab Initio Simulation Program (VASP)[55,56] were employed. Spin-polarized DFT calculations were performed with the exchange-correlation functional Perdew−Burke−Ernzerhof (PBE)[57,58] described within the generalized gradient approximation implemented with the projector augmented wave function (PAW)[59,60] method for representing the nonvalence core electrons. The calculations employed 5 × 5 × 1 *k*-points Monkhorst−Pack mesh sampling in the surface Brillouin zone. The plane-wave cutoff energy was optimized at 400 eV. The results were checked for convergence with respect to the energy cutoff and number of *k*-points. The Methfessel−Paxton smearing of order 2 with a value of smearing parameter σ of 0.2 eV was applied. The convergence criteria for electronic self-consistent iteration were set to 1.5×10^{-7} eV and the ionic relaxation loop was limited for all forces smaller than 0.035 eV/Å for free atoms.

The free energy diagrams of the electrochemical reactions for a given surface at 291.65 K were constructed according to the method proposed by Nørskov et al.[52] The method successfully described the overpotential of the oxygen reduction reaction on metal surfaces and CO_2 reduction to be methane on the Cu(211) surface.[36,52] Details of calculations are described very well in Peterson et al.[36] Also, our previous work[51] includes the calculation details, the applied values of zero-point energy (ZPE), $\int C_p dT$ and $T\Delta S$ correction terms of all adsorbed species and gas-phase species and the parameters taking into account the solvation effect on the adsorbate stabilization. The method[52] sets the reference potential to be the standard hydrogen electrode (SHE). This means, at $U \neq 0$, the free energy of the proton−electron pair can be treated by shifting the energy by $-eU$, where U is the electrode potential relative to SHE. The reference electrode in this work is the theoretical reversible hydrogen electrode (RHE), which can relate to the standard hydrogen electrode (SHE) as $U_{RHE} = U_{SHE} - (kT \times \text{pH} \times \ln 10)$, where the pH value in this work is 6.8.

3. RESULTS AND DISCUSSION

Figure 1 shows the eight and six electrons and protons transferred pathways for CO_2 reduction to methane and methanol, which are investigated in this work. The pathways share the common first-three proton and electron transfer steps (seen in the top reaction scheme in Figure 1) of (i) CO_2 protonation to be HOCO* (ii) the protonation of HOCO* to be HCOOH or to form CO* + H_2O(aq) and (iii) the protonation of CO* at C to form HCO* or at O to form COH. The second and third reaction scheme in Figure 1 shows the further proton and electron transfer steps when HCO* is favorable and when COH* is favorable, respectively. The protonation of HCO* (the second reaction scheme in Figure 1) at the C atom can form formaldehyde (OCH_2*) or at the O atom to form HCOH* leading to methane and methanol production. The protonation of COH* (the third reaction scheme in Figure 1) at the C atom can yield HCOH* or at the

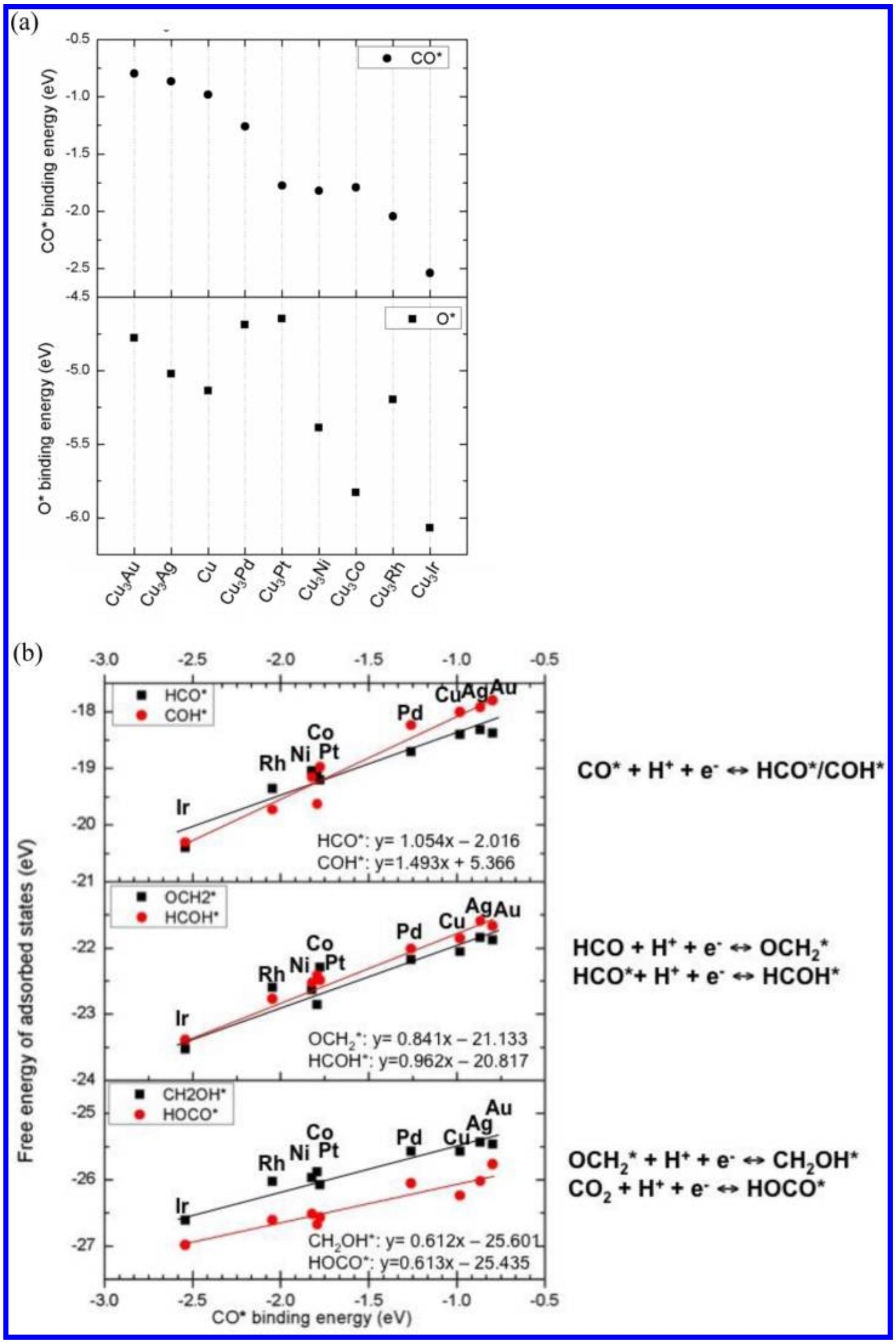

Figure 2. (a) CO* and O* binding energy (b) Linear scaling correlations of the free energy of the adsorbed HCO*, COH*, OCH_2*, HCOH*, CH_2OH*, and HOCO* on Cu_3X surfaces as a function of CO* binding energy. The X element is labeled at the data point. The binding energy is calculated by $E_{total} - E_{clean\ slab} - E_{isolated\ adsorbate(gas)}$. The free energy of the adsorbed states is calculated by $E_{total} - E_{clean\ slab}$ + (ZPE, entropy and enthalpy corrections). The binding is stronger with the more negative binding energy.

O atom can yield C*+H_2O leading to methane and methanol production as well. The theoretical work based on DFT calculations by Nørskov et al.[36,41] suggested that the lowest free energy pathway from CO_2 to CH_4 on Cu(211) surface proceeds through the adsorbed formaldehyde intermediate and methane production is more energetically favorable than methanol production. However, this disagrees with the experimental results that formaldehyde reduction leads to methanol product rather than methane.[44] Recently, Nørskov et al.[39] has suggested that methanol is possibly formed by the reduction of methanediol rather than formaldehyde, which could explain the contradiction. Their calculations showed that methandiol which is formed by hydration of formaldehyde is selectively reduced to methanol. Thus, methanol may be formed by reduction of methanediol rather than by reduction of adsorbed formaldehyde. This means the calculation results do not necessarily contradict the suggestion that CO/CO_2 reduction on Cu(211) surface goes through adsorbed formaldehyde intermediate to yield methane. In this work, we also include the investigation of methanediol reduction to methanol and hydrogen evolution reaction, which is a competitive side reaction.

3.1. Surface Interaction with Intermediate Species.

The affinity relation between intermediates and surfaces are of importance to the free energy change of the elementary steps. We begin with the analysis of the interaction between the key intermediates and the alloy surfaces (Figure 2). The most favorable adsorption configurations and adsorption energies of all intermediate species on Cu_3X surfaces are shown in Tables S1−S3 of Supporting Information. It was previously reported that the pure Au and Ag surfaces show weaker CO* interaction compared to that on the pure Cu surface, but the other pure metal surfaces (i.e., Pd, Pt, Ni, Rh, and Ir) show stronger CO* interaction.[47] Alloying the transition metals with copper reveals a similar general trend of CO* interaction with the pure metal surfaces. Figure 2a (top) shows that the CO* binding on Cu_3Ag and Cu_3Au surfaces are weaker than that on pure Cu surface and the CO* binding on the other alloy surfaces are stronger. The CO* intermediate binds strongest on Cu_3Ir and Cu_3Rh surfaces. The CO* adsorption energies on Cu_3Pt, Cu_3Ni and Cu_3Co are comparable. The O* binding energy trend on Cu_3X surfaces (Figure 2a) is similar to that of pure metals. Alloying Cu with metals which have weaker O* adsorption than Cu, namely, Ag, Au, Pd, and Pt, remain to have relatively weak O* adsorption and vice versa for the metals with strong O* adsorption, namely, Ni, Co, Rh, and Ir. In addition, we found that the high affinity of CO* with Cu, Pd, Co, and Rh may influence the segregation, resulting in relatively high composition of those metals on the surface and near surface atomic layers. The calculations show that the binding energy can be affected by the composition change. The CO* binding energies on the segregated structures (Figure S2, Supporting Information) are weaker than those on the nonsegregated structures by 0.02, 0.06, and 0.16 eV on Cu_3Pd, Cu_3Co and Cu_3Rh, respectively. The CO* binding energy on segregated Cu_3Ag structure is stronger than that on the nonsegregated structure by 0.02 eV. The sensitivity of CO* binding energy to the change of surface composition due to segregation tends to increase on the surface with relatively strong CO* interaction.

The good linear scaling correlations between the CO* binding energy and the surface interaction with the other key intermediates, that is, HCO*, COH*, OCH_2*, HCOH*, CH_2OH, and HOCO* on Cu_3X surfaces can be obtained as shown in Figure 2b. The coefficients determination (R^2) are in the range of 0.90−0.98, which represents a very strong relation between CO* binding energy and the surface interaction with those key intermediates. Similarly, the good correlation between adsorption energies of CO* and HCO* on pure transition metal (TM) surfaces was previously found as well.[47] Interestingly, the CO* interacts with the surfaces through the C atom, thus the CO* binding energies also show good linear scaling correlations with C* binding energies but very poor correlation with O* binding energies (Figure S3, Supporting Information). Although, the intermediate HCO* and COH* binds to the alloy surfaces through the C atom, HCO*/COH* binding energies do not correlate with C* binding energies. Yet, they show very good correlation with CO* binding energies.

The protonation of CO* forming HCO*/COH* is a crucial step. It was previously reported to be the limiting-potential step on pure Cu, Pd, Ni, Rh, Pt, and Cu_3Ag surfaces.[36,47,51] The favorability of CO* protonation products between HCO* and COH* can be affected by alloying. Alloying Rh and Co with Cu results in COH* being more stable. The stability of HCO* and COH* is comparable on Cu_3Ni surface. It is interesting that the relatively higher stability of COH* than HCO* may occur on catalysts with relatively strong CO* interaction energy (Figure 2b). Also, it was previously reported that the HCO* or COH* favorability may be affected by the solvation effect through water-assisted proton shuttling coupled with electron transfer.[37] We also found that the favorability of HCO* or COH* formation carries on, being the same on the segregated and nonsegregated structures. The sensitivity of HCO* binding energy due to segregation is low (<0.05 eV) on the surfaces with weak CO* interaction and it is large (>0.1 eV) on the surfaces with strong CO* interaction such as Cu_3Pd and Cu_3Co surfaces. The sensitivity of COH* binding energy due to segregation is larger so that the binding energy change ranges between 0.1 and 0.4 eV. Furthermore, the protonation of CO_2 to produce HOCO* was previously reported to be the limiting-potential step on pure Au, Ag, and Cu_3Au surfaces.[47,51] All the alloy surfaces show stronger HOCO* interaction than the Cu_3Au surface (Figure 2b). Thus, the significantly weak HOCO* interaction resulting in the CO_2 protonation to yield HOCO*, which proves to be the limiting-potential step, should not be problematic on the other alloy surfaces.

The electronic structures facilitate the understanding of the nature of CO bonding with the alloys surfaces. The charge density difference of CO* adsorption (Figure 3) on the Cu surface shows significant electron transfer from Cu surface atoms to C atom. However, on the Cu_3Co surface, electrons are mostly transferred from the Co surface atoms to the C atom rather than from the Cu surface atoms. The CO* adsorption trend on metal surfaces qualitatively agrees with the surface *d*-band center energy level trend (Table S4 of Supporting Information). The trends can be ascribed to the interaction between the metal *d* states and the CO $2\pi^*$ and 5σ states.[61] The *d*-band center energy levels of Cu_3Au and Cu_3Ag shift to lower energy than that of the Cu surface whereas the *d*-band center energy levels of the other alloy surfaces shift to higher energy compared to the Cu surface. This corresponds to the weaker chemisorption of CO* on Cu_3Ag and Cu_3Au surfaces than that on the Cu surface, whereas CO* adsorption is relatively stronger on the other alloy surfaces. Also, the *d* states

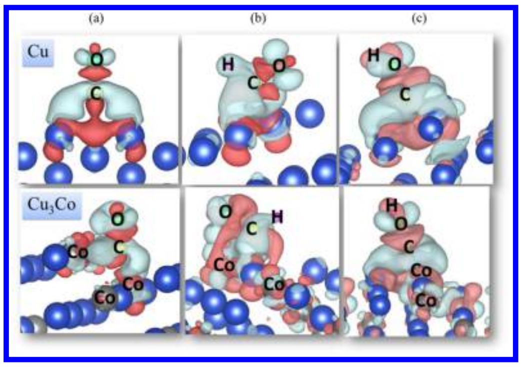

Figure 3. Isosurface of charge density differences of (a) CO* adsorption with the isosurface value of ±0.005 eV/Å^3; (b) HCO* adsorption with the isosurface value of ±0.002 eV/Å^3; and (c) COH* adsorption with the isosurface value of ±0.001 eV/Å^3. The top row is the adsorption on Cu(211) surface and the bottom row is the adsorption on Cu_3Co(211) surface. Red and green colors represent charge depletion and accumulation, respectively. The blue atom is Cu and the gray atom is Co.

Table 1. Summary of the Most Favorable Pathway, The Calculated Limiting-Potential Voltage, The Limiting-Potential Elementary Step, And the Calculated Onset Potential of H_2O Formation and HER on $Cu_3X(211)$ Surfaces

	most favorable pathway	limiting-potential elementary step	onset potential of the limiting-potential step (V_{RHE})	onset potential of $OH^* + H^+ + e^- \rightarrow H_2O$ (V_{RHE})	onset potential of HER (V_{RHE})
Cu	CH_4	$CO^* + H^+ + e^- \rightarrow HCO^*$	−0.75	−0.31	−0.10
Cu_3Au	CH_4	$CO_2 + H^+ + e^- \rightarrow HOCO^*$	−0.86	0.21	0.02
Cu_3Ag	CH_4	$CO^* + H^+ + e^- \rightarrow HCO^*$	−0.72	0.02	−0.01
Cu_3Pd	CH_3OH	$CO^* + H^+ + e^- \rightarrow HCO^*$	−0.72	0.16	−0.12
Cu_3Pt	CH_3OH	$CO^* + H^+ + e^- \rightarrow HCO^*$	−0.74	0.17	−0.21
Cu_3Ni	CH_4	$CO^* + H^+ + e^- \rightarrow COH^*$	-0.85	−0.44	−0.28
	CH_3OH	$CO^* + H^+ + e^- \rightarrow HCO^*$	−0.95		
Cu_3Co	CH_4	$COH^* + H^+ + e^- \rightarrow HCOH^*$	−0.67	−0.66	−0.27
		$OH^* + H^+ + e^- \rightarrow H_2O$	−0.66		
Cu_3Rh	CH_4	$CO^* + H^+ + e^- \rightarrow COH^*$	−0.49	−0.15	−0.42
Cu_3Ir	CH_4	$CO^* + H^+ + e^- \rightarrow HCO^*$	−0.32	−0.31	−0.47
		$OCH_2^* + H^+ + e^- \rightarrow OCH_3^*$	−0.33		

of Cu tends to interact with CO* rather than the *d* states of Au and Ag which manifests in the favorable CO* adsorption site to be on top of Cu on Cu_3Ag and Cu_3Au surfaces (see structures in Table S1 of Supporting Information). Similarly, the *d* states of the other X elements, namely, Pd, Pt, Co, Ni, Rh, and Ir, tend to interact with CO* rather than the *d* states of Cu, which results in the favorable CO* adsorption on a top site of those X atoms or the foot of the step site where CO* interacts with two X atoms (see structures in Tables S2−S3 of Supporting Information).

The common features of charge density difference analysis seen in HCO* and COH* adsorption on both Cu and Cu_3Co surfaces (Figure 3b,c) are that electrons transfer from the Cu surface to the C atom. In Figure 3b, electron accumulation (green) at the C−H bond and the electron depletion (red) at the C−O bond can be observed upon HCO* adsorption, whereas in Figure 3c, electron depletion (red) occurs at C−O and O−H bond upon COH* adsorption. Thus, electron depletion at both O−H and C−O bonds in COH* adsorption may induce the preference to COH* formation on a surface with a relatively high *d*-band center energy level and strong CO* adsorption, namely, Cu_3Ni, Cu_3Co, Cu_3Rh, and Cu_3Ir. Yet, electron accumulation at the C−H bond in HCO* adsorption may bring the favorability of HCO* formation on a surface with a relatively low *d*-band center energy level; namely Cu_3Au, Cu_3Ag, Cu, Cu_3Pd and Cu_3Pt. In addition, the poor correlation between HCO*/COH* adsorption energy with the C* adsorption energy may result from the difference of charge transfer characteristic at the C−H (HCO* adsorption) bond and at the O−H (COH* adsorption) bond. The charge transfer characteristic of the C−O bond in HCO* and COH* adsorption is similar, thus, CO* adsorption energy is a good descriptor for correlations with HCO* and COH* adsorption energy, as well as with OCH_2*, HCOH*, CH_2OH, and HOCO* adsorption energy.

3.2. Pathway Investigation. The investigated CO_2 reduction pathway to produce methane and methanol is shown in Figure 1. The pathways through COH* are considered on Cu_3Co, Cu_3Ni and Cu_3Rh surfaces because COH* formation is more favorable than HCO* formation on those surfaces. The pathways through HCO* are considered on Cu, Cu_3Ag, Cu_3Au, Cu_3Pd, and Cu_3Pt surfaces. The stability of adsorbed HCO* and COH* is comparable on Cu_3Ni and Cu_3Ir in which the free energies of HCO* and COH* states are very close with ∼0.1 eV difference. Thus, the pathways through both HCO* and COH* intermediates are considered on Cu_3Ni and Cu_3Ir surfaces. From a thermodynamic point of view, the limiting-potential indicates the highest electrode potential at which the free energy of every elementary step is downhill and the reaction begins to have an evident rate. By constructing the free energy diagrams as a function of potential, the energetically favorable pathway and the limiting-potential step on surfaces can be indicated. The free energy diagrams at 0 V_{RHE} are shown in Figures S4 and S5 of Supporting Information. The most favorable pathway, the limiting-potential elementary step, the limiting-potential voltage, and the onset potential of HER and the H_2O formation step are summarized in Table 1.

The calculated free energy diagrams indicate that the Cu-based alloy catalysts mostly are more energetically favorable to yield methane than methanol product. Methanol production is found to be favorable on Cu_3Pd, and Cu_3Pt surfaces. On Cu_3Ni surface, the reduction to methanol shows a slightly higher limiting-potential of 0.1 V than the reduction to methane. The CO* protonation producing HCO* or COH* is the limiting-potential step on most surfaces with the exception of Cu_3Au, and Cu_3Co surfaces. The protonation of CO_2 yielding HOCO* is the limiting-potential step on Cu_3Au surface. The water formation step and the protonation of COH* to form HCOH* are the limiting-potential steps on Cu_3Co surface. Figure 4 displays the onset potentials of the CO_2 protonation, CO* protonation, and the formic acid formation step. It can be seen that the overpotentials on Cu_3Co, Cu_3Rh, and Cu_3Ir surfaces are lower than that on pure Cu. The overpotentials on Cu_3Ag, Cu_3Pd, and Cu_3Pt surfaces are similar to that on pure Cu and they show the same limiting-potential step.

The Cu_3Au and Cu_3Ni surfaces show the highest limiting-potential of −0.86 V_{RHE} (Table 1, Figure 4). The very weak HOCO* adsorption on Cu_3Au (Figure 3b) contributes to the high limiting-potential of HOCO* formation. The HOCO* binding energies on the other surfaces are relatively stronger, thus, the HOCO* formation is not a challenging step on the other surfaces. Furthermore, the two protons and electrons transfer steps of CO_2 reduction to formic acid take place at low potential close to the equilibrium potential of formic acid formation (−0.20 V_{RHE}, eq 1) on Cu_3Pt, Cu_3Ni, Cu_3Co, and Cu_3Rh surfaces (Figure 4). This suggests that these surfaces are thermodynamically favorable for HCOOH production. The experiments showed that the addition of 10% Ni into Cu shifts the onset potential of HCOOH production in a positive

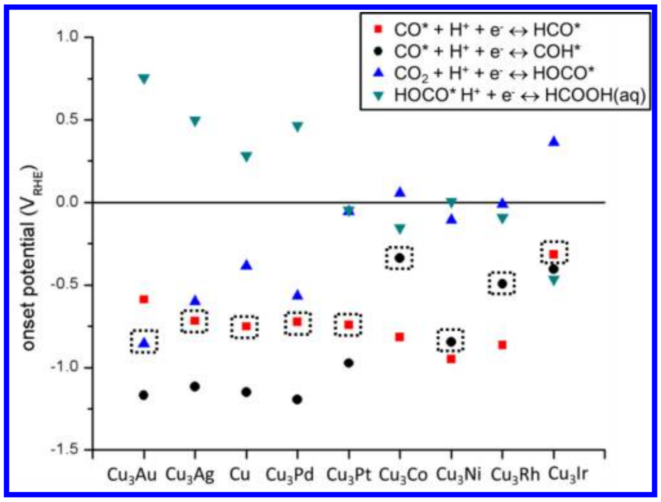

Figure 4. Onset potentials of the CO_2, HOCO*, and CO* protonation step. The dot squares indicate the calculated limiting-potential step on $Cu_3X(211)$ surfaces.

potential direction compared to Cu (~0.2 V).[48] The calculation results show the shift of HCOOH onset potential ~0.3 V on Cu_3Ni compared to Cu. Additionally, Cu−Ni experimentally showed the strong suppression of CO formation and is not a significant effect on faradaic efficiency or the overpotential for production.[48] This may result from the increase efficiency of HCOOH production, and consequently the suppression of CO formation.

The very strong CO* adsorption on Cu_3Ni induces the protonation of CO* to be potentially limited at −0.85 V_{RHE} resulting in a relatively high overpotential for methane production. The Cu_3Co, Cu_3Rh and Cu_3Ir surfaces also show very strong CO* and HCO*/COH* interaction (Figure 2b), however, the onset potentials of CO* protonation step on these surfaces are less negative (−0.3 to −0.5 V_{RHE}) than that on Cu_3Ni surface. The strong adsorption of CO* and HCO*/COH* is not essentially an indicator as to whether the onset potential of CO* protonation is likely to be at high negative potential, yet the relative interaction between CO* and HCO* or COH* on a surface is an important one. The difference in free energies of the adsorbed states of HCO* or COH* referenced on free energies of the adsorbed CO* state on Cu_3Co, Cu_3Rh, and Cu_3Ir are 2.9−3.1 eV, whereas that on Cu_3Ni is 2.55 eV and they are ~2.7 eV on Cu_3Ag, Cu, Cu_3Pt, and Cu_3Pd, which show a similar onset potential of the CO* protonation step. The larger of the free energy differences, the CO* protonation step tends to take place at the less negative onset potential. The lowest calculated onset potential of CO* protonation (−0.32 V_{RHE}) occur on Cu_3Ir surface in which the free energy difference is largest. The higher degree of CO* and HCO*/COH* adsorption energy decoupling pronounces, the onset potential of CO* protonation becomes less negative, which increases the thermodynamic favorability of the CO* protonation step. The theoretical overpotential on pure metal surfaces were shown to have a volcano-type relationship with copper situated near the top.[47] However, the volcano-type relationship is not seen on copper-based alloy surfaces.

3.3. Methanol Production.

The investigated reaction pathways for methanol production, as shown in Figure 1, may proceed through OCH_2*, HCOH* intermediates, and methanediol reduction. The equilibrium potential of $CO_2 + 6H^+ + 6e^- \rightarrow CH_3OH$ (aq) is 0.03 V_{RHE} (eq 4). The free energy diagrams reveal that methanol production is more thermodynamically favorable than methane production on Cu_3Pd and Cu_3Pt surfaces, yet with high overpotential (~0.7 V) for methanol production. The favorable pathway on Cu_3Pd is through OCH_2* intermediate and through HCOH* intermediate on Cu_3Pt. Then, the protonation of OCH_2* and HCOH* yields a common intermediate of CH_2OH*. This may suggest that the key of methanol selectivity is CH_2OH* formation favorability associated with the preference of CH_2OH* protonation at the C atom over the O atom. On Cu_3Ni surface, the most thermodynamically favorable production pathway for methane production proceeds through HCO* and OCH_2* and is only 0.1 V (Table 1) more energetically favorable than the methanol production pathway which goes through COH* intermediate. This comes from the onset potential of HCO* and COH* formation is only 0.1 V difference on Cu_3Ni surface. The surface affinity with key species HCO*/COH* also plays a role on methanol and methane selectivity. In addition, the Cu−Ni alloy with 10% of Ni added was experimentally reported to have CH_3OH production in the potential region from −0.1 to −1.1 V_{RHE} with the maximum production at −0.5 V_{RHE}, whereas it is absent on Cu and Ni catalysts.[48] The calculations in this work suggested that the onset potential of CH_3OH on Cu_3Ni is relatively high at −0.95 V_{RHE} and the OH* removal step initially occurs at −0.44 V_{RHE}, which may allow the high production at this potential.

The reduction of methanediol is also considered (Figure 1). Methanediol is formed via hydration of formaldehyde (OCH_2). At 0.0 V_{RHE}, the reduction of methanediol through CH_2OH* intermediate (the first pathway) is energetically favorable on Cu_3Co, Cu_3Rh, Cu_3Pt, and Cu_3Ni surfaces. Yet, the formation of CH_2OH* is the potential-limiting step on Cu, Cu_3Ag, Cu_3Au, and Cu_3Pd surfaces with the limiting potential of −0.30, −0.21, −0.19, and −0.08 V_{RHE}, respectively. The protonation of CH_2OH* to form CH_3OH is the potential-limiting step on Cu_3Ir surface with the limiting potential of −0.47 V_{RHE}. Additionally, an alternative pathway may occur with the protonation at carbon atoms of methanediol coupling with C−O breaking; $CH_2(OH)_2 + H^+ + e^- \rightarrow CH_3OH + OH^*$. The OH* removal step is an important one for this pathway. This alternative pathway is the lowest free energy pathway to produce CH_3OH at 0.0 V_{RHE} on most surfaces except Cu_3Pt and Cu_3Ir surfaces. However, the OH* removal step is a challenging step on Cu, Cu_3Ni, Cu_3Co, and Cu_3Rh surfaces, where the onset OH* removal step takes place at negative potentials (Table 1).

3.4. H_2 Evolution and OH Removal.

The OH* protonation to form water is a significant elementary step to inhibit the catalytic activity decrease via surface OH* poisoning. The OH* removal step to form H_2O is the potential-limiting step on Cu_3Co due to the excessively strong OH* binding energy (Figure 5). The OH* and H* binding energies are shown in Figure 5. Although the OH* removal step is not the potential-limiting step on the other surfaces with relatively high affinities for OH* (Figure 5), namely, Cu, Cu_3Ni, Cu_3Rh, and Cu_3Ir, the surfaces may be poisoned by OH* species due to the relatively high negative onset potential of the step (−0.2 to −0.7 V_{RHE}, Table 1). Thus, surface OH* poisoning may occur on the surface of Cu alloying with high OH affinity metals, namely, Co, Ni, Rh, and Ir. Likewise, alloying Cu with less affinity toward OH, namely, Au, Ag, Pd, and Pt metals improve

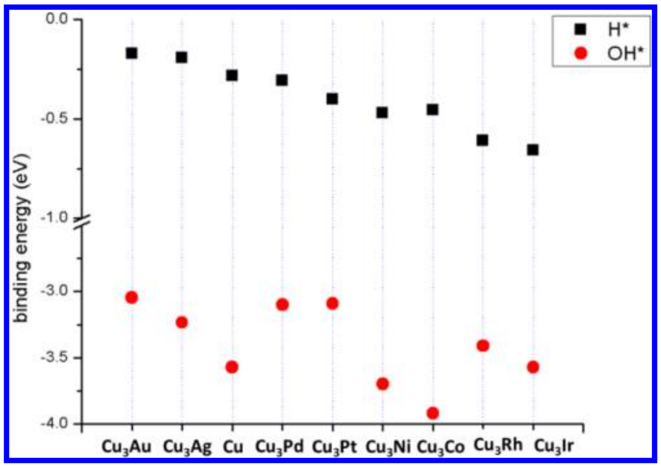

Figure 5. OH* and H* binding energies on Cu$_3$X(211) surfaces. The binding energy is calculated by $E_{\text{total}} - E_{\text{clean slab}} - E_{\text{isolated adsorbate(gas)}}$.

the OH* removal step and prove to be more efficient than pure Cu.

Furthermore, the efficient CO$_2$ conversion catalyst would be expected to not overly catalyze HER and therefore dominate over CO$_2$ reduction; consequently, the surface may mostly be covered by adsorbed H*. Also, the high activity of HER may lead to surface CO* poisoning which the adsorbed CO* is not further reduced. The pure Pd and Pt surfaces were experimentally shown to mainly produce CO and HCOOH and prevent further CO$_2$ reduction with significant H$_2$ evolved as a side reaction.[46] The pure Co, Rh, and Ir electrodes were experimentally shown to mainly produce H$_2$.[45] The HER on all alloy surfaces occurs at more negative potential than that on pure Cu with the exception on Cu$_3$Au and Cu$_3$Ag surfaces (Table 1). The approximately 0.0 V$_{\text{RHE}}$ of HER onset potential on Cu$_3$Ag and Cu$_3$Au surfaces possibly lead to much higher selectivity of H$_2$ on these surfaces.

The calculated HER on Cu surface is −0.1 V$_{\text{RHE}}$, but almost entirely H$_2$ production on Cu is experimentally[31] observed at approximately −0.5 V$_{\text{RHE}}$. This may result from H*, O*, and OH* binding to the same step sites and it would require the OH* removal step taking place in order to clear adsorbed OH* and enable H$_2$ evolution.[36] Similar to the Cu surface, the H$_2$ production on Cu$_3$Ni and Cu$_3$Co would occur at a more negative potential than the calculated HER onset potential shown in Table 1 and take place approximately at the onset potentials of their OH* removal step. Therefore, compared to the Cu surface, the HER would be suppressed due to high OH* coverage on the surfaces when alloying Cu with Ni, Co, and Ir. The H* binding energies shown in Figure 5 demonstrate that only H* on Cu$_3$Ag and Cu$_3$Au surfaces binds more weakly than on pure Cu surface. Thus, the Cu alloying results in the suppression of HER with the exception on Cu$_3$Ag and Cu$_3$Au surfaces.

4. CONCLUSIONS

This work systematically investigated thermodynamics of CO$_2$ electroreduction to methane and methanol on copper-based alloys (Cu$_3$X), where X are metals in groups 9−11 using DFT calculations associated with the standard hydrogen electrode model. The affinity relation between intermediates and surfaces are crucial to the free energy change of the elementary steps, consequently, determining the overpotential, the potential-limiting step, and the selectivity. The key intermediates are CO*, HCO*, COH*, CH$_2$OH*, HOCO*, OH*, and H*, and their interactions with the catalysts are required to be optimum in order to efficiently catalyze CO$_2$ conversion to methane and methanol, suppress H$_2$ production, and avoid OH* surface poisoning.

The CO* protonation producing HCO* or COH* is the limiting-potential step on most surfaces with the exception on Cu$_3$Au and Cu$_3$Co surfaces. In spite of the excessive strong CO* interaction which is even higher than that on pure Cu, the onset potentials of the CO* protonation step on Cu$_3$Co, Cu$_3$Rh, and Cu$_3$Ir surfaces can be at less negative potential than that on pure Cu surface. The strong adsorption of CO* and HCO*/COH* is not necessarily an indicator as to whether the onset potential of CO* protonation is likely to be at high negative potential. Instead, the higher degree of CO* adsorption energy and HCO*/COH* adsorption energy decoupling produces, the onset potential of CO* protonation becomes less negative. This shows that the CO* protonation step becomes more efficient. The selectivity between HCO* and COH* formation upon CO* protonation can be affected by alloying. The relatively higher stability of COH* than HCO* can be found on the surfaces with relatively strong CO* adsorption because they allow a relatively high degree of electron transfer to CO* corresponding to the electron deficiency at the O−H bond of COH*. The charge transfer characteristics of the C−O bond in HCO* and COH* adsorption is similar to that of CO*; therefore, CO* adsorption energy is a good descriptor for linear scaling correlations with HCO* and COH* adsorption energies, as well as with the other key intermediates of OCH$_2$*, HCOH*, CH$_2$OH*, and HOCO* binding energies. The selectivity of HCO* and COH* intermediates was not found to change due to the change of surface and near-surface compositions caused by segregation. Yet, the sensitivity of CO*, HCO*, and COH* binding energies to the change of surface and near-surface compositions can be somewhat significant.

The Cu-based alloy catalysts mostly are more energetically favorable to yield methane than methanol product, except on Cu$_3$Pd and Cu$_3$Pt surfaces. The protonation of CO$_2$ yielding HOCO* is the limiting-potential step on Cu$_3$Au due to the significant weak HOCO* adsorption. The water formation step and the protonation of COH* to form HCOH* are the limiting-potential steps on Cu$_3$Co surface. The two proton and electron transfer steps of CO$_2$ reduction to yield formic acid takes place at low potential close to the equilibrium potential of formic acid formation on Cu$_3$Pt, Cu$_3$Ni, Cu$_3$Co, and Cu$_3$Rh surfaces. Thus, it suggests that these surfaces are thermodynamically favorable for formic acid production.

Methanol production is found to be more favorable than methane production on Cu$_3$Pd and Cu$_3$Pt surfaces, yet they show high overpotential (~0.7 V). Both surfaces show that the key of methanol selectivity is CH$_2$OH* intermediate formation favorability associated with the preference of CH$_2$OH* protonation at the C atom over the O atom. The reduction of methanediol to methanol is energetically favorable at 0.0 V$_{\text{RHE}}$ on most Cu-based alloy surfaces. However, the OH* removal step is a significant and challenging step in which its onset potential may take place at negative potentials resulting in OH* surface poisoning.

Alloying Cu with high OH affinity metals, namely, Co, Ni, Ir, and Rh, worsen surface OH* poisoning compared to pure Cu surface, yet it possibly suppresses the HER. Likewise, alloying Cu with less affinity toward OH, namely, Au, Ag, Pd, and Pt, improves the OH* removal step to be more efficient than pure Cu, yet it may promote the HER. The HER on all alloy surfaces occurs at more negative potential than that on pure Cu, with the exception on Cu_3Au and Cu_3Ag surfaces where HER is very efficient with the onset potentials at ∼0.0 V_{RHE}.

■ ASSOCIATED CONTENT

Ⓢ Supporting Information

Clean surface model structures, adsorption energies, and configurations of adsorbed intermediate species, structures of CO* adsorption on segregated structures, plots between CO* binding energies and C* or O* binding energies, surface *d*-band center energy levels, and free energy diagrams of the most favorable CH_4 and CH_3OH pathway and the reduction of methanediol at 0 V_{RHE}. This material is available free of charge via the Internet at http://pubs.acs.org.

■ AUTHOR INFORMATION

Corresponding Author

*E-mail: pussana@nanotec.or.th.

Notes

The authors declare no competing financial interest.

■ ACKNOWLEDGMENTS

P.H. would like to thank Prof. Perla B. Balbuena (Texas A&M University) for her suggestions for the project proposal. P.H. thanks Mr. Robert Rose for his grammatical editorial assistance. The authors acknowledge the financial support from Thailand Research Funding (TRF) and the National Nanotechnology Center (NANOTEC), and the computing resource from National e-Science Infrastructure Consortium.

■ REFERENCES

(1) Kuhl, K. P.; Cave, E. R.; Abram, D. N.; Jaramillo, T. F. New Insights into the Electrochemical Reduction of Carbon Dioxide on Metallic Copper Surfaces. *Energy Environ. Sci.* **2012**, *5*, 7050−7059.

(2) Schouten, K. J. P.; Pérez Gallent, E.; Koper, M. T. M. Structure Sensitivity of the Electrochemical Reduction of Carbon Monoxide on Copper Single Crystals. *ACS Catal.* **2013**, *3*, 1292−1295.

(3) Le, M.; Ren, M.; Zhang, Z.; Sprunger, P. T.; Kurtz, R. L.; Flake, J. C. Electrochemical Reduction of CO_2 to CH_3OH at Copper Oxide Surfaces. *J. Electrochem. Soc.* **2011**, *158*, E45−E49.

(4) Varela, A. S.; Schlaup, C.; Jovanov, Z. P.; Malacrida, P.; Horch, S.; Stephens, I. E. L.; Chorkendorff, I. CO_2 Electroreduction on Well-Defined Bimetallic Surfaces: Cu Overlayers on Pt(111) and Pt(211). *J. Phys. Chem. C* **2013**, *117*, 20500−20508.

(5) Nie, X.; Griffin, G. L.; Janik, M. J.; Asthagiri, A. Surface Phases of Cu_2O(111) under CO_2 Electrochemical Reduction Conditions. *Catal. Commun.* **2014**, *52*, 88−91.

(6) Gattrell, M.; Gupta, N.; Co, A. A Review of the Aqueous Electrochemical Reduction of CO_2 to Hydrocarbons at Copper. *J. Electroanal. Chem.* **2006**, *594*, 1−19.

(7) Roy, S. C.; Varghese, O. K.; Paulose, M.; Grimes, C. A. Toward Solar Fuels: Photocatalytic Conversion of Carbon Dioxide to Hydrocarbons. *ACS Nano* **2010**, *4*, 1259−1278.

(8) Schouten, K. J. P.; Pérez Gallent, E.; Koper, M. T. M. The Influence of pH on the Reduction of CO and to Hydrocarbons on Copper Electrodes. *J. Electroanal. Chem.* **2014**, *716*, 53−57.

(9) Li, C. W.; Kanan, M. W. CO_2 Reduction at Low Overpotential on Cu Electrodes Resulting from the Reduction of Thick Cu_2O Films. *J. Am. Chem. Soc.* **2012**, *134*, 7231−7234.

(10) Rosen, B. A.; Salehi-Khojin, A.; Thorson, M. R.; Zhu, W.; Whipple, D. T.; Kenis, P. J. A.; Masel, R. I. Ionic Liquid−Mediated Selective Conversion of CO_2 to CO at Low Overpotentials. *Science* **2011**, *334*, 643−644.

(11) Hull, J. F.; Himeda, Y.; Wang, W.-H.; Hashiguchi, B.; Periana, R.; Szalda, D. J.; Muckerman, J. T.; Fujita, E. Reversible Hydrogen Storage Using CO_2 and a Proton-Switchable Iridium Catalyst in Aqueous Media under Mild Temperatures and Pressures. *Nat. Chem.* **2012**, *4*, 383−388.

(12) Angamuthu, R.; Byers, P.; Lutz, M.; Spek, A. L.; Bouwman, E. Electrocatalytic CO_2 Conversion to Oxalate by a Copper Complex. *Science* **2010**, *327*, 313−315.

(13) Barton Cole, E.; Lakkaraju, P. S.; Rampulla, D. M.; Morris, A. J.; Abelev, E.; Bocarsly, A. B. Using a One-Electron Shuttle for the Multielectron Reduction of CO_2 to Methanol: Kinetic, Mechanistic, and Structural Insights. *J. Am. Chem. Soc.* **2010**, *132*, 11539−11551.

(14) Lim, C.-H.; Holder, A. M.; Hynes, J. T.; Musgrave, C. B. Reduction of CO_2 to Methanol Catalyzed by a Biomimetic Organo-Hydride Produced from Pyridine. *J. Am. Chem. Soc.* **2014**, *136*, 16081−16095.

(15) Tripkovic, V.; Vanin, M.; Karamad, M.; Björketun, M. E.; Jacobsen, K. W.; Thygesen, K. S.; Rossmeisl, J. Electrochemical CO_2 and CO Reduction on Metal-Functionalized Porphyrin-Like Graphene. *J. Phys. Chem. C* **2013**, *117*, 9187−9195.

(16) Dhakshinamoorthy, A.; Navalon, S.; Corma, A.; Garcia, H. Photocatalytic CO_2 Reduction by TiO_2 and Related Titanium Containing Solids. *Energy Environ. Sci.* **2012**, *5*, 9217−9233.

(17) Woolerton, T. W.; Sheard, S.; Reisner, E.; Pierce, E.; Ragsdale, S. W.; Armstrong, F. A. Efficient and Clean Photoreduction of CO_2 to CO by Enzyme-Modified TiO_2 Nanoparticles Using Visible Light. *J. Am. Chem. Soc.* **2010**, *132*, 2132−2133.

(18) Hansen, H. A.; Varley, J. B.; Peterson, A. A.; Nørskov, J. K. Understanding Trends in the Electrocatalytic Activity of Metals and Enzymes for CO_2 Reduction to CO. *J. Phys. Chem. Lett.* **2013**, *4*, 388−392.

(19) Varley, J. B.; Hansen, H. A.; Ammitzbøll, N. L.; Grabow, L. C.; Peterson, A. A.; Rossmeisl, J.; Nørskov, J. K. Ni−Fe−S Cubanes in CO_2 Reduction Electrocatalysis: A DFT Study. *ACS Catal.* **2013**, *3*, 2640−2643.

(20) Centi, G.; Quadrelli, E. A.; Perathoner, S. Catalysis for CO_2 Conversion: A Key Technology for Rapid Introduction of Renewable Energy in the Value Chain of Chemical Industries. *Energy Environ. Sci.* **2013**, *6*, 1711−1731.

(21) Qiao, J.; Liu, Y.; Hong, F.; Zhang, J. A Review of Catalysts for the Electroreduction of Carbon Dioxide to Produce Low-Carbon Fuels. *Chem. Soc. Rev.* **2014**, *43*, 631−675.

(22) Hori, Y., Electrochemical CO_2 Reduction on Metal Electrodes. In *Modern Aspects of Electrochemistry*; Vayenas, C. G., White, R. E., Gamboa-Aldeco, M. E., Eds. Springer: New York, 2008; Vol. *42*, pp 89−189.

(23) Appel, A. M.; Bercaw, J. E.; Bocarsly, A. B.; Dobbek, H.; DuBois, D. L.; Dupuis, M.; Ferry, J. G.; Fujita, E.; Hille, R.; Kenis, P. J. A.; et al. Frontiers, Opportunities, and Challenges in Biochemical and Chemical Catalysis of CO_2 Fixation. *Chem. Rev. (Washington, DC, U. S.)* **2013**, *113*, 6621−6658.

(24) Kuhl, K. P.; Hatsukade, T.; Cave, E. R.; Abram, D. N.; Kibsgaard, J.; Jaramillo, T. F. Electrocatalytic Conversion of Carbon Dioxide to Methane and Methanol on Transition Metal Surfaces. *J. Am. Chem. Soc.* **2014**, *136*, 14107−14113.

(25) Hori, Y.; Kikuchi, K.; Murata, A.; Suzuki, S. Production of Methane and Ethylene in Electrochemical Reduction of Carbon Dioxide at Copper Electrode in Aqueous Hydrogencarbonate Solution. *Chem. Lett.* **1986**, 897−898.

(26) Hori, Y.; Kikuchi, K.; Suzuki, S. Production of CO and CH_4 in Electrochemical Reduction of CO_2 at Metal Electrodes in Aqueous Hydrogencarbonate Solution. *Chem. Lett.* **1985**, *14*, 1695−1698.

(27) Hori, Y.; Murata, A.; Takahashi, R.; Suzuki, S. Enhanced Formation of Ethylene and Alcohols at Ambient Temperature and Pressure in Electrochemical Reduction of Carbon Dioxide at a Copper Electrode. *J. Chem. Soc., Chem. Commun.* **1988**, 17−19.

(28) Noda, H.; Ikeda, S.; Oda, Y.; Ito, K. Potential Dependencies of the Products on Electrochemical Reduction of Carbon Dioxide at a Copper Electrode. *Chem. Lett.* **1989**, *18*, 289−292.

(29) Shibata, H.; Moulijn, J.; Mul, G. Enabling Electrocatalytic Fischer−Tropsch Synthesis from Carbon Dioxide over Copper-Based Electrodes. *Catal. Lett.* **2008**, *123*, 186−192.
(30) Centi, G.; Perathoner, S. Catalysis: Role and Challenges for a Sustainable Energy. *Top. Catal.* **2009**, *52*, 948−961.
(31) Hori, Y.; Murata, A.; Takahashi, R. Formation of Hydrocarbons in the Electrochemical Reduction of Carbon Dioxide at a Copper Electrode in Aqueous Solution. *J. Chem. Soc., Faraday Trans. 1* **1989**, *85*, 2309−2326.
(32) Hori, Y.; Takahashi, R.; Yoshinami, Y.; Murata, A. Electrochemical Reduction of CO at a Copper Electrode. *J. Phys. Chem. B* **1997**, *101*, 7075−7081.
(33) DeWulf, D. W.; Jin, T.; Bard, A. J. Electrochemical and Surface Studies of Carbon Dioxide Reduction to Methane and Ethylene at Copper Electrodes in Aqueous Solutions. *J. Electrochem. Soc.* **1989**, *136*, 1686−1691.
(34) Kim, J. J.; Summers, D. P.; Frese, K. W., Jr Reduction of CO_2 and CO to Methane on Cu Foil Electrodes. *J. Electroanal. Chem.* **1988**, *245*, 223−244.
(35) Hori, Y.; Murata, A.; Takahashi, R.; Suzuki, S. Electroreduction of Carbon Monoxide to Methane and Ethylene at a Copper Electrode in Aqueous Solutions at Ambient Temperature and Pressure. *J. Am. Chem. Soc.* **1987**, *109*, 5022−5023.
(36) Peterson, A. A.; Abild-Pedersen, F.; Studt, F.; Rossmeisl, J.; Norskov, J. K. How Copper Catalyzes the Electroreduction of Carbon Dioxide into Hydrocarbon Fuels. *Energy Environ. Sci.* **2010**, *3*, 1311−1315.
(37) Nie, X.; Luo, W.; Janik, M. J.; Asthagiri, A. Reaction Mechanisms of CO_2 Electrochemical Reduction on Cu(111) Determined with Density Functional Theory. *J. Catal.* **2014**, *312*, 108−122.
(38) Nie, X.; Esopi, M. R.; Janik, M. J.; Asthagiri, A. Selectivity of CO_2 Reduction on Copper Electrodes: The Role of the Kinetics of Elementary Steps. *Angew. Chem., Int. Ed.* **2013**, *52*, 2459−2462.
(39) Hansen, H.; Montoya, J.; Zhang, Y.-J.; Shi, C.; Peterson, A.; Nørskov, J. Electroreduction of Methanediol on Copper. *Catal. Lett.* **2013**, *143*, 631−635.
(40) Shaw, S. K.; Berna, A.; Feliu, J. M.; Nichols, R. J.; Jacob, T.; Schiffrin, D. J. Role of Axially Coordinated Surface Sites for Electrochemically Controlled Carbon Monoxide Adsorption on Single Crystal Copper Electrodes. *Phys. Chem. Chem. Phys.* **2011**, *13*, 5242−5251.
(41) Durand, W. J.; Peterson, A. A.; Studt, F.; Abild-Pedersen, F.; Nørskov, J. K. Structure Effects on the Energetics of the Electrochemical Reduction of CO_2 by Copper Surfaces. *Surf. Sci.* **2011**, *605*, 1354−1359.
(42) Calle-Vallejo, F.; Koper, M. T. M. Theoretical Considerations on the Electroreduction of CO to C2 Species on Cu(100) Electrodes. *Angew. Chem., Int. Ed.* **2013**, *52*, 7282−7285.
(43) Schouten, K. J. P.; Qin, Z.; Gallent, E. P.; Koper, M. T. M. Two Pathways for the Formation of Ethylene in CO Reduction on Single-Crystal Copper Electrodes. *J. Am. Chem. Soc.* **2012**, *134*, 9864−9867.
(44) Schouten, K. J. P.; Kwon, Y.; van der Ham, C. J. M.; Qin, Z.; Koper, M. T. M. A New Mechanism for the Selectivity to C1 and C2 Species in the Electrochemical Reduction of Carbon Dioxide on Copper Electrodes. *Chem. Sci.* **2011**, *2*, 1902−1909.
(45) Azuma, M.; Hashimoto, K.; Hiramoto, M.; Watanabe, M.; Sakata, T. Electrochemical Reduction of Carbon Dioxide on Various Metal Electrodes in Low-Temperature Aqueous $KHCO_3$ Media. *J. Electrochem. Soc.* **1990**, *137*, 1772−1778.
(46) Hori, Y.; Wakebe, H.; Tsukamoto, T.; Koga, O. Electrocatalytic Process of CO Selectivity in Electrochemical Reduction of CO_2 at Metal Electrodes in Aqueous Media. *Electrochim. Acta* **1994**, *39*, 1833−1839.
(47) Peterson, A. A.; Nørskov, J. K. Activity Descriptors for CO_2 Electroreduction to Methane on Transition-Metal Catalysts. *J. Phys. Chem. Lett.* **2012**, *3*, 251−258.
(48) Watanabe, M.; Shibata, M.; Kato, A.; Azuma, M.; Sakata, T. Design of Alloy Electrocatalysts for CO_2 Reduction: III. The Selective and Reversible Reduction of on Cu Alloy Electrodes. *J. Electrochem. Soc.* **1991**, *138*, 3382−3389.
(49) Christophe, J.; Doneux, T.; Buess-Herman, C. Electroreduction of Carbon Dioxide on Copper-Based Electrodes: Activity of Copper Single Crystals and Copper−Gold Alloys. *Electrocatalysis* **2012**, *3*, 139−146.
(50) Xu, Z.; Lai, E.; Shao-Horn, Y.; Hamad-Schifferli, K. Compositional Dependence of the Stability of Aucu Alloy Nanoparticles. *Chem. Commun. (Cambridge, U. K.)* **2012**, *48*, 5626−5628.
(51) Hirunsit, P. Electroreduction of Carbon Dioxide to Methane on Copper, Copper−Silver, and Copper−Gold Catalysts: A DFT Study. *J. Phys. Chem. C* **2013**, *117*, 8262−8268.
(52) Nørskov, J. K.; Rossmeisl, J.; Logadottir, A.; Lindqvist, L.; Kitchin, J. R.; Bligaard, T.; Jónsson, H. Origin of the Overpotential for Oxygen Reduction at a Fuel-Cell Cathode. *J. Phys. Chem. B* **2004**, *108*, 17886−17892.
(53) Nørskov, J. K.; Bligaard, T.; Logadottir, A.; Bahn, S.; Hansen, L. B.; Bollinger, M.; Bengaard, H.; Hammer, B.; Sljivancanin, Z.; Mavrikakis, M.; Xu, Y.; Dahl, S.; Jacobsen, C. J. H. Universality in Heterogeneous Catalysis. *J. Catal.* **2002**, *209*, 275−278.
(54) Ruban, A. V.; Skriver, H. L.; Nørskov, J. K. Surface Segregation Energies in Transition-Metal Alloys. *Phys. Rev. B* **1999**, *59*, 15990−16000.
(55) Kresse, G.; Furthmüller, J. Efficient Iterative Schemes for Ab Initio Total-Energy Calculations Using a Plane-Wave Basis Set. *Phys. Rev. B* **1996**, *54*, 11169−11186.
(56) Kresse, G.; Furthmüller, J. Efficiency of Ab Initio Total Energy Calculations for Metals and Semiconductors Using a Plane-Wave Basis Set. *Comput. Mater. Sci.* **1996**, *6*, 15−50.
(57) Perdew, J. P.; Burke, K.; Ernzerhof, M. Generalized Gradient Approximation Made Simple. *Phys. Rev. Lett.* **1996**, *77*, 3865−3868.
(58) Perdew, J. P.; Burke, K.; Ernzerhof, M. Generalized Gradient Approximation Made Simple [*Phys. Rev. Lett.* **1996**, *77*, 3865]. *Phys. Rev. Lett.* **1997**, *78*, 1396−1396.
(59) Blöchl, P. E. Projector Augmented-Wave Method. *Phys. Rev. B* **1994**, *50*, 17953.
(60) Kresse, G.; Joubert, D. From Ultrasoft Pseudopotentials to the Projector Augmented-Wave Method. *Phys. Rev. B* **1999**, *59*, 1758−1775.
(61) Hammer, B.; Morikawa, Y.; Nørskov, J. K. CO Chemisorption at Metal Surfaces and Overlayers. *Phys. Rev. Lett.* **1996**, *76*, 2141−2144.

Supplementary Information for
“CO_2 Electrochemical Reduction to Methane and Methanol on Copper Based Alloys: Theoretical Insight”

Pussana Hirunsit *[a], Wiwaporn Soodsawang [a], and Jumras Limtrakul [b,c]

[a] National Nanotechnology Center (NANOTEC), Thailand Science Park, Pathumthani 12120, Thailand

[b] Department of Chemistry and NANOTEC Center for Nanoscale Materials Design for Green Nanotechnology, Faculty of Science, Kasetsart University, Bangkok 10900, Thailand

[c]PTT Group Frontier Research Center, PTT Public Company Limited, 555 Vibhavadi Rangsit Road, Chatuchak, Bangkok 10900, Thailand

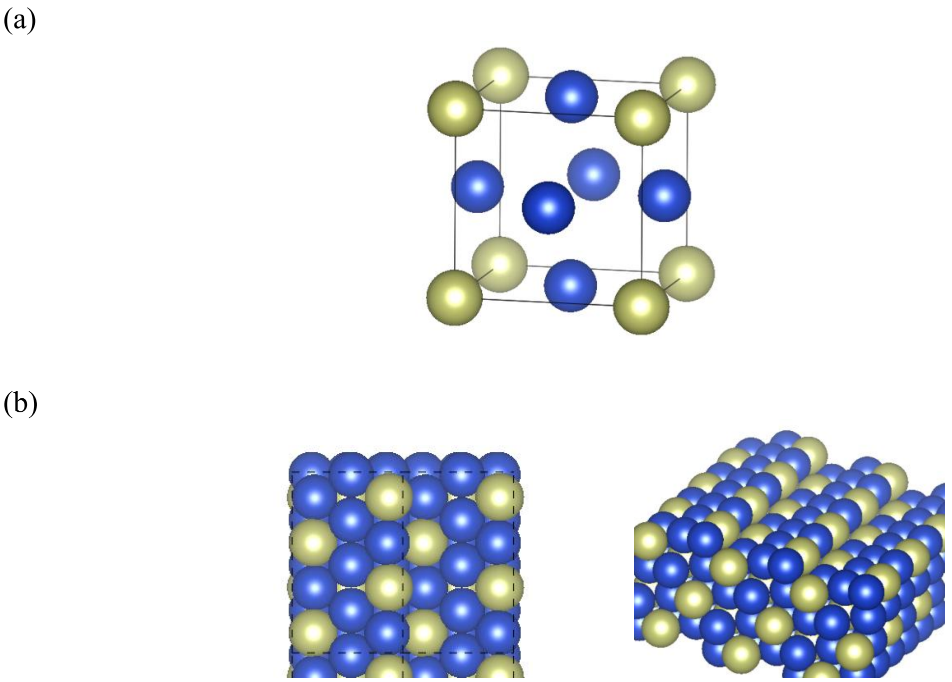

Top view side view

Figure S1. (a) The bulk $L1_2$ crystal lattice structure of Cu_3X , and (b) a unit cell of slab model of stepped (211) Cu_3X alloys surface. Cu atom-blue and X atom-green. The dashed line indicates a unit cell boundary.

Table S1. Adsorption energy of intermediate species, $B.E^{a}$, on Cu(211), Cu$_3$Ag(211), and Cu$_3$Au(211) in eV. Blue atom is Cu, gray atom is Ag, orange atom is Au, red atom is O, brown atom is C and white atom is H.

species	Cu(211)		Cu$_3$Ag(211)		Cu$_3$Au(211)	
	configuration	$B.E^{a}$	configuration	$B.E^{a}$	configuration	$B.E^{a}$
O	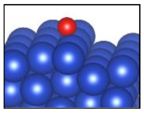	0.77	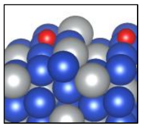	0.88	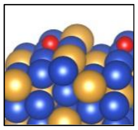	1.13
H	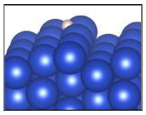	-0.28	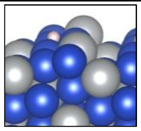	-0.19	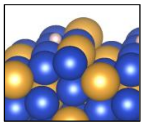	-0.17
C	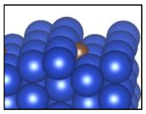	2.05	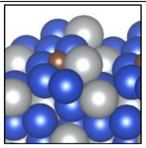	2.85	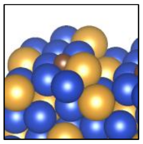	2.91
OH	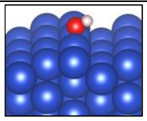	-0.28	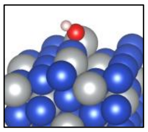	0.05	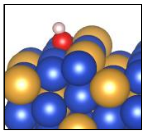	0.24
CO	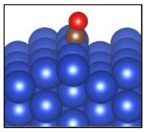	0.93	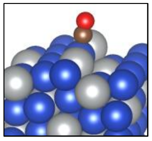	1.05	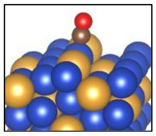	1.12
CH	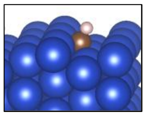	1.01	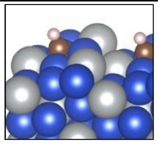	1.35	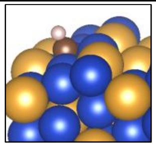	1.55
CH$_2$	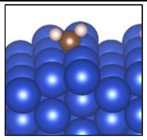	0.53	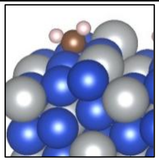	0.77	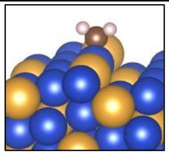	0.79
COH	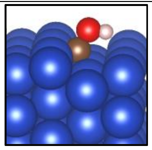	1.91	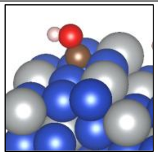	2.00	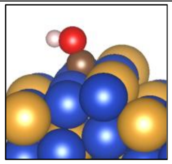	2.12
HCO	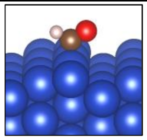	1.43	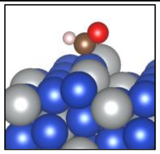	1.51	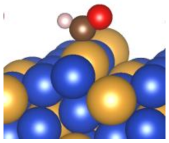	1.45

species	$Cu(211)$		$Cu_3Ag(211)$		$Cu_3Au(211)$	
	configuration	*B.E*[a]	configuration	*B.E*[a]	configuration	*B.E*[a]
HCOH	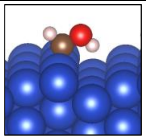	1.18	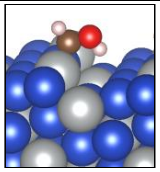	1.45	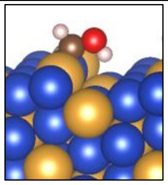	1.37
HOCO	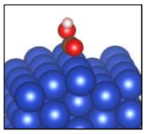	1.04	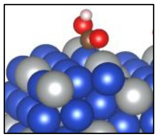	1.26	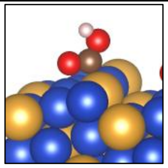	1.51
CH_3	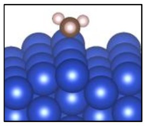	-0.61	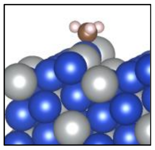	-0.39	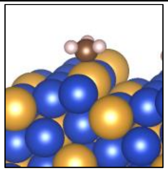	-0.40
OCH_2	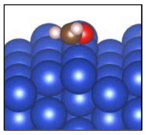	0.83	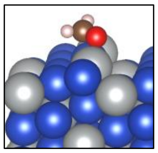	1.06	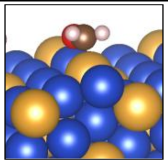	1.01
OCH_3	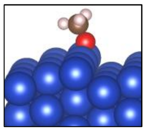	-0.27	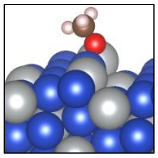	0.07	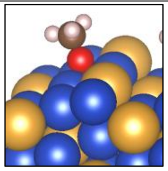	0.16
CH_2OH	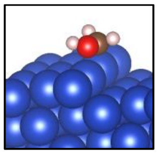	0.54	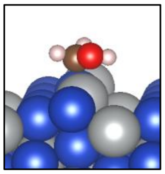	0.68	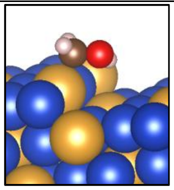	0.65

$^{a}B.E \ = \ E_{total(C_xH_yO_z)} - E_{slab} - xE(C) - yE(H) - zE(O)$

Where $E_{total(C_xH_yO_z)}$ is the total energy of the state, E_{slab} is the energy of the clean slab, $E(C)$is energy of C atom referenced to graphene, $E(H)$ is the energy of H atom referenced to $1/2H_2$ and $E(O)$ is the energy of O atom referenced to ($H_2O - H_2$)

Table S2. Adsorption energy of intermediate species, *B.E*[a], on $Cu_3Pd(211)$, $Cu_3Pt(211)$, and $Cu_3Co(211)$ surfaces in eV. Blue atom is Cu, gray atom is Pd or Pt, dark blue atom is Co, red atom is O, brown atom is C and white atom is H.

species	$Cu_3Pd(211)$		$Cu_3Pt(211)$		$Cu_3Co(211)$	
	configuration	*B.E*[a]	configuration	*B.E*[a]	configuration	*B.E*[a]
O	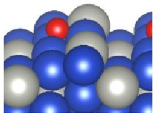	1.22	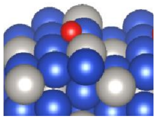	1.26	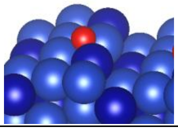	0.08
H	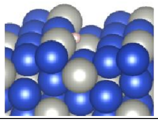	-0.31	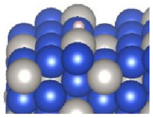	-0.40	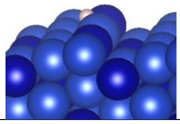	-0.46
C	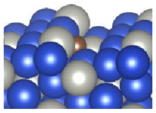	1.93	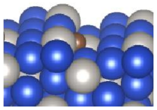	1.34	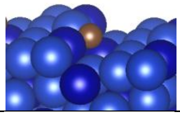	1.67
OH	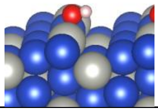	0.18	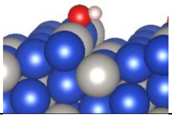	0.19	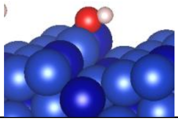	-0.63
CO	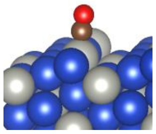	0.66	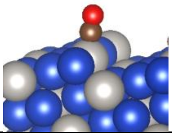	0.14	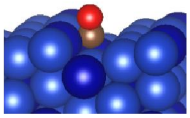	0.13
CH	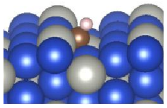	1.09	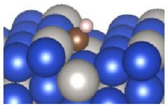	0.53	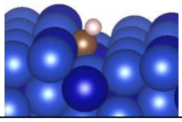	-0.15
CH_2	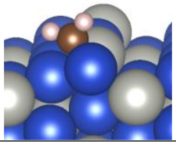	0.60	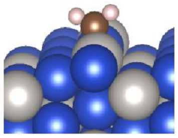	0.11	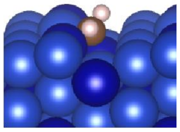	-0.18
COH	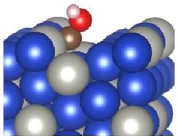	1.68	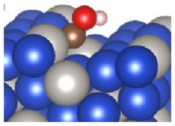	0.94	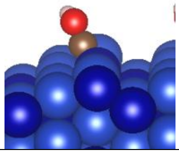	0.29
HCO	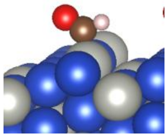	1.12	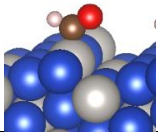	0.62	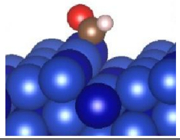	0.68
HCOH	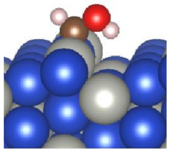	1.02	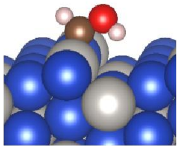	0.55	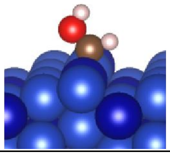	0.61

species	$Cu_3Pd(211)$		$Cu_3Pt(211)$		$Cu_3Co(211)$	
	configuration	*B.E*[a]	configuration	*B.E*[a]	configuration	*B.E*[a]
HOCO	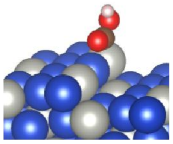	1.23	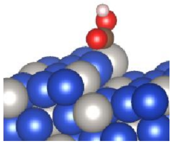	0.71	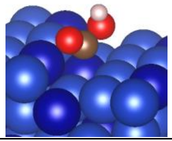	0.60
CH_3	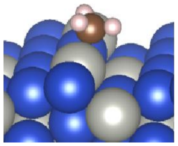	-0.51	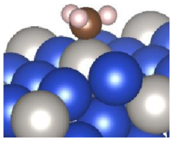	-0.84	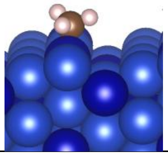	-0.83
OCH_2	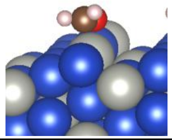	0.71	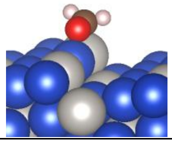	0.59	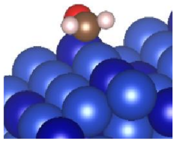	0.03
OCH_3	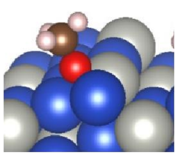	0.34	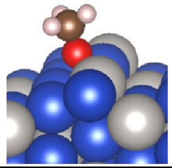	0.42	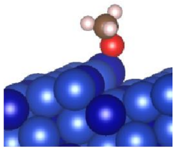	-0.42
CH_2OH	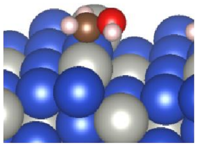	0.54	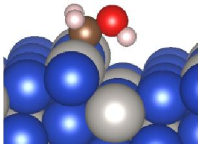	0.04	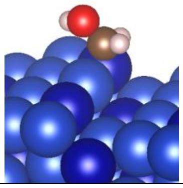	0.22

[a] $B.E = E_{total(C_xH_yO_z)} - E_{slab} - xE(C) - yE(H) - zE(O)$

Where $E_{total(C_xH_yO_z)}$ is the total energy of the state, E_{slab} is the energy of the clean slab, $E(C)$ is energy of C atom referenced to graphene, $E(H)$ is the energy of H atom referenced to $1/2H_2$ and $E(O)$ is the energy of O atom referenced to ($H_2O - H_2$)

Table S3. Adsorption energy of intermediate species, *B.E*^{a}, on Cu$_3$Ni(211), Cu$_3$Rh(211), and Cu$_3$Ir(211) surfaces in eV. Blue atom is Cu, gray atom is Ni or Rh, green atom is Ir, red atom is O, brown atom is C and white atom is H.

species	Cu$_3$Ni(211)		Cu$_3$Rh(211)		Cu$_3$Ir(211)	
	configuration	*B.E*^{a}	configuration	*B.E*^{a}	configuration	*B.E*^{a}
O	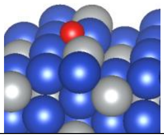	0.52	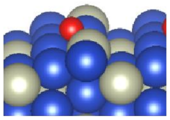	0.71	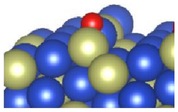	-0.16
H	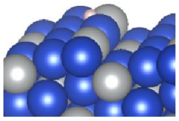	-0.47	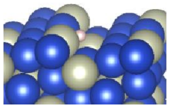	-0.61	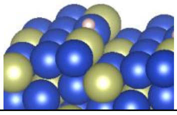	-0.66
C	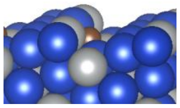	0.75	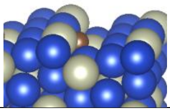	0.33	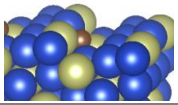	-0.12
OH	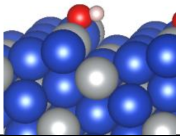	-0.41	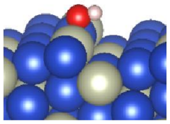	-0.12	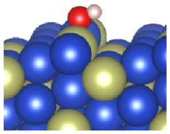	-0.29
CO	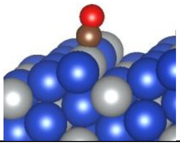	0.10	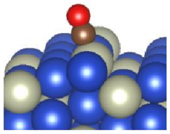	-0.13	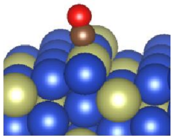	-0.62
CH	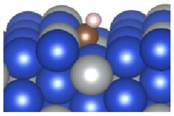	0.11	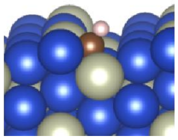	-0.10	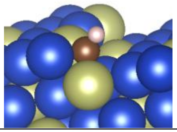	-0.60
CH$_2$	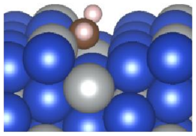	0.09	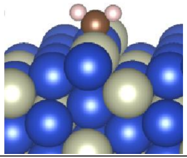	-0.13	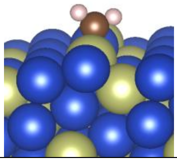	-1.59
COH	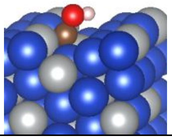	0.77	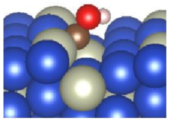	0.19	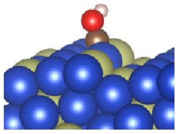	-0.39
HCO	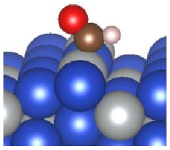	0.79	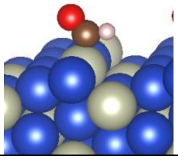	0.48	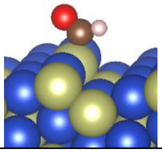	-0.57

species	$Cu_3Ni(211)$		$Cu_3Rh(211)$		$Cu_3Ir(211)$	
	configuration	*B.E*[a]	configuration	*B.E*[a]	configuration	*B.E*[a]
HCOH	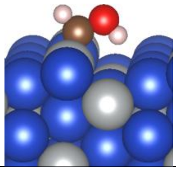	0.51	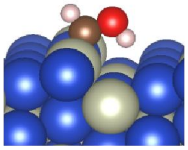	0.26	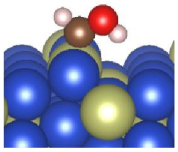	-0.36
HOCO	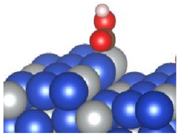	0.76	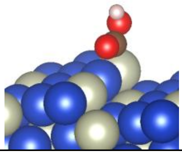	0.67	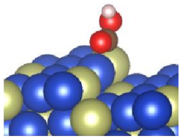	0.30
CH_3	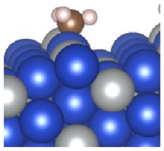	-0.90	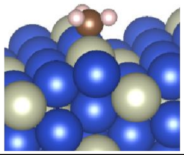	-0.86	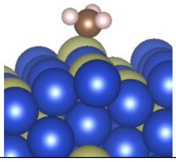	-2.11
OCH_2	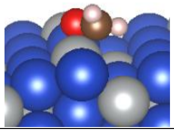	0.25	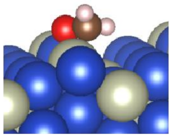	0.29	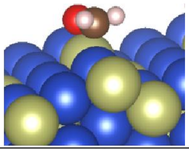	-0.64
OCH_3	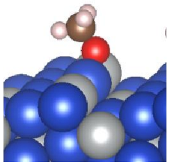	-0.37	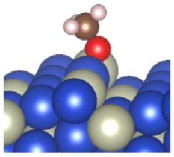	-0.06	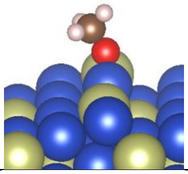	-0.70
CH_2OH	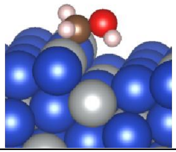	0.14	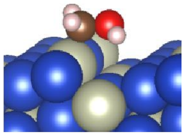	0.09	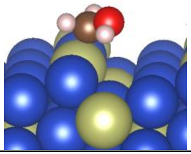	-0.50

[a] $B.E = E_{total(C_xH_yO_z)} - E_{slab} - xE(C) - yE(H) - zE(O)$

Where $E_{total(C_xH_yO_z)}$ is the total energy of the state, E_{slab} is the energy of the clean slab, $E(C)$ is energy of C atom referenced to graphene, $E(H)$ is the energy of H atom referenced to $1/2H_2$ and $E(O)$ is the energy of O atom referenced to ($H_2O - H_2$)

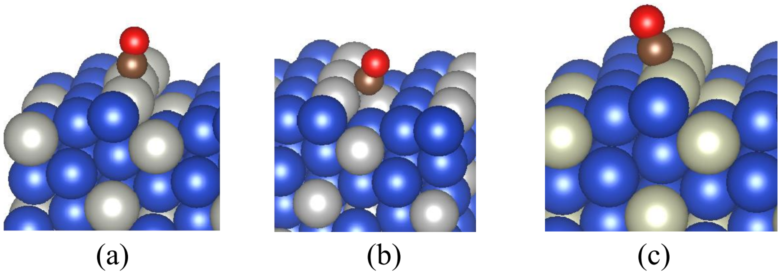

(a) (b) (c)

Figure S2. Structures of CO* adsorption on segregated structures of (a) $Cu_3Pd(211)$, (b) $Cu_3Co(211)$ and (c) $Cu_3Rh(211)$ surfaces.

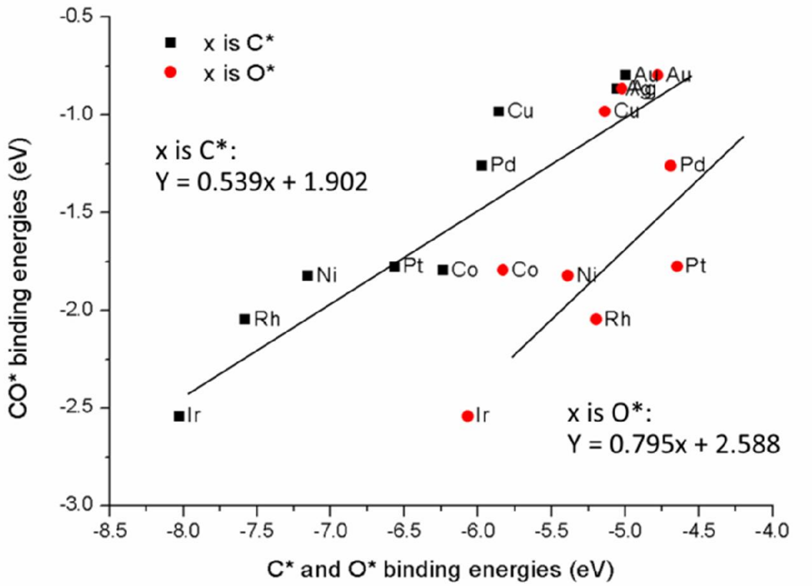

Figure S3. Linear scaling correlations between CO* binding energies and C* or O* binding energies on $Cu_3X(211)$ surfaces. The X element is labeled at the data point. The binding energies are calculated by $E_{total} - E_{clean\ slab} - E_{adsorbate\ (gas)}$.

Table S4. Surface *d*-band center energy level referenced on Fermi energy level.

$Cu_3X(211)$	*d*-band center energy level (eV)
Cu_3Ag	-2.68
Cu_3Au	-2.54
Cu	-2.16
Cu_3Pd	-1.83
Cu_3Pt	-1.85
Cu_3Ni	-1.49
Cu_3Co	-1.76
Cu_3Rh	-1.52
Cu_3Ir	-1.68

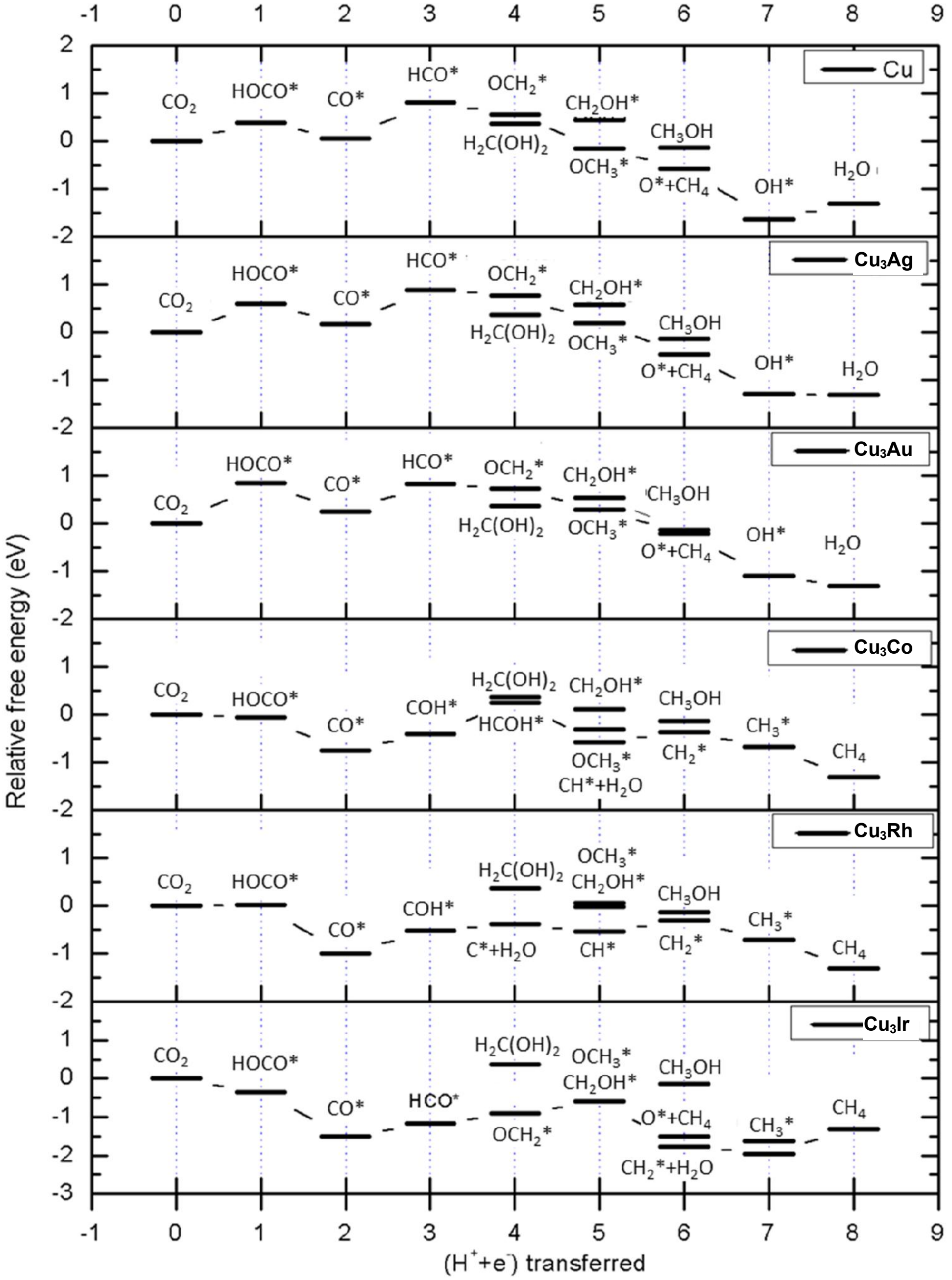

Figure S4. Free energy diagrams of the most favorable CH_4 pathway and the reduction of methanediol at 0 V_{RHE} on Cu, Cu_3Ag, Cu_3Au, Cu_3Co, Cu_3Rh, and Cu_3Ir (211) surfaces.

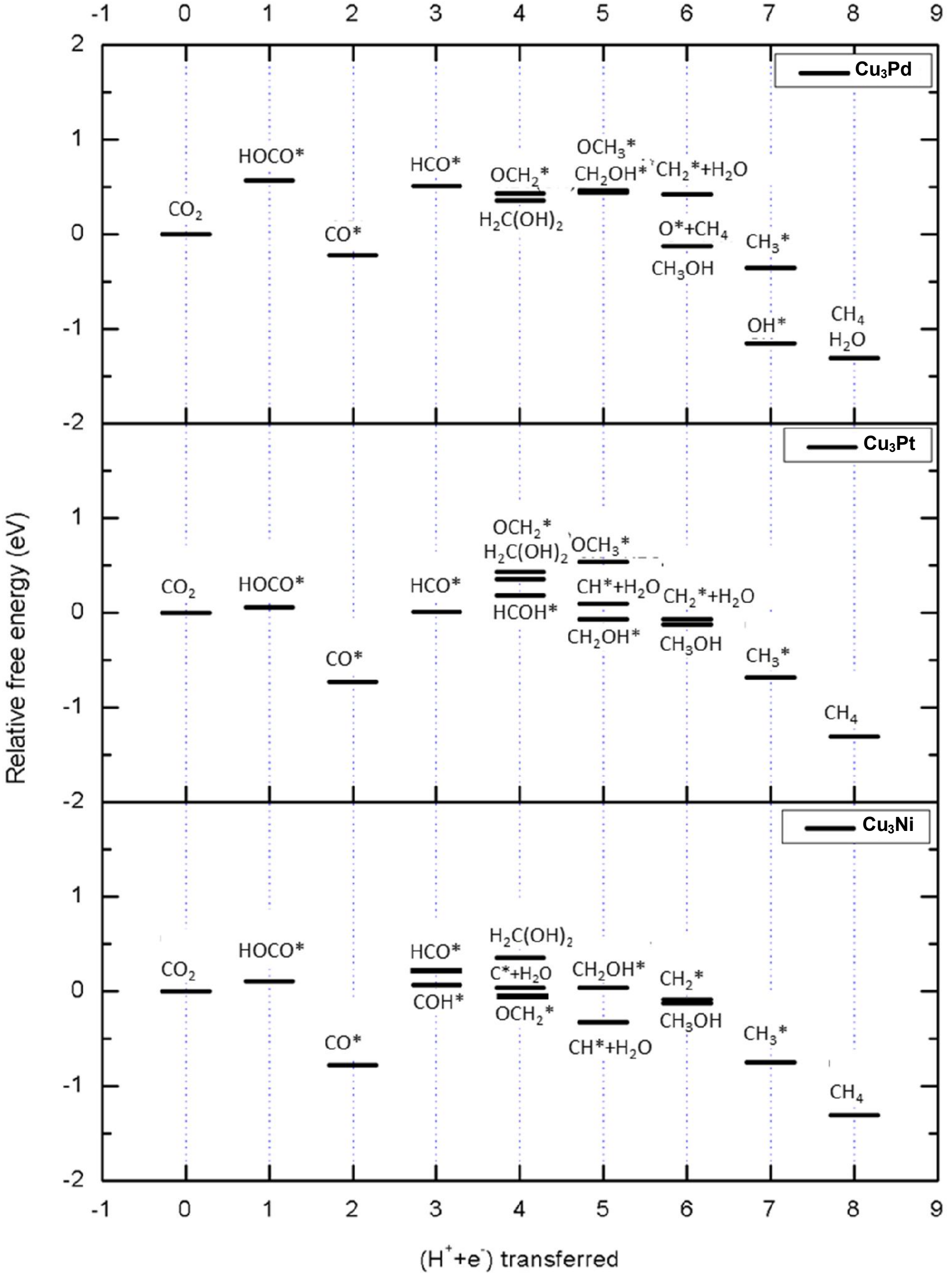

Figure S5. Free energy diagrams of the most favorable CH_3OH, CH_4 pathway and the reduction of methanediol at 0.0 V_{RHE} on Cu_3Pd, Cu_3Pt, and Cu_3Ni (211) surfaces.

SMS
Smart Materials and Surfaces
BANGKOK 2014

International Conference
26 - 28 August 2014

Sheraton Grande Sukhumvit Hotel
Bangkok - Thailand

Organizer

SETCOR
Conferences & Events

www.setcor.org

In collaboration with

IAAM
International Association
of Advanced Materials

www.iaamonline.org

AIT
Asian Institute
of Technology

www.ait.ac.th

AIT CONSULTING
Technology . Engineering . Environment . Development . Management

www.consulting.ait.asia

Reactivity Trend of CO_2 Electroreduction on Copper Alloys from First Principles

Pussana Hirunsit [1,*] Wiwaporn Soodsawang [1], Jumras Limtrakul [2,3]
[1] National Nanotechnology Center (NANOTEC), National Science and Technology Development Agency (NSTDA), Pathumthani, Thailand
[2] Department of Chemistry and NANOTEC Center for Nanoscale Materials Design for Green Nanotechnology, Faculty of Science, Kasetsart University, Bangkok, Thailand
[3] PTT Group Frontier Research Center, PTT Public Company Limited, Bangkok, Thailand

Abstract: The electroreduction of CO_2 to valuable hydrocarbon products is a promising process that would allow recycling waste CO_2 into usable hydrocarbons without high temperature reactions requirement and the production rate can be varied to follow the availability of electricity produced from clean resources such as solar cells. The critical challenges for the CO_2 electroreduction process are that the reaction must be at a low overpotential as well as being selective. The electrode material is crucial in that it plays essential roles in determining the overpotential, efficiency and selectivity. A Copper electrode was found to perform the direct reduction of CO_2 to hydrocarbons (methane and ethylene) with a reasonable rate but very low efficiency (Hori *et al.,* 1986). It is an important challenge to discover promising electrode materials (electrocatalysts) which provide high efficiency and high hydrocarbon product selectivity. In this talk, we will present the thermodynamic investigation of CO_2 conversion to CH_4 on copper-based alloy with transition metals in group 9-11 using density functional theory calculations associated with standard hydrogen electrode model (Nørskov *et al.,* 2004) (Hirunsit, 2013). The key intermediate species, the theoretical overpotential, the potential-limiting step and the theoretical onset potential of key elementary steps are discussed. The scaling correlation of the key intermediate adsorbed free energies and their electronic structures provide the fundamental understanding of the interaction with surfaces. Also, the reactivity toward the competitive reaction of hydrogen evolution and the favorability of OH* surface poisoning will be discussed.

Keywords: density functional theory, heterogeneous catalysis, electrocatalysts, CO_2 reduction, and copper alloys.

References:

Hori, Y.; Kikuchi, K.; Murata, A.; Suzuki, S. (1986), Production of methane and ethylene in electrochemical reduction of carbon dioxide at copper electrode in aqueous hydrogencarbonate solution, *Chem. Lett.*, 897-898

Nørskov, J. K.; Rossmeisl, J.; Logadottir, A.; Lindqvist, L.; Kitchin, J. R.; Bligaard, T.; Jónsson, H. (2004), Origin of the Overpotential for Oxygen Reduction at a Fuel-Cell Cathode, *J.Phy.Chem.B*, 108 (46), 17886-17892

Hirunsit, P. (2013), Electroreduction of Carbon Dioxide to Methane on Copper, Copper–Silver, and Copper–Gold Catalysts: A DFT Study, *J.Phy.Chem.C,* 117 (16), 8262-8268.